Aus dem

Walter-Brendel-Zentrum für experimentelle Medizin

Komm. Direktor: Prof. Dr. med. dent. Reinhard Hickel

Ehem. Direktor: Prof. Dr. med. Ulrich Pohl

5'-adenosine monophosphate-activated protein kinase (AMPK) modulates myoendothelial junctions

Dissertation

zum Erwerb des Doktorgrades der Medizin an der Medizinischen

Fakultät der Ludwig-Maximilians-Universität zu München

Jiehua Qiu

Jiangxi, China

2018

Mit Genehmigung der Medizinischen Fakultät
der Universität München

Berichterstatter:	Prof. Dr. med. Ulrich Pohl
Mitberichterstatter:	Prof. Dr. med. Andreas Schober
	Prof. Dr. med. Stefan Brunner
Mitbetreuung durch die promovierten Mitarbeiter:	Kai-Michael Schubert, PhD
	Dr. med. Holger Schneider
Dekan:	Prof. Dr. med. dent. Reinhard Hickel
Tag der mündlichen Prüfung	01.03.2018

Index

List of Figures: 5
List of Tables: 7
Summary: 8
List of Abbreviations: 12
1. Introduction: 16
1.1. Cell–Cell Communication 16
1.2. Myoendothelial junction (MEJ) in the vasculature 17
1.3. Plasminogen activator inhibitor-1 20
1.4. 5'-adenosine monophosphate-activated protein kinase 22
1.5. Hypotheses and aim of the Study 25
2. Materials and Methods: 27
2.1. Buffer solutions and drugs. 27
2.2. Probes and Antibodies 31
2.3. Animals, isolation and cannulation of resistance-type arteries. 32
2.4. Recording of MEJ dynamics and live imaging. 36
2.5. Immunofluorescence. 37
2.6. Assessment of heterocellular dye transfer. 37
2.7. Calcein spreading and diffusion. 37
2.8. Image analysis. 38
2.9. Acetylcholine (Ach) dose response curves. 39
2.10. Protein isolation from intact arteries. 40
2.11. Cell culture, siRNA transfection and protein harvest. 41
2.12. Western blot 42
2.13. Mouse genotyping via PCR 43
2.14. Statistics 44
3. Results 45
3.1. Observation of actin-rich circular and cone-like structures in mesenteric arteries. 45
3.2. Characterization of WLS. 48
3.3. The dark area around the actin cone of WLS represents endoplasmatic reticulum (ER). 53
3.4. AMPK modulated MEJ dynamics. 54
3.5. AMPK α1-KO, but not α2-KO, enhanced Ach-induced artery dilation 57
3.6. More MEJs and IEL holes in AMPK α1-KO, but not in AMPK α2-KO mice. 59

3.7. PAI-1 expression was higher in AMPK α1-KO than WT artery, but not in AMPK α2-KO.....63
3.8. Active-PAI-1 increased MEJs in intact artery. 65
3.9. AMPK activation reduced PAI-1 expression in intact artery 67
3.10. AMPK activation reduced the PAI-1 expression in PCASMC.....70
3.11. PAI-1 expression was increased after AMPK silencing with SiRNA in porcine and human VSM. 72
3.12. PAI-1 expression was not significantly changed after AMPK silencing in HUVEC.. 73
3.13. SHP expression was inhibited in vessels of both AMPK α1 and AMPK α2-KO mice……..…….74
4. Discussion.....76
4.1. A short recapitulation of the most important findings 76
4.2. Research models for MEJ ……..……..76
4.3. Cell protrusions and / or MEJ?.....78
4.4. Dynamics of MEJs vs. connexins / Gap junctions.....79
4.5. MEJ as interactomes.....79
4.6. AMPK, a universal cell regulator. 80
4.7. AMPK expression in blood vessels. 81
4.8. Verification of the AMPK activation state.....81
4.9. AMPK α1 modulation of MEJ dynamics 82
4.10. AMPK regulates MEJ dynamics via PAI-1. 83
4.11. Endothelial vs. smooth muscle regulation.....84
4.12. ACh-induced dilatation in AMPK α1 KO mice: related to the higher amount of MEJ?.....85
4.13. Potential physiological relevance of the mechanism.....86
References.....89
Acknowledgements.....103
Conference and Publications Papers during doctor study: 105
Conference: 105

List of Figures:

Figure 1. Schematic structure of MEJ. 20
Figure 2. Preparation of mesenteric arteries. 33
Figure 3. Preparation of saphenous artery. 34
Figure 4. Pressure myograph system (Isobaric arteriography). 35
Figure 5. Setup under the confocal microscope. 36
Figure 6. The calcium measuring and diameter registration system. 40
Figure 7. Localization of MEJs and Podosomes in intact arteries of LifeAct mouse. ... 46
Figure 8. Calcein staining co-localizes with the actin signal around MEJs. 47
Figure 9. Circular structures are PRs. 49
Figure 10. Cx37 and 43 is enhanced on WLS of intact mesenteric arteries. 50
Figure 11. PAI-1 signal is enhanced on WLS of intact mesenteric arteries. 50
Figure 12. Gap junction inhibition blunts heterocellular dye transfer from ECs to VSMC. 51
Figure 13. Calcein recovery in smooth muscle after bleaching starts from the WLS. .. 52
Figure 14. ER was enriched around the actin core of a WLS in intact artery. 53
Figure 15. Development of new WLS in a mesenteric artery of a LifeAct mouse after CC incubation. 55
Figure 16. AMPK inhibition boosted MEJ development compared to time control. 56
Figure 17. Inhibition of AMPK increased the fraction of holes filled by WLS and enhanced Ach-mediated dilation of the artery. 56
Figure 18. Inhibition of AMPK decreased calcein transfer from EC to VSMC, and enhanced formation of vesicles along nuclei. 57
Figure 19. Left shift of the Ach dose response curve in AMPKα1-KO mice compared to their respective WT controls. 58
Figure 21. Ach dose response curve was not changed in AMPKα2-KO mice, compared to their respective controls (WT). 59
Figure 21. The total hole area per unit IEL was higher in vessels of AMPKα1-KO mice. 60
Figure 22. The fraction of hole filled with WLS was higher both in mesenteric and muscle arteries from AMPK α1-KO than WT mice. 61
Figure 23. Compound C increased the fraction of hole filled with WLS in mesenteric arteries from AMPK α 1 WT mice, but not in KO mice. 62
Figure 24. No difference with regard to the fraction of hole filled with WLS in mesenteric arteries between AMPKα2-KO and WT mice. 63

Figure 25. AMPK α1 KO arteries expressed more PAI-1 protein. 64
Figure 26. NO change of PAI-1 expression in AMPK α2 KO artery compared to WT. ... 65
Figure 27. Active PAI-1 increased the fraction of WLS. 66
Figure 28. Activated AMPK reduced the PAI-1 expression in intact artery. 68
Figure 29. CC alone in unstimulated arteries did not affect PAI-1 expression. 69
Figure 30. Activated AMPK reduced the PAI-1 expression in PCASMC. 71
Figure 31. AMPK silencing increased the PAI-1 protein expression in PCASMC. 72
Figure 32. AMPK silencing increased the PAI-1 protein expression in HUVSMC. 73
Figure 33. AMPK silencing did not change the PAI-1 protein expression in HUVEC. ... 74
Figure 34. Lower SHP expression in AMPK α1 KO mice compared to its littermate WT mice. 75
Figure 35. Lower SHP expression in AMPK α2 KO mice compared to its littermate WT mice. 75

List of Tables:

Table 1. The detailed contents of MOPS buffer 27
Table 2. The detailed contents of PBS+ buffer 28
Table 3. The detailed contents of RIPA buffer 28
Table 4. The detailed contents of sample lysis buffer 28
Table 5. The detailed contents of loading buffer 29
Table 6. The detailed contents of loading buffer 29
Table 7. The detailed contents of washing buffer (pH to 7.6) 29
Table 8. The detailed contents of transfer buffer. 29
Table 9. The information about the drugs used in experiment 30
Table 10. The information of the probes and antibodies 31
Table 11. The detailed contents of DNA extraction buffer and tissue 44
Table 12. The protocol of DNA extraction 44
Table 13. The protocol of PCR cycling 44
Table 14. The comparison of characteristics between MEJ and Podosome. 48

Summary:

Cell-to-cell communication plays an important role in multicellular tissues. It is also pivotal in the modulation of vessel functions, such as the regulation of vessel tone. Heterocellular communication between endothelial cells (EC) and vascular smooth muscle cells (VSMC) via myoendothelial gap junctions (MEGJs) represents an important communication pathway in resistance arteries and arterioles. Myoendothelial junctions (MEJ) are, however, not only the site of direct cell communication via gap junctions but also represent a signaling microdomain critical for localizing, concentrating, and organizing cell-signaling components and regulating various vascular biological processes such as endothelium dependent hyperpolarization (EDH) of vascular smooth muscle. Therefore, a better understanding of MEJ's physiological functions allows new insights into regulation of vessel function. Up to now, little is known, however, about the regulation for MEJ formation.

The 5'-adenosine monophosphate-activated protein kinase (AMPK) is not only one of the most important enzymes controlling cell catabolic metabolism, but has been shown to influence vascular tone, thereby augmenting blood and oxygen supply as required for catabolic pathways. It has not yet been studied, however, whether AMPK could also affect MEJ. Thus, the aim of this project was to elucidate the impact of AMPK on MEJ dynamics and its potential mechanism of action.

We studied isolated small mesenteric and skeletal muscle resistance arteries of mice using a pressure myograph system developed in our laboratory. Using confocal and two photon excitation fluorescence microscopy we identified the internal elastic lamina, which in these vessels exhibits small holes that allow direct contact between endothelial and smooth muscle cells. On average, we found that in about 35% of the holes, structures with a bright actin core as assessed by using F-actin fluorescence in LifeAct mice or by staining with phalloidin which we could define as sites of MEJ. These structures showed expression of Cx37 and Cx43 suggesting that MEGJs were also localized in these structures. We found that endoplasmic reticulum (ER) was enriched around MEJs which is consistent with MEJs acting as active signaling domains. Over observation time of up to 2 hours, we found that the number and localization of these MEJ varied, while they always showed expression in the area of

holes of IEL only. Thus, for the first time we could investigate MEJ dynamics. AMPK negatively regulates MEJ expression, since in AMPK α1, but not in α2 knockout (KO) mice, the number of MEJ was significantly increased. In accordance, in wild type mice, incubation with the AMPK inhibitory compound C (CC) significantly augmented the number of MEJ while the AMPK stimulator A76 did not further decrease them during the observation time. Furthermore, we found that the KO of AMPK α1, in intact mice as well as in cultured human and porcine smooth muscle cells, went along with an increase in PAI-1 expression. Accordingly, incubation of arteries with exogenous PAI-1 also increased the number of MEJ. The negative effect of AMPK on PAI-1 could be explained by enhanced expression of the silencer of the PAI-1 gene, small heterodimer partner (SHP). PAI-1 expression in arteries from AMPK α2 KO mice was unchanged compared to arteries from WT mice.

Since MEJ are also involved in EDH, we studied whether the expression of MEJ correlated with EDH induced vasodilation. The higher amount of MEJs in α1 KO mice went indeed along with a left shift of acetylcholine (ACh) -induced dilation dose effect curve.

In summary, this work describes for the first time a role of AMPK as a potent modulator of MEJ dynamics. This effect is selectively mediated by the α1 subunit of AMPK which is probably mediated by controlling PAI-1 expression. Our data also for the first time demonstrate a dynamic regulation of MEJ expression in intact blood vessels. Since MEJ represent a gateway for the communication between EC and VSMC and are involved in EDH, our observations may point towards a new target with therapeutic potential in small resistance vessels.

Zusammenfassung:

Die Zell-zu-Zell-Kommunikation spielt in multizellulären Geweben eine wichtige Rolle. Diese Kommunikation ist auch bei der Modulation der Gefäßfunktion, wie beispielsweise bei der Regulierung des Gefäßtonus von großer Bedeutung. Myoendotheliale gap junctions (MEGJs) ermöglichen eine heterozelluläre Kommunikation zwischen Endothelzellen (EC) und glatten Gefäßmuskelzellen (VSMC). Sie sind in myoendothelialen Junctions (MEJ) lokalisiert. MEJ stellen darüber hinaus eine Signalmikrodomäne dar, die für die Lokalisierung, Konzentration und Organisation von Zellsignalen und die Regulierung verschiedener vaskulärer Prozesse von entscheidender Bedeutung ist. Dazu gehört auch die endothel-abhängige Hyperpolarisation (EDH) der Gefäßmuskulatur welche eine Gefäßerweiterung auslöst. Ein besseres Verständnis der Dynamik der MEJ kann daher neue Einsichten in die Regulation von Gefäßfunktionen vermitteln.

Die 5'-Adenosinmonophosphat-aktivierte Proteinkinase (AMPK) ist nicht nur eines der wichtigsten Enzyme für die Kontrolle der Zellmetabolismus sondern spielt auch eine wesentliche Rolle bei der Kontrolle des Gefäßtonus. Die Enzymaktivierung führt zu einer Vasodilatation welche die Blut- und Sauerstoffversorgung der Gewebe verbessert. Es wurde jedoch bisher noch nicht untersucht, ob AMPK auch die Bildung von MEJ beeinflusst. Daher war es das Ziel dieses Projekts, den Einfluss von AMPK auf die MEJ-Dynamik und potentielle Mechanismen, die diesem Einfluss zu Grunde liegen, aufzuklären.

Unsere Untersuchungen führten wir in kleinen Widerstandsarterien durch, welche aus der Skeletmuskulatur bzw. dem Mesenterium von Mäusen frisch isoliert wurden. Unter Verwendung von konfokaler und 2-Photonen Mikroskopie konnten wir in diesen Gefäßen die Lamina Elastica Interna (IEL) darstellen, welche Endothel- und Gefäßmuskelzellen voneinander trennt, aber zahlreiche Löcher aufweist. Nur in diesen Bereichen ist ein direkter Kontakt zwischen Endothel und Gefäßmuskelzellen möglich. Bei genauer Analyse fanden wir heraus, dass in etwa 35% der Löcher Strukturen sichtbar waren, welche gleichermaßen von Gefäßmuskulatur und Endothel ausgingen und sich durch ein sehr deutliches F-Aktin Fluoreszenz-Signal auszeichneten (LifeAct oder Phalloidin Staining) und die wir als myoendotheliale Junctions (MEJ) definieren konnten. In diesen Strukturen ließen sich auch die Connexine Cx37 und Cx43 nachweisen, was auf das Vorhandensein von

myoendothelialen Gap Junctions in diesen Bereichen hinwies. Im Bereich der MEJ war ebenfalls endoplasmatisches Retikulum nachzuweisen, was zusätzlich darauf hinwies, dass es sich um eine signalaktive Domäne handelte. Während Beobachtungszeiten von bis zu 2 Stunden variierte die Zahl und Lokalisation der MEJ, war jedoch stets nur im Bereich von Löchern der LEI nachzuweisen. Damit war es zum ersten Mal möglich, die Dynamik von MEJ zu untersuchen. Die Untersuchungen identifizierten AMPK als negativen Regulator der MEJ. In AMPKα1 KO Mäusen war die Zahl der MEJ signifikant erhöht, während in AMPKα2 KO Mäusen keine Veränderungen gegenüber Wildtyp Kontrollen nachweisbar waren. In Übereinstimmung mit diesen Beobachtungen nahm die Zahl der MEJ auch nach akuter Gabe des AMPK Inhibitors Compound C signifikant zu, während es unter pharmakologischer Stimulation der AMPK zu keiner weiteren Abnahme kam. Der Knockout von AMPKα1 in isolierten Gefäßen bzw. auch in kultivierten Gefäßmuskelzellen (mittels siRNA) ging mit einer signifikanten Zunahme der Expression von Plasminaktivator Inhibitor 1 (PAI-1) einher. Die akute Gabe von PAI-1 führte ebenfalls zu einer Zunahme von MEJ. Der negative Effekt von AMPK auf die PAI-1 Expression war möglicherweise über eine Hemmung der PAI-1 Genexpression durch SHP (small heterodimer partner) verursacht, da SHP in AMPK KO vermindert exprimiert war.

Da die EDH über MEJ vermittelt wird, untersuchten wir auch, ob eine gesteigerte Zahl von MEJ mit einer verstärkten EDH einhergeht. In der Tat war die durch Acetylcholin ausgelöste und durch EDH vermittelte Gefäßdilatation in Gefäßen von AMPKα1 KO Mäusen signifikant verstärkt.

Zusammenfassend beschreibt diese Arbeit erstmalig eine Dynamik der MEJ in intakten kleinen Blutgefäßen. Sie zeigt aber auch eine Rolle von AMPK bei der Kontrolle der MEJ Expression, welche vermutlich über PAI-1 vermittelt wird. Da MEJ eine zentrale Schnittstelle zwischen Endothel und Gefäßmuskel, u. a. für die EDH, darstellen, tragen unsere Untersuchungen dazu bei, MEJ und AMPK als mögliche Angriffspunkte für die therapeutische Beeinflussung der Gefäßfunktion in den Blick zu nehmen.

List of Abbreviations:

ACC:	**Acetyl-CoA carboxylase**
ACh:	**Acetylcholine**
AMPK:	**AMP-activated protein kinase**
AMP:	**Adenosine monophosphate**
ADP:	**Adenosine diphosphate**
ADP:	**Adenosine triphosphate**
AICAR:	**5-aminoimidazole-4-carboxamide ribonucleoside**
AID:	**Auto-inhibitory domain**
AEBSF:	**4-(2-Aminoethyl) benzenesulfonyl fluoride hydrochloride**
A76:	**A769662**
BD:	**Binding domain**
BKca:	**Large conductance calcium-activated potassium channel**
BSA:	**Bovine serum albumin**
CaMKKb:	**Calcium/calmodulin-dependent protein kinase kinase**
CBS:	**Cystathionine β synthase**
CC:	**Compound C, dorsomorphin**
CTD:	**C-terminal domain**
CVD:	**Cardiovascular disease**
Ca^{2+}:	**Calcium**
Cx:	**Connexin**
DRC:	**Dose response curve**
DNA:	**Deoxyribonucleic acid**
DMSO:	**Dimethyl sulfoxide**
DRP-1:	**Dynamin-related protein 1**
EEL:	**External elastic lamina**
EC:	**Endothelial cell**
EDH:	**Endothelium-dependent hyperpolarization**
EDHF:	**Endothelium-derived hyperpolarizing factor**

EDTA: **Ethylenediaminetetraacetic acid**

eNOS: **Endothelial nitric oxide synthase**

ER: **Endoplasmic Reticulum**

FRAP: **Fluorescence recovery after photobleaching**

F Actin: **Filamentous actin**

G Actin: **Globular actin**

GAPDH: **Glyceraldehyde-3-phosphate dehydrogenase**

GJ: **Gap junction**

GBD: **Glycogen binding domain**

GFP: **Green fluorescent protein**

GTPCH1: **GTP cyclohydrolaseI**

HRP: **Horseradish peroxidase**

HUVEC: **Human umbilical vein endothelial cell**

HUVSMC: **Human umbilical vein smooth muscle cell**

IEL: **Internal elastic lamina**

IL: **Interleukin**

INDO: **Indomethacin**

KD: **Kinase domain**

KO: **Knockout**

LKB1: **Liver kinase B1**

L-NAME: **Nω-Nitro-L-Arginine Methyl-Ester-Hydrochloride**

M: **Muscarinic receptor**

MA: **Mesenteric Artery**

MDD: **Major Depressive Disorder**

MEJ: **Myoendothelial junction**

MEGJ: **Myoendothelial gap junction**

mM: **mmol/L (Millimoles per liter)**

µM: **µmol/L(Micromoles per liter)**

mmHg: **Millimetre(s) of mercury**

min: Minute

MMP: Matrix metallopeptidase

MOPS: 3-morpholinopropanesulfone

NAFLD: Non-alcoholic fatty liver

NE: Norepinephrine

NO: Nitric oxide

NOS: Nitric oxide synthase

nM: Nanomole per liter

PAI-1: Plasminogen activator inhibitor-1

PBS+: Phosphate-buffered saline with divalent cations

PCR: Polymerase Chain Reaction

PCASMC: Porcine coronary artery smooth muscle cells

PFK2: 6-phosphofructo-2-kinase

PGC-1α: Proliferator-activated receptor-gamma coactivator 1α

PGI: Prostacyclin

PLN: Phospholamban

PR: Podosome

PT1: 2-Chloro-5-[[5-[[5-(4,5-Dimethyl-2-nitrophenyl)-2-furanyl] methylene]-4,5-dihydro-4-oxo-2-thiazolyl] amino]benzoic acid

PVDF: Polyvinylidene fluoride

RPM: Revolutions per minute

ROI: Regions of interest

RIMs: Regulatory subunit interacting motifs

ROS: Reactive oxygen species

siRNA: Small interfering RNA

SDS: Sodium dodecyl sulphate

SDS-PAGE: Sodium dodecyl sulphate polyacrylamide gel electrophoresis

SECRA: Sarco/endoplasmic reticulum Ca^{2+} ATPase

SHP: **Small heterodimer partner**

SEM: **Standard error of the mean**

TBST buffer: Tris-buffered saline with Tween 20 buffer

TNFα: **Tumour necrosis factor α**

t-PA: **Tissue-type plasminogen activator**

TEM: **Transmission electron microscopy**

TNT: **Tunnelling nanotube**

u-PA: **Urokinase-type plasminogen activator**

VSMC: **Vascular smooth muscle cell**

VCCC: **Vascular cells co-culture**

v/v: **Volume / Volume**

WB: **Western Blot**

WT: **Wildtype**

w/v: **Weight / volume**

α: **alpha**

β: **beta**

γ: **gamma**

1. Introduction:

1.1. Cell–Cell Communication

Cell-to-cell communication is essential for biological processes such as differentiation, development and for maintaining normal function in multicellular organisms (Bloemendal & Kück 2013). Communication happens both in homotypic and heterotypic cells. The communication can be divided into two types according to the distance between cells: distant and local communication (Ha et al. 2016). The distant communication occurs through hormones, such as insulin which is secreted from pancreas, and reaches their target cells via the blood stream. By distant communication, various types of cells and organs in whole body expressing the respective receptor can be regulated (Röder et al. 2016). Recently, a novel distant intercellular communication via exosomes has been reported (Kowal et al. 2016). Exosomes are membrane vesicles which contain various contents, among them including proteins and RNAs. They can reach their target cells via the blood stream or other biological fluids. After contact with the target cells they release their constituents (Junyan Xu et al. 2017). The local communication include short range diffusion of transmitters and paracrine factors (indirect contact) such as synaptic transmission, and the direct intercellular exchange of (signal) molecules or electric signals via gap junctions (GJ) or tunneling nanotubes (TNT) (Ha et al. 2016; Nawaz et al. 2017; Rustom et al. 2014; Abounit & Zurzolo 2012). GJs are present in a wide variety of cells and play pivotal roles in a variety of biological processes, like development, differentiation, neural activity, immune response and vascular tone (Maeda & Tsukihara 2011; Zhang & Ducsay 2014). GJs were discovered more than 50 years ago (Revel & Karnovsky 1967). With ongoing research, it became evident that GJs are channels which allow the exchange of small molecules and current between adjacent cells. An intercellular GJ channel is comprised of two connexons formed with six connexin monomers in hexagonal configuration (Yeager & Harris 2007) being located in the corresponding membrane sites of two adjacent cells. There are 21 different connexins in humans, of which the connexins 37, 40, 43 and 45 are verified to be present in vascular cells (Isakson & Duling 2005; Heberlein et al. 2009).

Cell-cell communication also plays a pivotal role in the regulation of blood vessel function (Figueroa & Duling 2009). The vascular system principally consists of

arteries, veins and capillaries. Normally, the resistance arteries and arterioles are responsible for controlling the magnitude and the distribution of organ blood flow (Jacob et al. 2016). The arterial wall can be subdivided into tunica adventitia, media and intima, which are separated by external elastic lamina (EEL) and internal elastic lamina (IEL) respectively (Dora 2001; Welsh & Taylor 2012). The adventitia is mostly composed of connective tissue, fibroblasts and the nerves; the media is mostly composed of vascular smooth muscle cell (VSMC) and the intima is composed of a monolayer of endothelial cells (EC) (Tennant & Mcgeachie 1990). According to the structure of wall, there are homocellular and heterocellular communications in the blood vessel. The homocellular communications mainly include the VSMC-VSMC and EC-EC communications. These communications play an important role in the cell synchronization and coordination of a vessel (Schmidt et al. 2008). The heterocellular communications not only include nerve-EC and nerve-VSMC communications (Dora 2001) but**,** in addition, heterocellular communications between EC and VSMC are named as the myoendothelial junctions (MEJs) (Sandow & Hill 2000b). MEJs not only exists myoendothelial gap junctions (MEGJs) pathway for the communication between EC and VSMC, but also represent a signaling microdomain critical for localizing, concentrating, and organizing cell-signaling components and regulating various vascular biological processes such as endothelium dependent hyperpolarization (EDH) of VSMC in resistance arteries and arterioles (Sandow et al. 2002).

1.2. Myoendothelial junction (MEJ) in the vasculature

Myoendothelial junctions (MEJs) are the regions where VSMCs and ECs get in close contact to each other through the fenestrations of IEL via their projections (Straub et al. 2014). In these areas also myoendothelial gap junctions (MEGJ) can be formed. MEJs were first found sixty years ago at the ultrastructure level in a transmission electron microscopy (TEM) study on small canine arteries (Moore & Ruska 1957). Fifty years ago, its high resolution images were obtained from rabbit kidney arterioles, and MEJs were proposed to serve as channels for communications between ECs and VSMCs (Rhodin 1967). Nearly twenty years ago, an exquisite three dimensional reconstruction of MEJ was performed from TEM sections which confirmed again that MEJ exists between EC and VSMC (Sandow & Hill 2000b). With regard to the morphology of the cellular processes, MEJs can be divided into three

different types: first, VSMC protrusions contact with EC through the IEL; second, EC protrusions contact with VSMC through IEL; third, VSMC and EC protrusions contact halfway between each other cell in the IEL (Michel et al. 1995). The shape of MEJ are club-like or flat appositions, about 0.5 µm in width by 0.5 µm in depth (Straub et al. 2014). The different shapes may relate to different specific functions or developmental stages of MEJs (Heberlein et al. 2009). On a subcellular basis, it has been found that endoplasmic reticulum (ER), cytoskeletal components, caveolae, IP3-R1 and some ion channels such as $K_{Ca}2.3$ channel, $K_{Ca}3.1$ channel are enriched in MEJs (Dora et al. 2009; Heberlein et al. 2009) together with gap junctions. Connexin 37, 40, 43 have been reported to be present in MEJ so far (Haddock et al. 2006; Isakson, A. K. Best, et al. 2008; Sandow et al. 2006). They can form gap junctions but also exert channel independent functions (Kameritsch et al. 2015). The structure of a MEJ is shown schematically in **(Figure 1).** The frequency of MEJs in vasculature is variable depending on the organs and species. The accepted tendency is that in the adult state MEJs do not exist in aorta and large arteries, whereas in the microcirculation, MEJs are expressed and their number increases with decrease vessel diameter (Sandow et al. 2012).

In general, it is now widely accepted that the MEJs do not only allow for direct transfer of substances between EC and VSMC through gap junctions located in this area (Straub et al. 2014), but also represent a signaling microdomain critical for localizing, concentrating, and organizing cell-signaling components and regulating various vascular biological processes (Heberlein et al. 2009). The nitric oxide (NO) generating enzyme endothelial nitric oxide synthase (eNOS), which is an important factor regulating the vascular tone and for preventing proliferation of VSMC, exists in close apposition to MEJ (Straub et al. 2011; Straub et al. 2012). MEJs can also specifically enable control of the abluminal pool of eNOS in EC (Biwer et al. 2016). Endothelium-dependent hyperpolarization (EDH) is another of the three important endothelial dilator mechanisms, and the MEJ has been shown to be essentially involved in EDH of VSM (Sandow & Hill 2000a; Sandow et al. 2002). Moreover, our group reported that MEGJs regulate the bidirectional Ca^{2+}-signal propagation between EC and VSMC (Pogoda et al. 2014). MEGJs also join in the regulation of coronary VMSC differentiation by shear stress (Zhang et al. 2016). The transfer of VSMC from contractile to synthetic phenotype plays a pivotal role in intimal

hyperplasia of vessels in atherosclerosis. As a consequence, MEJs dysfunction might be involved in arteriosclerosis (Zhang et al. 2016).

MEGJs are very dynamic with regard to their permeability as well as their expression in the membrane. The regulation of gap junction permeability occurs via posttranslational modification of the cytosolic parts of the connexins, in particular, the C-terminus. (Segal & Bagher 2010). For example, our group has shown that NO can reduce the calcium signal exchange via MEJ via tyrosine de-phosphorylation of connexin37 (Cx37) at position 332 (Pogoda et al. 2017).

In contrast, our knowledge about which factors influence the formation and regression of MEJ which are required for formation of MEJ are still limited. However, one of the regulators in the coagulation system, the plasminogen activator inhibitor-1 (PAI-1) has been reported to play an important role on MEJ formation (Segal & Bagher 2010; Heberlein et al. 2010). To study the role of MEJ, mostly cell co-culture models have been used (Wallace et al. 2007). TEM was used in intact arteries (Heberlein et al. 2010). These approaches do, however, allow neither to study the dynamics of the MEJ in living tissue *in situ* nor the consequences on the regulation of vascular tone.

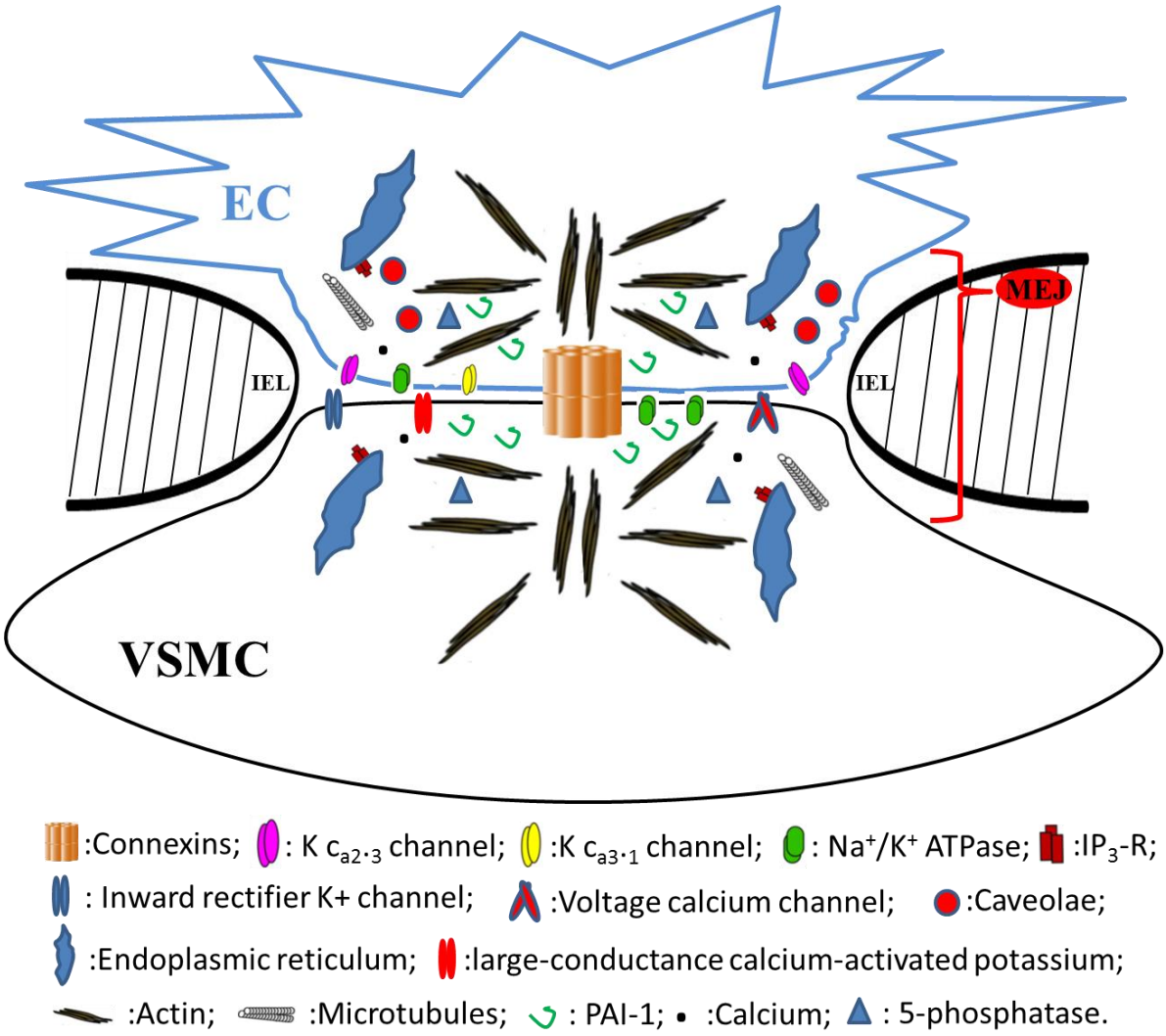

Figure 1. Schematic structure of MEJ.

A MEJ is formed by protrusions of EC and VSM in a hole of the IEL. In this functional domain many channels and subcellular structures are located. For more details, see text.

1.3. Plasminogen activator inhibitor-1

Plasminogen activator inhibitor-1 (PAI-1) is a serine protease inhibitor. It is a glycoprotein and was discovered more than 30 years ago (Pannekoek et al. 1986). Many cell types can synthesize PAI-1, among them are VSMC, EC, hepatocytes and some other mesenchymal cells (Dimova & Kietzmann 2008). Platelets can also synthesize PAI-1, and they can store it in alpha granules (Brogren et al. 2004; Erickson et al. 1984). PAI-1 exists in three states: active, latent and inactive (Lindahl et al. 1989). Normally, PAI-1 is secreted in the active state and will be converted into the inactive state with a half life time of about 1-2 hours at 37 °C (Lindahl et al. 1989). The important function of PAI-1 is to serve as an inhibitor of urokinase-type

plasminogen activator (u-PA) and tissue-type plasminogen activator (t-PA), thereby modulating the balance between blood coagulation and the fibrinolytic process (Rijken & Lijnen 2009). However, additional functions of PAI-1 are being unveiled. Recently, the influence of PAI-1 on MEJ dynamics has also been described (Segal & Bagher 2010; Heberlein et al. 2010)

With regard to blood vessels, PAI-1 has so far been found to play a role mainly under pathophysiologic conditions. PAI-1 is involved in many vascular diseases, such as atherosclerosis, neointima hyperplasia (Zhu et al. 2001; Deyoung et al. 2001) and restenosis (Prisco et al. 2001), via its influence on VSMC migration, detachment and adhesion. High level of PAI-1 represents also an independent factor for predicting development of type 2 diabetes mellitus (DM) (Festa et al. 2002), which is positively linked to development of cardiovascular disease (CVD).

As PAI-1 seems to be a crucial factor for CVD, DM and some others diseases, the research activities regarding its regulation are increasing. The regulation of PAI-1 synthesis can occur at both, the transcriptional and the post-transcriptional level (Agirbasli 2005). Inflammation seems to be a potent stimulator of PAI-1 production. For example, interleukin-1(IL-1) (Emeis & Kooistra 1986) and tumor necrosis factor-α (TNF-α) (Sawdey et al. 1989) can stimulate cultured EC to increase PAI-1 expression, and hypoxia is also a stimulator for increasing PAI-1 synthesis in EC (Gerber et al. 1993)**.** Moreover, high glucose level can enhance PAI-1 gene expression by activation of PAI-1 promoter via Sp1 site (Chen et al. 1998). Recently, some studies have shown that 5'-adenosine monophosphate-activated protein kinase (AMPK) may play a role in regulating PAI-1 expression. Metformin, a potential AMPK activator can inhibit PAI-1 expression in the liver (Bergheim et al. 2009). Likewise, another AMPK stimulator, adiponectin, can reduce PAI-1. This occurs via activation of AMPK in 3T3-L1 Cells (Komiya et al. 2014) and via an influence of AMPK on the NFkB pathway in human umbilical vein endothelial cells (HUVEC) (Chen et al. 2017)**.** With regard to a potential signaling pathway, fenofibrate can downregulate PAI-1 gene expression via AMPK-orphan nuclear receptor small heterodimer partner (SHP) pathway in hepatocytes (Chanda et al. 2009). An upregulation of SHP by AMPK has also been reported for its classic activator metformin in hepatocytes (Kim et al. 2012). SHP is an important repressor of many genes (Seol et al. 1996). Thus, AMPK may play an important role on the regulation of PAI-1 expression. It is, however, still

unknown whether and how AMPK affects PAI-1 production and release in vascular cells.

1.4. 5’-adenosine monophosphate-activated protein kinase

The virtually ubiquitously expressed 5’-adenosine monophosphate-activated protein kinase (AMPK) is one of the most important enzymes for the metabolism of many cells like hepatocytes and skeletal muscle cells (Hardie & Ashford 2014; I. Salt & Hardie 2017). In 1973, Carlson and colleagues discovered a novel kinase being able to phosphorylate acetyl-CoA carboxylase (ACC) and inhibit its function (Carlson & Kim 1973). Carling et al. discovered later that the enzyme can be activated by 5’-adenosine monophosphate (AMP) which led to its denomination as AMPK (Carling et al. 1989). AMPK is a serine/threonine kinase in nearly all eukaryotes (Steinberg & Kemp 2009a; Hardie & Ashford 2014) serving as an energy sensor involved in signaling pathways of anabolism and catabolism (D. Grahame Hardie et al. 2012; Carling et al. 2012; Russo et al. 2013).

AMPK is a heterotrimeric enzyme which is composed of a catalytic alpha (α) subunit and two regulatory subunits: beta (β) and gamma (γ) (Steinberg & Kemp 2009a; Hardie & Ashford 2014). Each of these subunits has several isoforms. According to the literature, α-subunit exists in two isoforms: α1 and α2; the β-subunit also has two isoforms (β1 and β2) and there exists three isoforms of the γ-subunit (γ1, γ2 and γ3). In mammals, PRKAA1 and PRKAA2 genes encode α1 and α2; PRKAB1 and PRKAB2 genes encode β1 and β2; PRKAG1, PRKAG2 and PRKAG3 genes encode γ1, γ2 and γ3 respectively (Hardie 2015)**.** The isoforms of each subunits can assemble in different combinations to generate 12 different potential AMPK complexes (Fiona A. Ross et al. 2016). The isoforms show different expression in species and tissues which may have specific roles in cellular metabolic processes (Steinberg & Kemp 2009b).

An AMPK activation is considered to be reflected by the phosphorylation of threonine residue (Thr-172) in the α kinase domain (S. A. Hawley et al. 1996) and can further be confirmed by phosphorylation of its classic substrate ACC. There are two major upstream kinases: liver kinase B1 (LKB1) (Shaw et al. 2004; Woods et al. 2003) and calcium/calmodulin-dependent protein kinase kinase (CaMKKβ) (Hawley et al. 2005; Woods et al. 2005; Hurley et al. 2005), which catalyze the phosphorylation of Thr-172

in AMPK α-kinase domain. Enhanced energy consumption, such as it occurs under exercise, or energy depletion like under conditions of glucose deprivation or hypoxia, lead to activation of AMPK due to the increase in the ratio of AMP/ATP or ADP/ATP (Evans et al. 2016; D Grahame Hardie et al. 2012). AMP binding to γ-subunit of AMPK can activate it by three potent mechanisms: (1) by promoting the Thr172 phosphorylation which is catalyzed by LKB1; (2) by allosteric activation; (3) by inhibiting the dephosphorylation of Thr172 by phosphatases (Sakamoto et al. 2004). All of them can be inhibited by ATP (Gowans et al. 2013; Fiona A Ross et al. 2016). AMPK can also be activated by some hormones, such as adiponectin (Bang et al. 2017), urocortin2 (Li et al. 2013) and ciliary neurotrophic factor (Watt et al. 2008). At the same time, some pharmacological agents are commonly applied to activate AMPK in cells or *in vivo* research. These agents are divided into five classes (I. Salt & Hardie 2017). Class Ⅰ is the mitochondrial inhibitor such as metformin and berberine. Class Ⅱ is glycolytic inhibitor such as 2-Deoxyglucose. Both of these agents activate AMPK by increasing AMP level (Hawley et al. 2010). Class Ⅲ is one type of nucleoside which can be converted to equivalent nucleotide when it is taken up by the cells, such as compound 5-aminoimidazole-4-carboxamide ribonucleotide (AICAR), and mimicking the AMP function (Corton et al. 1995). Class Ⅳ can be converted into AMP analog C2 and activating AMPK (Gomez-Galeno et al. 2010). Class Ⅴ includes compounds which can bind with N-lobe on the α sub-unit and β-CBM of AMPK, then inducing its allosteric change and activation, such as A769662 (A76) through β-subunit and 2-Chloro-5-[[5-[[5-(4,5-Dimethyl-2-nitrophenyl)-2-furanyl] methylene]-4,5-dihydro-4-oxo-2-thiazolyl]amino] benzoic acid (PT1) through α-subunit (Xiao et al. 2013; Pang et al. 2008). Compared to so many specific pharmacological activators of AMPK, there is still not specific inhibitor available. However, dorsomorphin (compound C, CC) is considered to act as relatively specific inhibitor of AMPK in research studies (Bain et al. 2007).

AMPK is considered as a cellular energy sensor, inhibiting anabolic pathways and promoting catabolic pathways of cell metabolism (Hardie & Ashford 2014). Its activation is involved in the regulation of carbohydrate homeostasis, lipid metabolism, protein metabolism, mitochondrial biogenesis, feeding and body weight (Angin et al. 2016). Therefore, there are substantial research activities focusing on AMPK function

in liver (Smith et al. 2016; M. Zhang et al. 2017) and skeletal muscle (Angin et al. 2016; Koh 2016). At the same time, AMPK has also shown to play important roles in some blood cells as well as in the cardiovascular system (I. Salt & Hardie 2017; Daskalopoulos et al. 2016). In human and murine organisms, AMPK α1 plays an important role in platelet aggregation via VASP, cofilin and cytoskeletal reorganization (Onselaer et al. 2014). AMPK α2 shows a key role in platelet αIIbβ3 integrin signaling via affecting Fyn activity which can lead to clot retraction and thrombus stability (Randriamboavonjy et al. 2010). AMPK is present in neutrophils and can regulate NADPH oxidase activity in human (Alba et al. 2004). In heart, AMPK can be activated by no-flow ischemia in perfused rat hearts and increase of heart workload (Kudo et al. 1995; Coven et al. 2003). AMPK can also promote anaerobic metabolism and the uptake of glucose by two core enzymes: phosphorylating Akt and 6-phosphofructo-2-kinase (PFK2) (Fukuda 2011). It also shows the function on the long regulation of cardiac energetic homeostasis via peroxisome proliferator-activated receptor-gamma coactivator 1α (PGC-1α) (Patten & Arany 2012) and forkhead box O (FoxO) (Kubli & Gustafsson 2014).

With the ongoing research, AMPK's roles on regulation of vascular function have been elucidated step by step. AMPK-α1 is the major isoform and accounts for the majority of total AMPK activity in EC and VSMC (Stahmann et al. 2010; Francoise Goirand et al. 2007). AMPK regulates endothelial nitric oxide (NO) via several different mechanisms: (1) increasing the activity of eNOS by phosphorylation at its Ser633 and Ser1177 (Chen et al. 1999); (2) increasing eNOS association with Hsp90 (Fujimura et al. 2012); (3) increasing tetrahydrobiopterin (BH4) concentrations via GTP cyclohydrolaseI (GTPCH1) (An et al. 2016); and then inducing VSMC relaxation, but inhibiting VSMC proliferation and migration, platelet aggregation, leukocyte adhesion and proinflammatory signaling (Siragusa et al. 2016). The anti-inflammatory effects of AMPK in VSMCs and ECs have also been reported. AMPK activation can inhibit NFκB activity which is stimulated by TNFα (Cacicedo et al. 2004) and by IL-6-stimulated Janus kinase-STAT signaling in EC (Rutherford et al. 2016). As in VSMCs, AMPK activation inhibits NFκB activity and secretion of IL-6 (He et al. 2015).

AMPK activation has also been reported to show a regulatory function on vasodilation in different types of arteries (from small artery to aorta) and various

species' vascular beds (Rubin et al. 2005; F Goirand et al. 2007; E. A. Bradley et al. 2010; Ford & Rush 2011; Ford et al. 2012). Accordingly, treatment with unspecific AMPK activators has been shown to reduce arterial blood pressure *in vivo* (Buhl et al. 2002; Ford et al. 2012). Our group found by using a pressure myograph system (isolated intact arteries under pressure) that AMPK activation modulates intracellular calcium homeostasis immediately by large conductance calcium-activated potassium (BKca) channel and sarco/endoplasmic reticulum Ca^{2+} ATPase (SERCA) (Holger. Schneider et al. 2015). And recently, we also uncovered that AMPK activation dilates resistance artery by a novel, Ca^{2+}-independent pathway via the regulation of the G and F actin filament dynamics (Schubert et al. 2017). These results suggested that AMPK stimulators may not only act as potent anti-diabetic drugs (Gruzman et al. 2009; Hardie 2013) but also as efficient drugs to treat vascular disease, particularly in states with metabolic syndrome (Holger Schneider et al. 2015). The existing literature suggests, that the communications between EC and VSMC, via MEJs, can also play an important role in modulating blood pressure as well as control of vascular tone. However, little is known about the role of AMPK in MEJ and its impact in regulating the vessel tone.

1.5. Hypotheses and aim of the Study

MEJs are close appositions between EC and VSMC which enable fast and direct communication between them, partly via MEGJ (Straub et al. 2014). MEJs have also been described as micro-signaling domains critically regulating calcium handling between EC and VSMC and thus, contractility of resistance arteries (Sandow et al. 2002; Tran et al. 2012). Although some studies offer regulatory pathways on how MEJ assemble (Heberlein et al. 2010; Heberlein et al. 2012), little is known about the dynamics and regulation of MEJ formation (Straub et al. 2014), in particular in intact arteries. Since resistance arteries are the main vessels regulating blood supply to match metabolic demands of the tissues (Sarelius & Pohl 2010). The aims and hypotheses of this project are following:

1st aim to develop a method to identify MEJs in intact arteries and to get quantitative information about their expression and to correlate it with vascular function.

2nd aim to test the hypothesis that MEJ formation may be controlled by AMPK.

3rd aim to test the hypothesis that AMPK may do so by regulating the expression of PAI-1

Consequently, in this study we try to elucidate the role of the AMPK on MEJ formation and function in resistance artery tone, and its potential molecular mechanisms.

2. Materials and Methods:

2.1. Buffer solutions and drugs

Buffer solutions used in this experimental study included (3-morpholinopropanesulfone acid)-buffered salt solution (MOPS) (manufactured by the pharmacy of the Munich University Hospital "Apotheke Klinikum der Universität München", Munich, Germany) (**Table 1**), phosphate-buffered saline with divalent cations buffer (PBS+) (manufactured by the pharmacy of the Munich University Hospital "Apotheke Klinikum der Universität München", Munich, Germany) (**Table 2**), radio immunoprecipitation assay buffer (RIPA buffer) (**Table 3**), sample lysis buffer (**Table 4**), loading buffer (**Table 5**), running buffer **(Table 6)**, washing buffer or Tris-buffered saline with Tween 20 (TBST) (**Table 7**), transfer buffer (**Table 8**), and blocking buffer which was 5 % bovine serum albumin (BSA) or non-fat milk in TBST. The other drugs or agents used in this study are listed in (**Table 9**).

Table 1. Detailed contents of MOPS buffer

Agents (Dissolved in distilled water)	Concentration (mM)
$CaCl_2 \times 2H_2O$	3.0
$MgSO_4 \times 7H_2O$	1.17
Glucose	5.0
$NaH_2PO_4 \times 1H_2O$	1.2
EDTA	0.02
MOPS	3.0
NaCl	145
KCl	4.7
Pyruvate	2.0

Table 2. Detailed contents of PBS+ buffer

Agents (Dissolved in distilled water)	Concentration (mM)
$MgSO_4 \times 7H_20$	0.3
$CaCl_2 \times 2H_2O$	0.9
$MgCl_2 \times 6H_2O$	0.3
$NaH_2PO_4 \times 1H_2O$	0.8
KH_2PO_4	0.4
$NaHCO_3$	3.6
KCl	5.4
NaCl	136.9
glucose	5.6

Table 3. Detailed contents of RIPA buffer

Agents (Dissolved in distilled water)	Concentration
NaCl	150 mM
Tris/HCl	50 mM
EDTA	5 mM
Na deoxycholate	0.5 % (w/v : g/100 ml)
SDS	0.1 % (w/v : g/100 ml)
Triton X-100	0.1 % (v/v)

Table 4. Detailed contents of sample lysis buffer

Agents (Dissolved in distilled water)	Concentration
Glycerol	20 % (v/v)
Tris/HCl	125 mM
SDS	4% (w/v: g/100 ml)

Table 5. Detailed contents of loading buffer

Agents (Dissolved in distilled water)	Concentration
SDS	4% (w/v: g/100 ml)
2-mercaptoethanol	10 % (v/v)
Glycerol	20 % (v/v)
Bromophenol blue	0.004 % (w/v: g/100 ml)
Tris-HCl	125 mM

Table 6. Detailed contents of loading buffer

Agents (Dissolved in distilled water)	Concentration
SDS	1% (w/v: g/100 ml)
Glycine	190 mM
Tris-HCl	25 mM

Table 7. Detailed contents of washing buffer (pH 7.6) (TBST buffer).

Agents (Dissolved in distilled water)	Concentration
NaCl	150 mM
Tris	20 mM
Tween 20	0.1 % (v/v)

Table 8. Detailed contents of transfer buffer.

Agents (Dissolved in distilled water)	Concentration
Methanol	20 % (v/v)
Tris	25 mM
Glycine	190 mM

Table 9. Drugs and chemicals used in the experiments

Drugs or Agents	Company
cheluminate-HRP PicoDetect solution A and B (A3417, 1200 A and B)	PanReac AppliChem (Gatersleben, Germany)
Non-fat dried milk powder (A0830,0500)	
Albumin fraction V(A1391, 0100)	
Antipain	
Bromophenol blue	
DMSO	
KCl	
MgSO4	
Na4P2O7	
NaCl	
SDS	
Tris	
KH_2PO_4	
$CaCl_2$	
EDTA	
Na_3VO_4	Alexis Corporation (Lausen, Switzerland)
Manganese (II) chloride tetrahydrate	Sigma Aldrich (Deisenhofen, Germany)
L-NAME(N5501)	
Indomethacine (17378)	
Acetycholine (Ach)	
Heptanol	
Meflumic acid	
Porcine smooth muscle cell growth medium (P311_500)	
NaOH	Merck Millipore (Billerica, MA, USA)
Ethanol	

NaF	
Norepinephine	Aventis Pharma (Frankfurt, Germany)
A769662	Tocris (Bristol, UK)
compound C	
Aprotinin (A162.1)	Carl Roth (Bavaria, Germany)
Leupeptin (CN33.1)	
Distilled water (Aqua ad iniectabilia)	B/BRAUN (Melsungen,Germany)
Endothelial cell growth medium	Promocell (Heidelberg, Germanz)

2.2. Probes and Antibodies

The probes and antibodies which were used in this experimental study are showed in the **(Table 10)**.

Table 10. Probes or antibodies

Probes and Antibodies	Company
Calcein Red-Orange-AM	Thermo Fisher Scientific (Waltham, MA, USA)
ER-Tracker™ Green (BODIPY® FL Glibenclamide)	
Glycine	
Phalloidin-Alexa546	
MPPSense645	PerkinElmer (Waltham, MA, USA)
Fura2-AM	LifeTechnologies (Carlsbad, CA, USA)
Active PAI-1	MolecularInnovations (Novi, USA)
anti-Cx37 antibody	A Diagnostics (San Antonio, USA)
anti-Cx43 antibody	
Anti-AMPKα1/2 antibody	Abcam (Cambridge, UK)
Anti-phospho-AMPKα1/2 antibody	Cell Signaling (Danvers, MA, USA)
Anti-phospho-ACC antibody	
Anti-SHP antibody(sc-271511)	Santa Cruz (Heidelberg, Germany)
Anti-PAI-1antibody(sc-9 5297)	

Anti-GAPDH antibody	Merck Millipore (Billerica, MA, USA)
KAPA mouse genotyping Kits	Sigma Aldrich (Deisenhofen, Germany)

2.3. Animals, isolation and cannulation of resistance-type arteries

All animal care and experimental protocols were conducted in accordance with German federal animal protection laws. C57BL6/N mice were purchased from Charles River Laboratories (Sulzfeld, Germany). LifeAct mice were kindly provided by Reinhard Fässler (MPI of Biochemistry, Martinsried). AMPKα-1 and α-2 knockout (KO) and their respective littermate wildtype (WT) mice were from the Jackson Laboratory (USA). The mice were killed by cervical dislocation, the mesentery or the legs of the mouse were removed and pinned onto a silicon-coated petri dish for subsequent vessel dissection (**Figure 2A** and **3A**). Fine dissection of mesenteric or muscle (saphenous) arteries was performed in ice-cold MOPS buffer. For mesenteric arteries, first order to fourth order branches of the superior mesenteric artery were dissected **(Figure 2B**). For muscle arteries, the whole saphenous artery was dissected **(Figure 3B**). Isolated arteries were then cannulated as described before (Steffen-Sebastian Bolz et al. 1999) (**Figure 4**).

Briefly, the glass pipettes (GB100F-10:0.58*1.00*100 mm, SCIENCE PRODUCTS GmbH) were pulled into two equally pointed cannula with a laser-based micropipette puller (P-2000, SUTTER INSTRUMENTS CO., Novato, USA), then they were fixed on the setups on both sides via a screw. Both cannulas were then connected to the three-way stopcock via a silicone tubing (TYGON® 3350, Pro Liquid). One cannula became the inlet; the other became the outlet of the vessel. The inlet was connected to a tube (original perfusor line) (B/Braun, Germany) stuck onto a 20 ml syringe (B/BRAUN, Germany) and filled with MOPS. Secondly, the proximal end of artery was mounted onto the inlet cannula and secured with the help of two knots made from 10-0 ethilon sutures (Georgia, USA). Then the lumen of artery was flushed with MOPS to remove the remaining blood. Afterwards, the distal end of the artery was mounted onto the outlet pipette by the way as mentioned above, followed by a test for leakage (leaving the artery first at 60 mmHg pressure and then closing both 3-way stopcocks whilst observing for possible collapse; then the stopcocks were opened again whilst watching out for any re-expansion of the vessel. Leaky arteries were

discarded. Lastly, the artery was stretched gently in axial direction at 60 mmHg transmural pressure until no more lateral buckling occurred.

When used for experiments with subsequent protein extraction, all mesenteric arteries were dissected and divided into equal parts as required by the number of experimental groups.

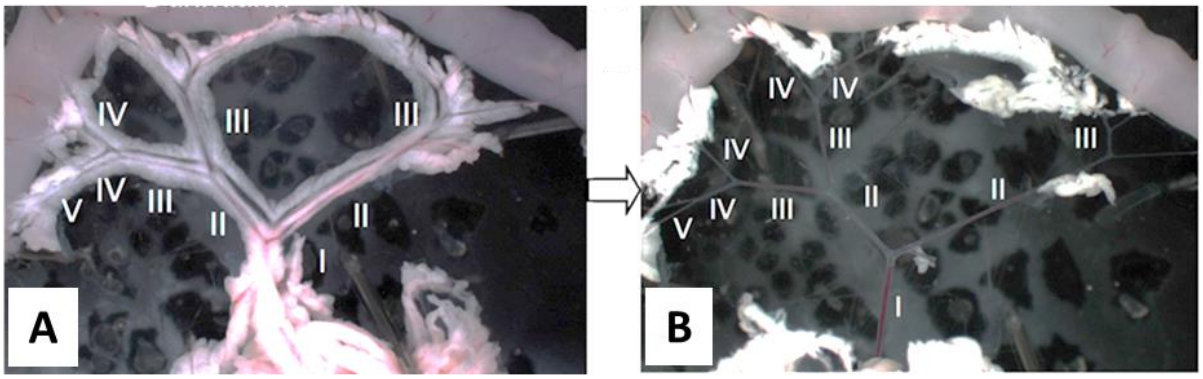

Figure 2. Preparation of mesenteric arteries.

In this image, the intestine was left *in situ* to clarify the anatomic relations to the supplying vessels. (A): The whole mesentery supplying the small intestine was dissected sharply from intestine, then it was pinned onto a silicon-coated petri dish with the fatty-tissue segments containing the vessels spread out in a the fan-like shape. (B): The adjacent vein, fatty and connective tissue were carefully removed until the desired order branch had been totally cleared. Vessels of first (I) to fourth (IV) order were used in experiments requiring protein extraction. Vessels of second (II) to third (III) order were used in the other experiments in this project. Subsequently, the arteries were transferred to an organ bath or a cell culture dish as outlined below.

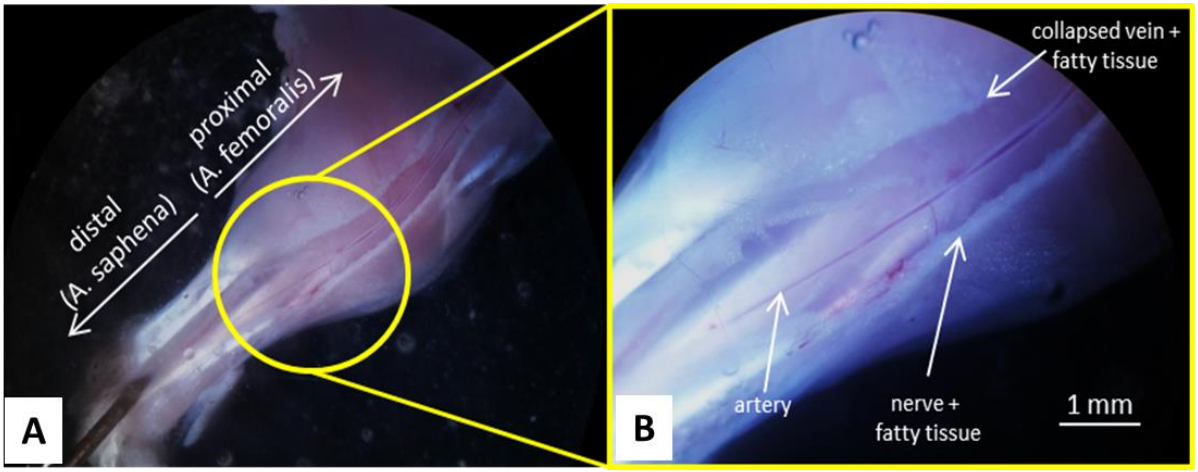

Figure 3. Preparation of saphenous artery.

For functional studies (Ach DRC), saphenous arteries with a maximal outer diameter of roughly 350 µm were prepared. **(A):** The skin was removed from the groin to the paws and the leg was then separated from the rest of the body. Afterwards, it was pinned onto a silicon-coated petri dish with cannulae. **(B)**: The adjacent vein, nerve as well as attached fatty and connective tissues were carefully removed by sharp dissection, and the isolated saphenous artery was transferred to an organ bath for subsequent experiments.

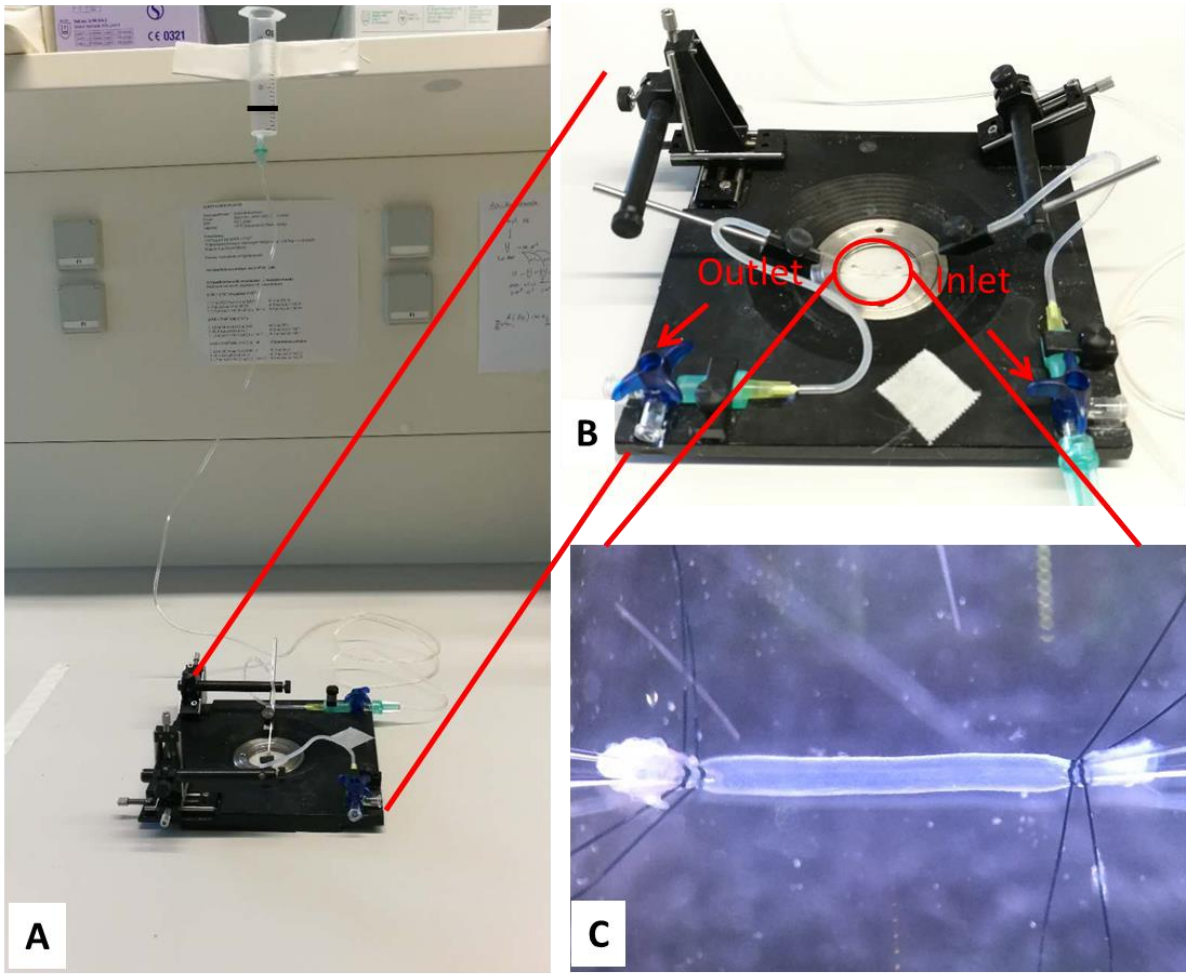

Figure 4. Pressure myograph system (Isobaric arteriography).

The freshly isolated vessel was fixed by 10-0 sutures to glass pipettes mounted on holders whose position could be controlled by micromanipulators. Firstly, artery was mounted on both sides and flushed free of blood with MOPS solution. Thereafter, the artery was stretched to in situ length and exposed to a hydrostatic pressure of 60 mmHg via the inlet whereas the outlet three-way stopcock remained closed. **(A):** Overview of the pressure myograph system. The inlet syringe with MOPS was fixed at a height corresponding to a hydrostatic pressure of 60 mmHg during the experiments. **(B):** The whole setup with the mounted artery. **(C):** Magnified image of the living artery at physiological pressure.

2.4. Recording of MEJ dynamics and live imaging.

Arteries from LifeAct-GFP mice were isolated, cannulated and pressurized at 60mmHg. Respective live-dyes were added to the cells via the intra-luminal route (infused through the silicone tubings, Calcein-AM red orange [1µM], Bodipy-Gibenclamide ER-Tracker [1 µM]) or via the abluminal route (Added to the organ chamber, Alexa633 [0.2 µM]). After thorough washing with PBS+, transmural image stacks as time-lapse recordings at the same area or for quantification purposes at different areas along the vessel length were obtained in the respective vessels using a Leica TCS SP5 confocal microscope (Leica Microsystems, Wetzlar, Germany) **(Figure 5)** or two photon excitation fluorescence microscope(Leica, Germany)**.** Images were analyzed in a blinded manner with Fiji ImageJ Software (ImageJ 1.x) (Schneider et al. 2012).

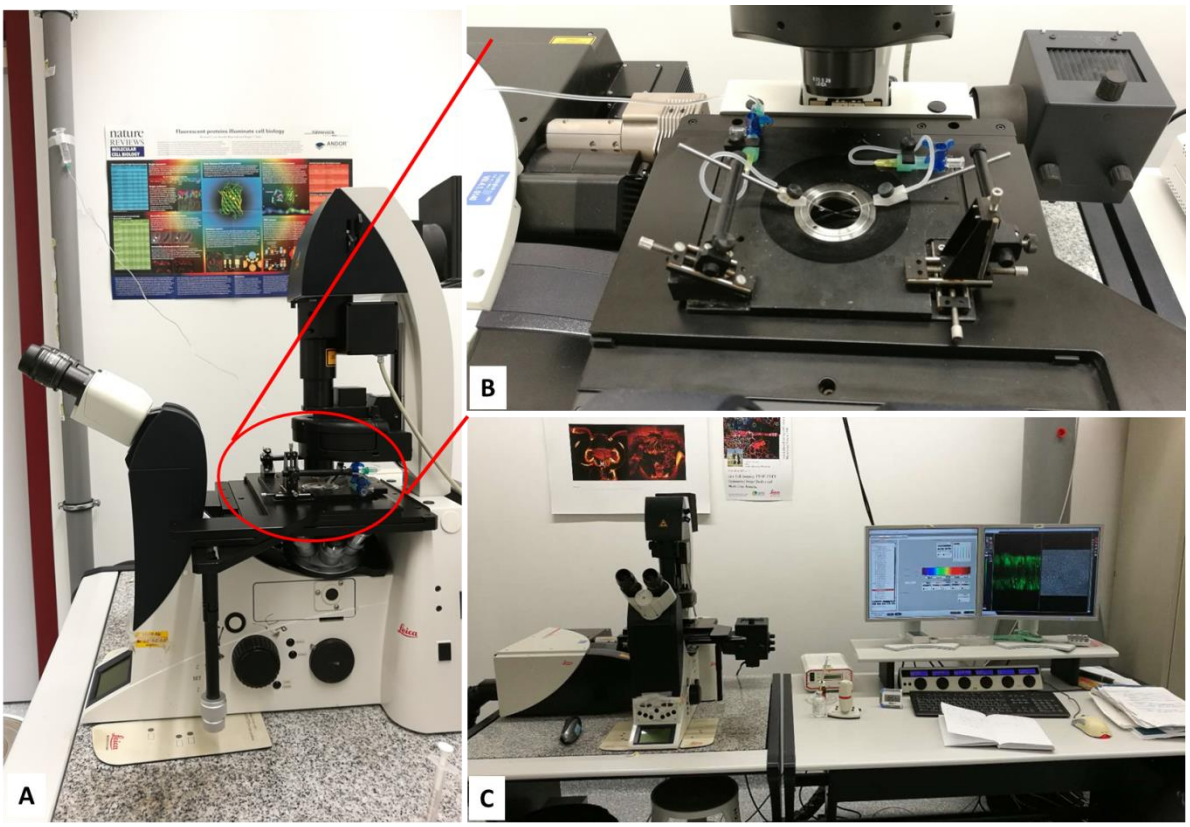

Figure 5. Setup under the confocal microscope.

The mouse arteries and immunofluorescence images were acquired with the SP5 confocal microscope (Leica microsystems, Wetzlar, Germany). **(A and B):** The setup with the mounted and pressurized artery was fixed on the confocal microscope. **(C):** The overview of the confocal microscope.

2.5. Immunofluorescence.

Cannulated and pressurized arteries from C57BL6/N mice were fixed for one hour with 3.7% formaldehyde. Thereafter, the vessels were intra- and extra-luminally permeabilized for 30 minutes with 0.5% Triton X-100, blocked with 1% BSA in phosphate-buffered saline with divalent cations (PBS+) followed by the addition of primary antibodies overnight at room temperature (PAI-1, AMPKα1/2, Cx37, Cx43, Cortactin and MMP14). Then, they were incubated for two hours with the respective secondary antibodies coupled to fluorescent dyes. Finally, images were acquired with a Leica TCS SP5 confocal microscope (Leica Microsystems) **(Figure 5)**. Images were analyzed with the help of Fiji Imaging software (ImageJ Version 5.2) (Schneider et al. 2012).

2.6. Assessment of heterocellular dye transfer.

In another set of experiments with the cannulated and pressurized arteries, MOPS solution containing calcein-AM (1 µM) was perfused through the artery lumen for 10 min to enable the selective loading of dye into endothelial cells. Afterwards, the lumen was flushed with MOPS buffer and the artery was incubated from the abluminal side with Alexa 633 for the visualization of the IEL (Internal elastic lamina). The time of calcein dye loading was kept constant at 20 min in all experiments. Meflumic acid (100 µM) and heptanol (250 µM) were used to block gap junctions. They were added to the organ chamber 30 min prior to calcein loading, and remained present during the loading and imaging periods. Vessel Images were obtained using a Leica TCS SP5 confocal microscope (Leica Microsystems). Arteries were excited at 543 nm for calcein-AM red-orange and at 633 nm for Alexa 633 imaging. The emission filters were set at 550-600 nm and 640-660 nm, respectively. Fluorescence was excited and registered through a 60x water immersion objective using the same laser, pinhole (0.5 AU), photomultiplier and HyD-detector settings in all experiments. Z-stacks through the wall of the artery were obtained in 0.35 µm steps (Leica Application Suite X software Version: 2.0).

2.7. Calcein spreading and diffusion.

Calcein spreading and diffusion was determined by using fluorescence recovery after photobleaching (FRAP) technique. A pressurized artery was loaded luminally with calcein-AM red-orange (1 µM) in calcium-free MOPS solution for 20 min which

remained in the lumen while imaging was performed. A 40x12 µm area in the VSMC layer with a typical calcein MEJ structure was recorded and afterwards bleached for 5 second with 100 % intensity of the 534 nm laser. Afterwards, the diffusion of the calcein signal in different regions of interests (ROI) in the VSMC over time (30 min) was recorded.

2.8. Image analysis.

For the analysis of MEJs and IEL hole count, EC-VSMC calcein transfer, MMPsense signal quantification, Alexa633 IEL thickness quantification in intact arteries, Fiji ImageJ software was adopted. MEJs in muscle and mesenteric arteries were quantified by counting bright calcein-AM red orange stainings in IEL holes. IEL holes were quantified by constructing a Fiji ImageJ Plugin. Shortly, raw images were pre-processed (unsharp masking and bandpass filter to compensate for inhomogeneous staining intensities and slightly oblique IEL level), a grey value threshold applied and fenestrations with a minimal diameter were analyzed:

```
Run("Unsharp Mask...", "radius=5 mask=0.60 stack");

Run("Enhance Contrast...", "saturated=5");

Run("Bandpass Filter...", "filter_large=40 filter_small=3 suppress=None tolerance=5 autoscale saturate");

getRawStatistics(nPixels, mean, min, max);

t2 = 0.3*mean;

t1 = min;

setThreshold(t1, t2);

setOption("BlackBackground", false);

Run("Convert to Mask");

Run("Analyze Particles...", "size=1-Infinity show=[Overlay Masks] display clear include summarize");
```

2.9. Acetylcholine (Ach) dose response curves.

The saphenous arteries were treated as published before (S.-S. Bolz et al. 1999). Briefly, the prepared arteries were mounted on the setups and pressurized at 60 mmHg **(Figure 5).** Then the setup was transported to the stage of a modified inverted microscope (Diaphot 300, Nikon, Düsseldorf, Germany) equipped with a 20x lens (D-APO 20 UV / 340, Olympus) and a video camera (Watec, WAT-902B) **(Figure 6)**. The organ bath temperature was slowly raised to 37 °C. The arteries were loaded with the Ca^{2+} indicator Fura2-AM (2 µM, LifeTechnologies, Carlsbad, CA, USA) in an incubation period of 90 min. Before the Ach dose response curve (DRC), the arteries were pre-incubated with 30 µM L-NAME (Nω-nitro-l-arginine methyl ester) and 30 µM indomethacine for 45 min. The measured Fura2 signals were corrected for background fluorescence (as measured at the end of each experiment after quenching with 8 mM $MnCl_2$). Simultaneously with the measurement of cytosolic Ca^{2+} concentrations $[Ca^{2+}]_i$, vascular outer diameters were recorded by video-microscopy and displayed with the help of BVA software (Hasotec, Rostock, Germany) **(Figure 6)** (Schubert et al. 2017). Increasing concentrations of Ach (3 nM or 10 nM-3 µM) were added for 2-4 min after pre-constriction of the arteries with norepinephrine (NE) (1 µM). Peak Ach-dilations and concomitant Ca^{2+}-decreases were used for quantification.

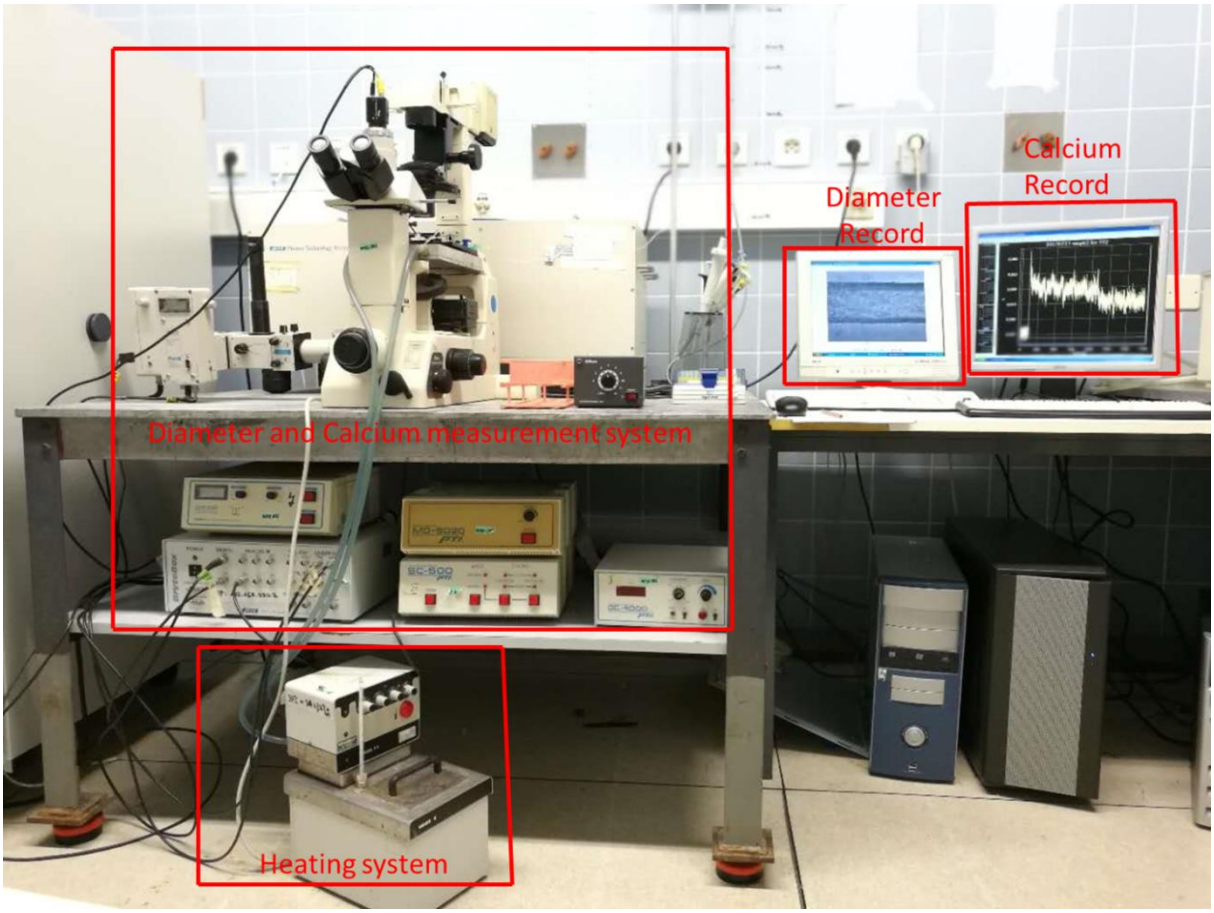

Figure 6. The calcium measuring and diameter registration system.

The heating system allowed to keep the pressurized arteries at a constant temperature of 37 °C. A detailed description of the total setup has been published earlier in doctoral dissertation from our institution (Kreutz 2013). Briefly, the illumination unit generated monochromatic light of the wavelengths 340 nm and 380 nm for the excitation of the vessel loaded with Fura-2. The resulting emission wavelength (510 nm) was transmitted to a photomultiplier. The excitation wavelengths were excluded from the analysis with the help of a bandpass filter. For the diameter registration, the vessel was illuminated by red light (to minimize interference with the simultaneous calcium measurement) which was transmitted to a CCD camera. Both signals were digitalized in a Bryte box and fed to a personal computer where they could be simultaneously displayed and recorded. These signals were exported to Microsoft Excel to subtract the background fluorescence. In parallel to the digital records, the artery image was displayed live on a second computer directly connected to the camera.

2.10. Protein isolation from intact arteries.

For the detection of PAI-1, SHP, GAPDH and total AMPK in arteries from AMPK α1 and α2 knockout (KO) and wild type (WT) mice were used (the respective littermate

WT for each strain). The mice were sacrificed by cervical dislocation and the α1 genotype was checked by examining the spleen. Afterwards, the whole arteries of a murine mesenterium were isolated, cannulated on one side, flushed free from intraluminal blood, divided into two roughly equal parts. Afterwards, the samples were snap-frozen in liquid nitrogen. Concerning the arteries from C57BL6/N (male mice, Charles River, Sulzfeld, Germany), the whole mesenteric arteries (MA) were isolated, and flushed free from intraluminal blood; secondly, the arterial tree was divided into three or four roughly equal parts; Subsequently, the arteries were transferred to a cell culture dish filled with MOPS buffer and incubated them for 15 min at 37 °C; thirdly, the arteries were treated with DMSO (0.01 %), 10 µM A76, 10 µM A76 plus 10 µM CC or 10 µM CC (all in MOPS buffer) at 37 °C for 1 hour, respectively. At the end of the experiment, the arteries were harvested by snap-freezing in liquid nitrogen. The arterial protein was extracted as previously described (Holger Schneider et al. 2015). Briefly, if half of the MA was used, the sample was minced thoroughly in a starting volume of with 20 µl lysis buffer in glass mortar, the pestle was minced thoroughly, rinsed with another 10 µl lysis buffer and the sample was centrifuged. This procedure was repeated until there were 50 µl lysis buffer in the mortar; if single arteries were used, the starting volume was 10 µl, rinsing volume remained 10 µl and the final volume was 30 µl, Then the suspension was pipetted up and down until only foam was left in the mortar. The foam was then transferred to a new reaction vial. Afterwards, the foam was spun down at 18000 revolutions per minute (rpm) and 4 °C for 15 min; at the end, the supernatant containing the protein was transferred to a new vial and stored at -80 °C until a conventional Western Blot (WB) was performed.

2.11. Cell culture, siRNA transfection and protein harvest.

Porcine coronary artery smooth muscle cells (PCASMCs, Sigma Aldrich, Deisenhofen, Germany) and human umbilical vein smooth muscle cells (HUVSMCs) were cultured according to the provider's instructions in a humidified chamber with ambient conditions of 5 % CO_2 and 95 % O_2. Porcine smooth muscle cell growth medium was applied for PCASMC culture. AMPK knockdown: siRNA against both AMPK α-subunits (sc-45312) or control siRNA (sc-28 37007) both Santa Cruz, Heidelberg, Germany) was transfected into PCASMC cells using Lipofectamine RNAiMAX Transfection Reagent (ThermoFisher, Waltham, MA, USA) according to the manufacturer's protocol. Cells grown in six well plates were transfected in Opti

MEM medium for 4 hours. Afterwards, 4 ml culture medium was added on top. The culture medium included 1 % penicillin-streptomycin solution (10000 U penicillin and 10 mg streptomycin/ml). After 3 days of culture, protein was harvested by removing the medium and adding 150 µl of ice cold RIPA buffer with protease and phosphatase inhibitors in each well. The retrieved solution was the stored at -80 °C until subjected to conventional WB. The human umbilical vein endothelial cells (HUVECs) were purchased from Promocell and were cultured with specific culture medium (Medium 199 (Gibco, 31150-022) supplemented with 20 % NBCS and 1 % penicillin-streptomycin (10000 U penicillin and 10 mg streptomycin/ml) and substituted with endothelial cell growth medium (Promocell, C22010 at a 1:2 dilution)). Like in PCASMCs, the siRNA against both AMPK α-subunits (sc-45312) or control siRNA was transfected into HUVECs using Lipofectamine 2000 transfection reagent according to the following protocol (6 well plate): cells were grown to 70-80 % confluency, the medium was removed and cells were washed one with PBS, opti MEM medium was added (700 µl per well) together with the siRNA mixture. Then HUVECs were incubated for 6 hours, the transfection reagents were removed and HUVEC medium was applied onto the cells (medium199: endothelial cell growth medium=1:1) 3 ml for each well. After 2 days of culture, protein was harvested as described for HUVSMC. The brief harvesting protocol: cells were scraped from the bottom of the culture dish with a scraper; the lysate was transferred into a reaction vial (1.5 ml Eppendorf reaction vial); the vial with the cell lysate was vigorously vortexed for 30 sec to 1 min, then it was incubated on ice for 10 min; this procedure was repeated 5 times. Afterwards, the sample was stored at -80 °C (dry ice) for 20 min. Then, the sample was centrifuged at 18000 rpm and 4 °C for 15 min; at the end, the supernatant containing the protein was transferred to a new vial, and stored at -80 °C until conventional WB was performed.

2.12. Western blot.

The harvested proteins were separated via sodium dodecyl sulfate polyacrylamide gel electrophoresis (SDS-PAGE) in Mini-PROTEAN Tetra system (BIO-RAD, USA) via a constant current of 25 milliamperes (mA) per gel for 1 hour, transferred onto a 0.2 µm PVDF membrane (BIO-RAD, USA) in a Trans-blot Turbo Transfer system (BIO-RAD, USA) via constant current of 2.5 A for 7 min, blocked in 5 % milk powder in TBST for 1 hour, then incubated with the primary antibody in 5 % BSA in TBST

buffer (anti-total-AMPK (α1 and α2) antibody dilution 1:1000, anti-phosphor-AMPK (α1 and α2 (T172)) antibody dilution 1:1000, anti-PAI-1 antibody dilution 1:200, anti-SHP antibody dilution 1:100, anti-phospho-ACC antibody dilution 1:1000 and anti-GAPDH antibody dilution 1:10000). The incubation period was 12 or 36 hours on a shaker at 4 °C. Afterwards, the membranes were washed with TBST buffer for 4 times with gentle shaking, each time for 5 min, and then incubated with the corresponding horseradish peroxidase (HRP)-conjugated secondary antibody (dilution 1:1000) for 1 hour. After this, the membranes were again washed with TBST buffer for 4 times, each time for 5 min. Finally, bound secondary antibody was visualized by HRP-mediated luminol oxidation (AppliChem, Darmstadt, Germany) which was detected with a CCD camera. The images were analyzed with Fiji ImageJ Software and the band intensities were quantified with Image Studio software (LI-COR Biosciences) (Miller 2010).

2.13. Mouse genotyping via PCR.

The genotypes of all mice of the AMPK α1 and α2 strains was determined by PCR according to the KAPA Mouse Genotyping Kit (KAPABIOSYSTEMS 2016) in duplicate (ear sample after birth and tail plus ear after sacrifice).

DNA extraction: The detailed contents of DNA extraction buffer and its protocol are shown in **Table 11 and 12**.The samples were centrifuged briefly to pellet cellular debris and the extract was diluted 10-fold with 10 mM Tris-HCl. Then the samples were stored at -20 °C. The PCR master mix was prepared as follows: PCR-grade water 25 µl, 2 KAPA2G fast genotyping Mix (Containing DNA polymerase for fast PCR, $MgCl_2$ (1.5 mM), dNTPs(0.2 mM)) with dye 12.5 µl, forward primer 1.25 µl (Final concentration 0.5 µM), reverse primer 1.25 µl (Final concentration 0.5 µM) and 1 µl of prepared DNA extract. The protocol for PCR is shown in **Table 13.** After PCR, samples were separated by agarose gel electrophoresis. AMPK α1 KO forward primer: 5´CCT TCC TGA AAT GAC TTC TGG 3´, AMPK α1 KO reverse primer: 5´GGG CTG CAG GAA TTC GAT ATC 3´, AMPK α1 WT forward primer: 5´AGC CGA CTT TGG TAA GCA TG 3´, AMPK α1 WT reverse primer: 5´CCC ACT TTC CAT TTT CTC CA 3´.AMPK2_neo_up primer: 5´GCT TAG CAC GTT ACC CTG GAT GG 3´, AMPK2_neo_down primer: 5´ GTT ATC AGC CCA ACT AAT TAC AC 3´.

Table 11. Detailed contents of DNA extraction buffer

Component	Per 100 µL reaction (µL)
PCR-grade water	88
10X KAPA Express Extract Buffer	10
1 U/µL KAPA Express Extract Enzyme	2

Table 12. DNA extraction protocol

Step	Temperature(°C)	Duration(min)
Lysis Step	75	10
Enzyme inactivation	95	5

Table 13. PCR cycle protocol

Step	Temperature(°C)	Duration	Cycles
Initial denaturation	95	3 min	1
Denaturation	95	15 s	33
Annealing	60	15 s	
Extension	72	15 s	
Final extension	72	7 min	1

Afterwards, the this system was cooled to 4°C.

2.14. Statistics.

For data presentation and computation of statistical tests SigmaPlot (Systat, Erkrath, Germany) was applied. Statistical tests comprised parametric tests, i.e. one way ANOVA, t-test, and paired t-test when the data were normally distributed. Mann-Whitney Rank Sum Test was used when the data were not normally distributed. Two way ANOVA was used in the compare of acetylcholine response curve in different artery. For descriptive reasons, all values are presented as means ± standard error of the mean (SEM). Differences were considered statistically significant when the alpha error probability was < 0.05.

3. Results

3.1. Observation of actin-rich circular and cone-like structures in mesenteric arteries.

In the endothelium of isolated and pressurized mesenteric arteries of LifeAct-GFP mice, we observed structures which were characterized by <1µm cone-like actin core surrounded by a virtually actin free zone of about 7 µm in radius around the cone except for thin intersection which gave the structure an appearance of a wheel with hub and spokes (“wheel like structure”, WLS). All of them being exclusively located in the area of holes in the IEL **(Figure 7A)**. Actin staining with phalloidin and, surprisingly, also calcein red-orange stained the exactly same pattern or WLS in mesenteric arteries from C57BL6/N mice **(Figure 8 A).** Calcein stain was more intense than the LifeAct-GFP signal. Due to the calcein loading from the endothelial side calcein stain was pronounced in ECs and less intense in adjacent VSMCs, so that MEJ structures on the endothelial side were easier to detect. All WLS stained with calcein in the endothelial layer had a corresponding actin hub when stained simultaneously with phalloidin (n=3). Further structural characteristics of the WLS in LifeAct mice are listed in **(Table 11).** WLS were exclusively located in holes of the IEL, the only areas where endothelial cells and smooth muscle cells can get direct contact **(Figure 7A, Figure 8 A and C).** We found that there were 1.86 ± 0.17 WLS and 5.35 ± 0.5 IEL holes per 10^3*µm² IEL in mouse mesenteric arteries (>250 µm in size, n=10) **(Figure 8B)**, and so about 35 % ± 1.8 % of IEL holes exhibited WLS **(Figure 8C)**.

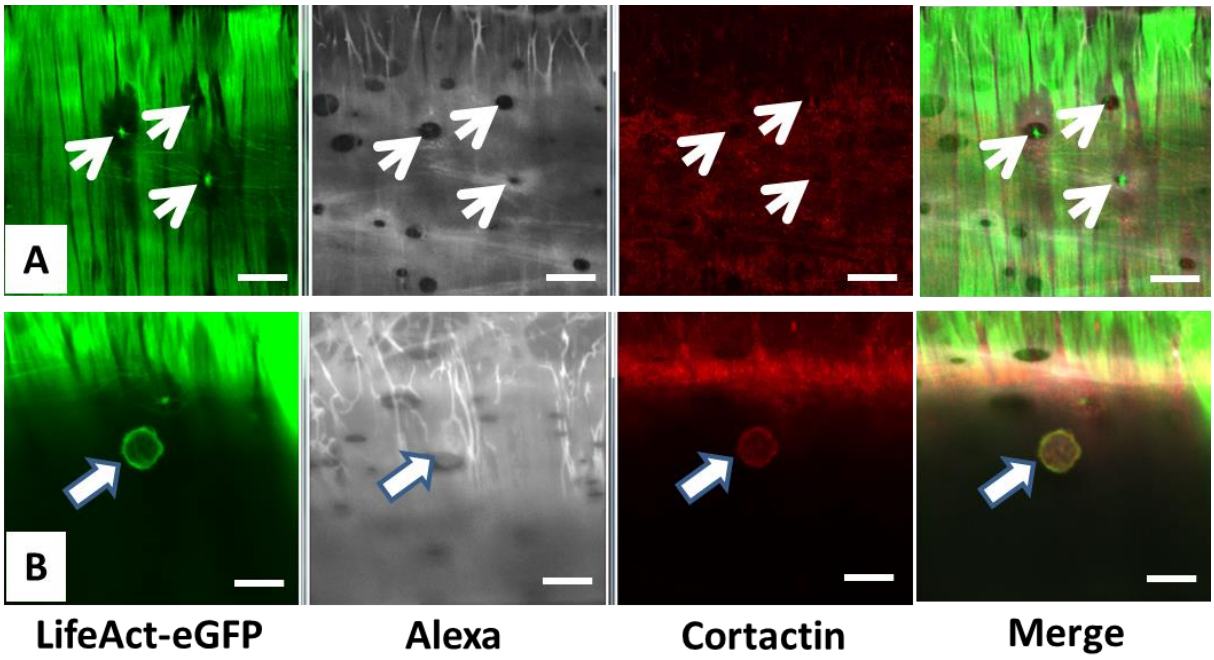

Figure 7. Localization of MEJs and Podosomes in intact arteries of LifeAct mouse.

Mesenteric arteries from LifeAct-GFP mice were cannulated, pressurized, and co-stained with cortactin (red) and Alexa 633 (grey, for IEL). Images were taken using a Leica TCS SP5 confocal microscope (Leica Microsystems). **(A)**: Wheel-like or cone-like LifeAct structures were observed always located in IEL holes and are negative for cortactin. These structures were identified as MEJs (marked by arrow). **(B)**: Round actin containing structures was also observed in LifeAct vessels. These structures were positive for cortactin and were not located in IEL holes, suggesting that these structure represented podosome rosettes (arrows). Scale bar is 10 µm.

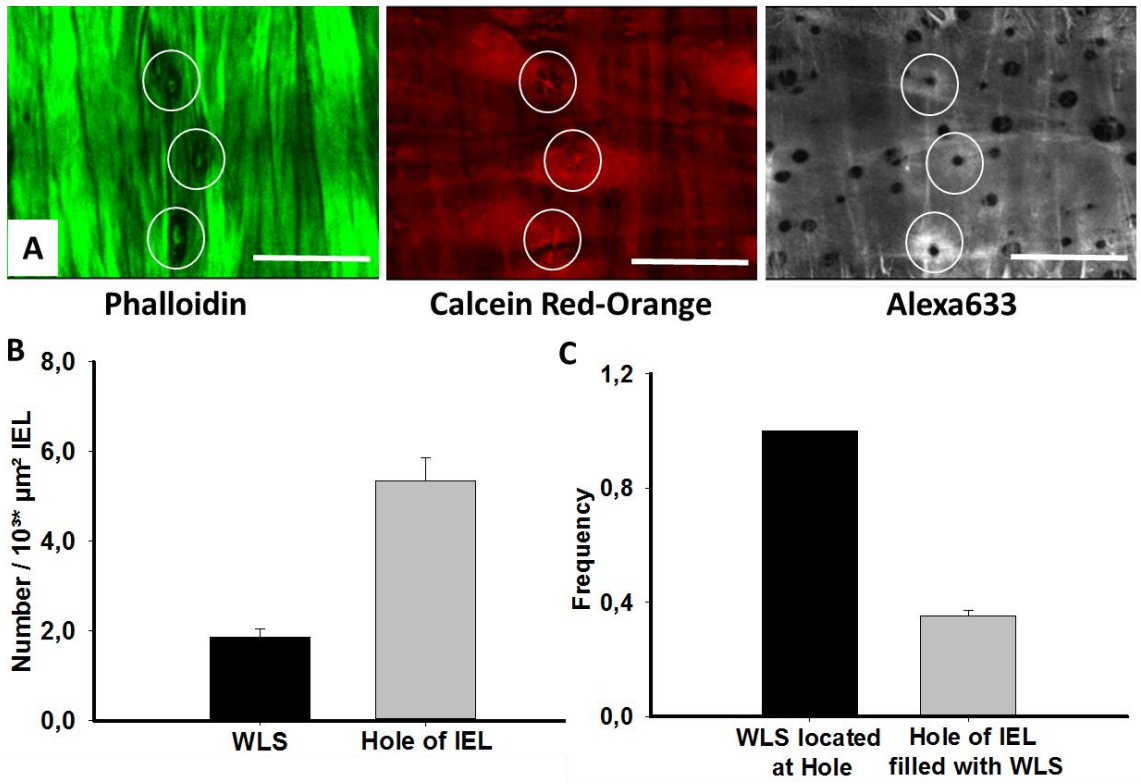

Figure 8. Calcein staining co-localizes with the actin signal around MEJs.

The wheel like structures as observed in LifeAct-GFP mouse arteries could also be detected when using the F-actin stain phalloidin in permeabilized vessels. Surprisingly, after loading the intact endothelium with calcein red-orange AM, the same structures could be identified which allowed long term observation of the dynamics of the structures. **(A)**: Images of vessels treated with the different stains. **(B)**: Quantification of the number of WLS and holes in IEL. There were 1.86 ± 0.17 WLS and 5.35 ± 0.5 IEL holes in 10^3*µm² IEL (n = 10). **(C)**: 100% of the WLS were located in the area of holes whereas 35 % ± 1.8 % of IEL holes were "filled" with MEJs in mesenteric arteries (n = 10). Scale bar is 20 µm.

Table 14. The comparison of characteristics between WLS and ring-like structures (RLS).

	WLS	RLS
Cortactin positive Staining	No	Yes
MMP14 positive staining	No	Yes
Cx37/ Cx43 postive staining	Yes	No
Actin impression on the smooth muscular side	Low ~ 1µm	Flat: a few hundred nm
Endothelial-sided actin structure	Wheel-shaped/ Star-shaped	Circular
Position to the IEL hole	Central	On the edge
Position to overlying muscle cells	Regularly between two muscle cells	More often under a single muscle cell

3.2. Characterization of WLS.

To distinguish these structures, from other actin rich structures, so called podosomes, some markers for podosomes where studied. The WLS were not positive for a co-staining with cortactin (Markers for Podosome) **(Figure 8A)** though morphologically different, larger ring like structures stained positive for cortactin and MMP-14 **(Figure 7B and Figure 9)**. Those were not always located near holes of the IEL **(Figure 9)**. The WLS stained positive for Cx43 (95 % ± 2.5 %), PAI-1 (100 %) and partially for Cx37 (46.6 % ± 2.3 %), proteins that have been described to be enriched in MEJ **(Figures 10, 11)**. WLS were therefore considered to represent cell (EC and VSM) protrusions which corresponded through holes of the IEL containing connexins known to be enriched in myoendothelial gap junctions (MEGJs). We therefore defined these WLS as MEJs and this term will be used further in the results section. The endothelial wheel-like structure was enhanced by staining with calcein red-orange **(Figure 8A**, **Figure 11)**.

To further support the conclusion that WLS contained gap junctions, gap junction inhibitors were used. Incubation of pressurized arteries with meflumic acid (100 µM) and heptanol (250 µM) reduced the staining of vascular smooth muscle cells with the gap junction permeable dye calcein which was loaded from the luminal side by 52.8 % (n=4) (**Figure 13**). To analyze further, whether calcein passed through MEJ one additional experiment was applied in which calcein was bleached and the recovery of the calcein signal in smooth muscle was studied in in regions of interest with different

distances from a MEJ. The results indicated that recovery of the calcein signal was faster in regions near the MEJ **(Figure 14).** These were not continued since bleaching could not be restricted exclusively to smooth muscle cells.

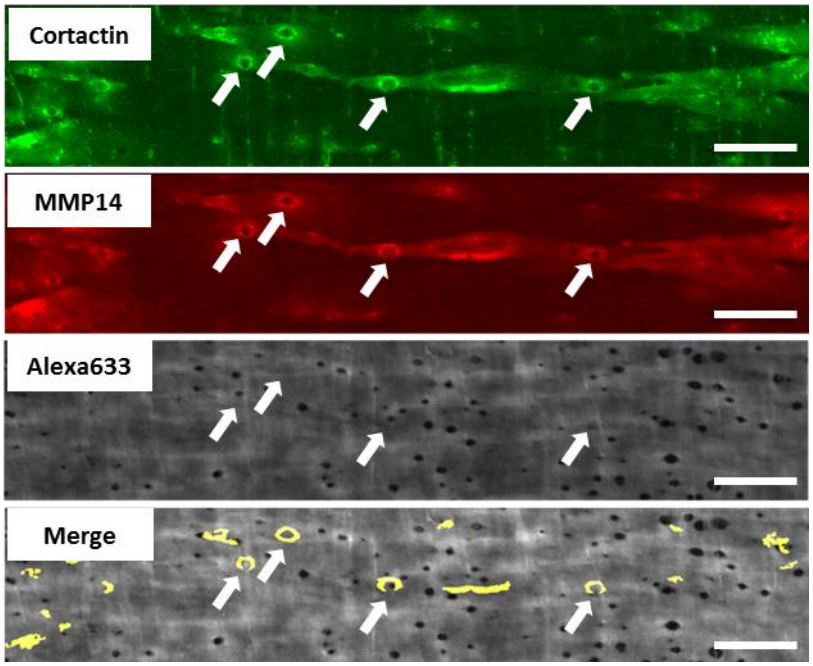

Figure 9. Circular structures are podosome rosettes (PRs).

To identify and localize PRs in artery, C57BL6/N mice were used. The pressurized arteries were stained with PR markers (cortactin and MMP14). Results showed that the circular structures were positive for cortactin and MMP14 while the structures were not in the IEL holes (as shown by arrow), suggesting that they were PRs. Scale bar is 20 µm.

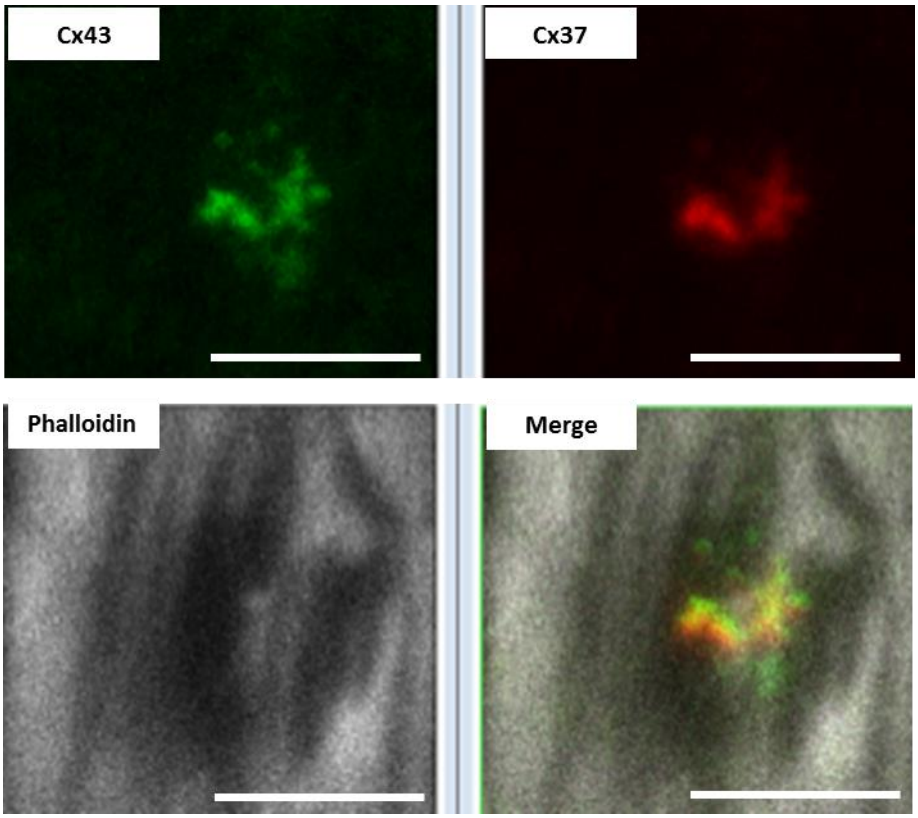

Figure 10. Cx37 and 43 is enhanced on WLS of intact mesenteric arteries.

Typical example of a vessel co-stained with Phalloidin (Mimicking the LifeAct structure), Cx37 and Cx43. The image shows an enhance Cx37 and Cx43 signal in the area of the WLS, suggesting close enrichment of Cx37 and Cx43 in this area. Scale bar is 5 µm.

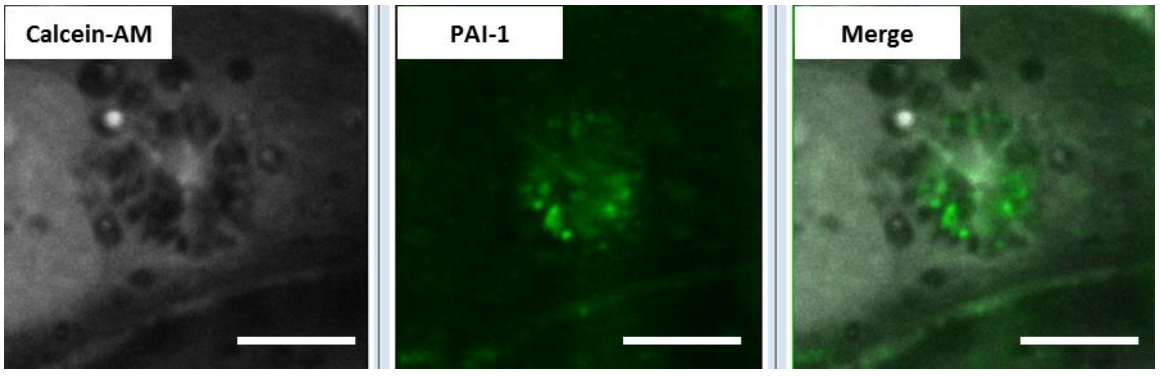

Figure 11. PAI-1 signal is enhanced on WLS of intact mesenteric arteries.

Typical example of a vessel co-stained with calcein and PAI-1. The image shows an enhanced PAI-1 signal in the area of the WLS, suggesting enrichment of PAI-1 in this area. Scale bar is 5µm.

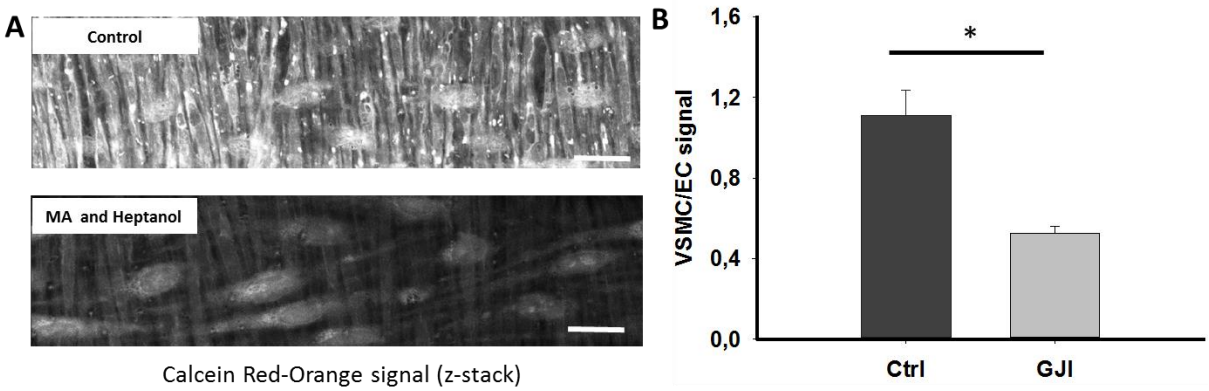

Figure 12. Gap junction inhibition blunts heterocellular dye transfer from ECs to VSMC.

Mesenteric arteries from C57BL6/N mice were incubated with the gap junction blockers meflumic acid (MA, 100µM) and heptanol (250µM) before calcein loading from the luminal side was performed. Under these conditions the calcein staining of smooth muscle cells /vertical cells structures) was reduced, indicating that calcein was being reaching smooth muscle mainly through gap junctions. After gap junction inhibition, the heterocellular dye transfer was reduced. Compared to the control, the treated artery decreased heterocellular dye transfer by 52.8%. **(A)**: Representative images of muscle staining with calcein Red-Orange with and without gap junction blockers; **(B)**: Quantification of the ratio of VSM to EC intensity signal with and without gap junction blockade (t-test (Shapiro-Wilk), *$p<0.05$, $n = 4$). Scale bar is 20 µm.

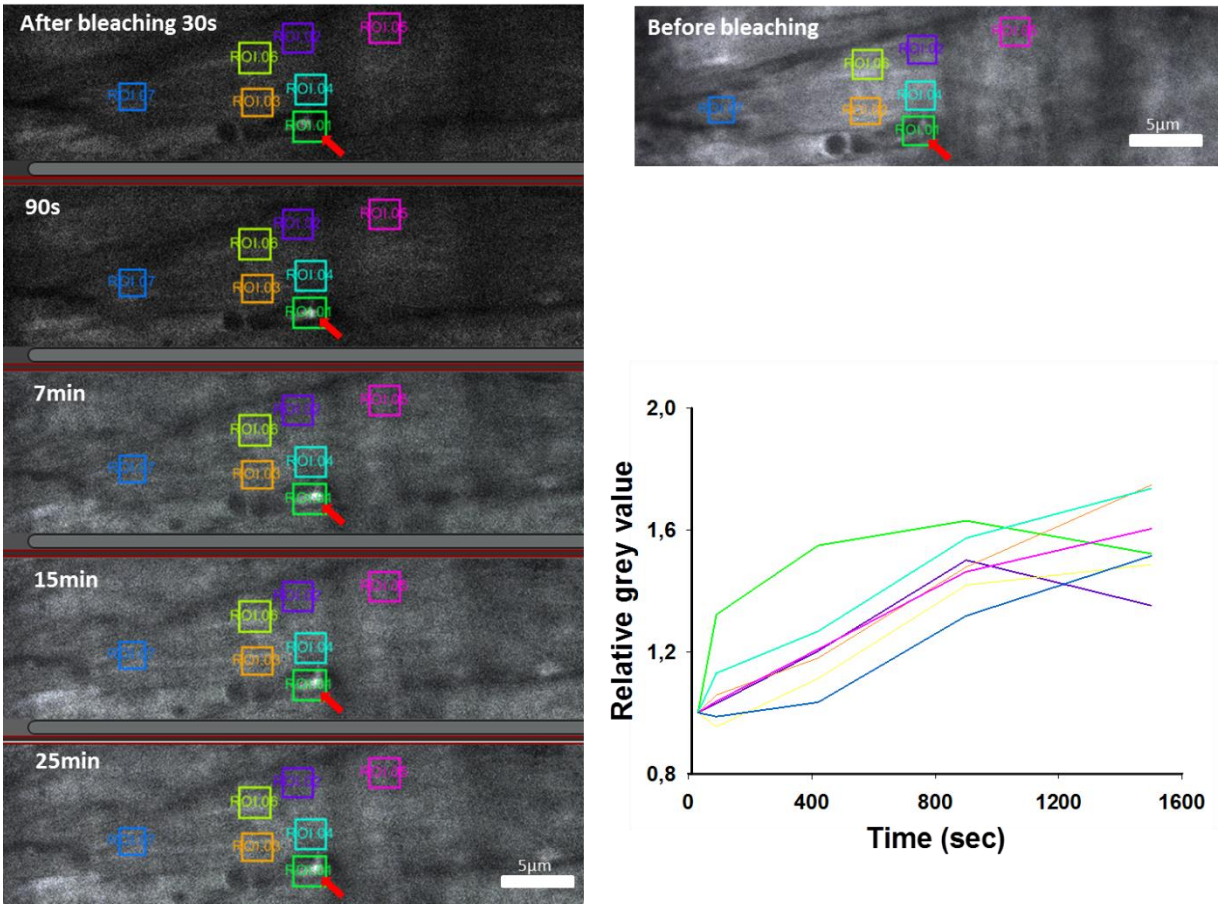

Figure 13. Calcein recovery in smooth muscle after bleaching starts from the WLS.

To confirm that the WLS were the sites of MEJ dye transfer, the calcein signal was bleached and the recovery of the calcein signal was analyzed in different ROIs at various distances from a WLS. The calcein signal increased first at the WLS (green), followed by areas adjacent to the WLS (light blue) and areas in intermittent distance to the WLS (violet, purple, orange and yellow) before it finally reached the area farthest away from a WLS (blue). The red arrow shows the position of WLS or MEJ. The diffusion velocity of the calcein signal was with 0.6 µm/min comparable to data published before (Bathany et al. 2011).

3.3. The dark area around the actin cone of WLS represents endoplasmic reticulum (ER).

We asked the question what the dark area as observed with LifeAct/phalloidin as well as calcein staining could represent **(Figure 7A and Figure 8A)**. The ER has been shown to be expressed around MEJ structures (Tran et al. 2012). Consequently, we tested if ER is enriched around MEJ using the ER specific stain ER-Tracker™Green (ER-Bodipy) (n=3). ER staining showed indeed that ER was enriched in the dark area **(Figure 14)**. The density of the ER stain in WLS area was significantly higher than in other areas (t-test, $p<0.05$, n=3).

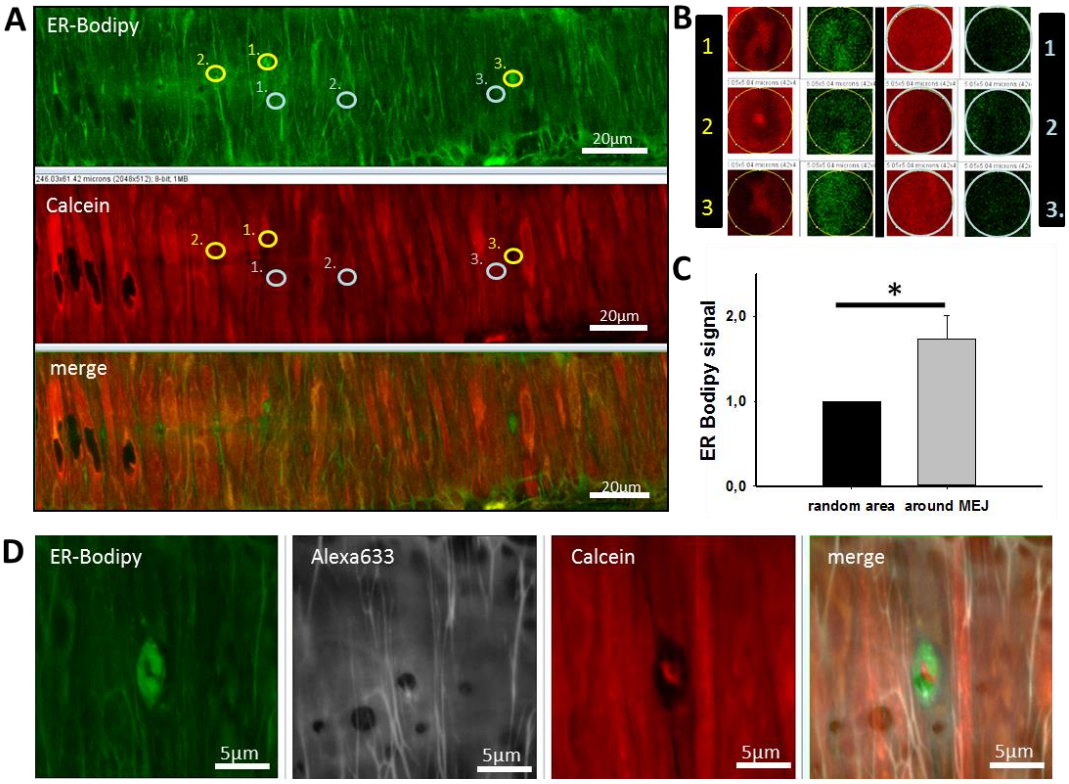

Figure 14. ER was enriched around the actin core of a WLS in intact artery.

Mesenteric arteries were co-stained with ER-Bodipy (ER Tracker) (green), calcein (red) and Alexa 633 (grey). WLS were compared with remote areas randomly selected. **(A)**: Representative images of a vessel with simultaneous ER-Bodipy and calcein staining, showing three independent WLS and non-WLS areas 1-3. **(B):** Magnified images of these areas demonstrating that the ER-Bodipy signal was higher in WLS as compared to non-WLS areas as quantified in **(C)** (Normality Test (Shapiro-Wilk), *$p<0.05$, n = 3). **(D)**: Magnified image of a WLS showing intense ER staining around the actin core. Values are normalized to random area ER Bodipy signal.

3.4. AMPK modulated MEJ dynamics.

Lately, we reported that AMPK is important for the control of actin dynamics in the vascular smooth muscle of small vessels. We also have shown that AMPK can stimulate the SERCA. In view of these effects we studied a potential role on expression and dynamics of MEJ. To this end, we incubated cannulated LifeAct mouse arteries with either compound C (CC; 10 µM), an inhibitor of the AMPK, or A769662 (A76; 10µM), an activator of the AMPK, or DMSO as the vehicle control. The MEJ dynamics were monitored under confocal microscopy (**Figure 15**). After 4 hour incubation, the number of MEJs was found to be augmented in CC treated arteries as compared with the sham treated time controls **(Figure 16)**. In CC treated vessels we found that the number of IEL holes “filled” with a WLS increased to 51.0 % ± 7.1 % in vessels treated with CC as compared with 35.2 % ± 6.2 % in vessels treated with DMSO (n=3). The number of IEL holes was not changed in arteries treated with the AMPK-inhibitor CC. The increase in MEJ numbers went along with better ACh-mediated dilation **(Figure 17B).** A76 incubation had no effect on MEJs density as compared to time controls (39.1 % ± 3.3 % n=3**)** within the observation period **(Figure 17A)**. A significant decrease of heterocellular calcein transfer was observed when arteries treated with CC **(Figure 18)**.

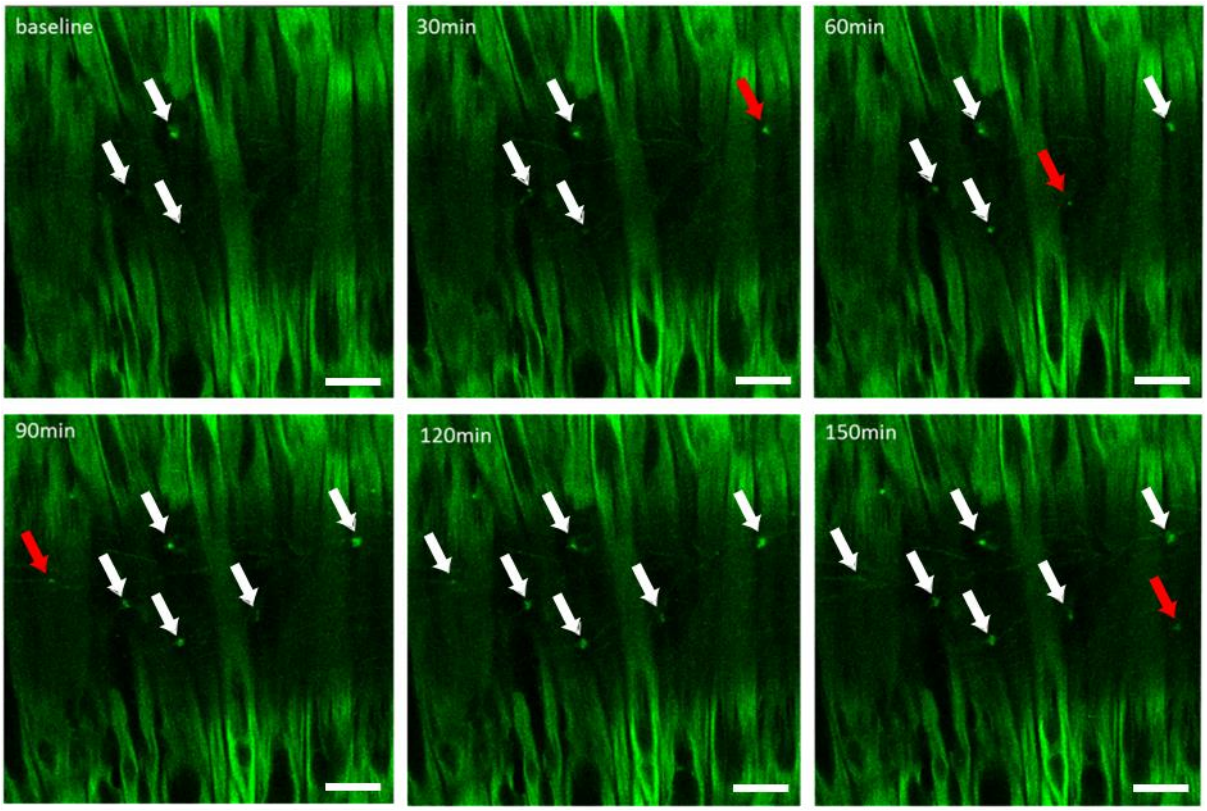

Figure 15. Development of new WLS in a mesenteric artery of a LifeAct mouse after CC incubation.

A mesenteric artery of a LifeAct-GFP mouse was incubated with AMPK inhibitor CC (10 µM) and a time lapse series over 150 minutes recorded. White arrows indicate already existing actin bridges, red arrow depict newly appearing actin bridges during the subsequent observation periods. Scale bar is 10 µm.

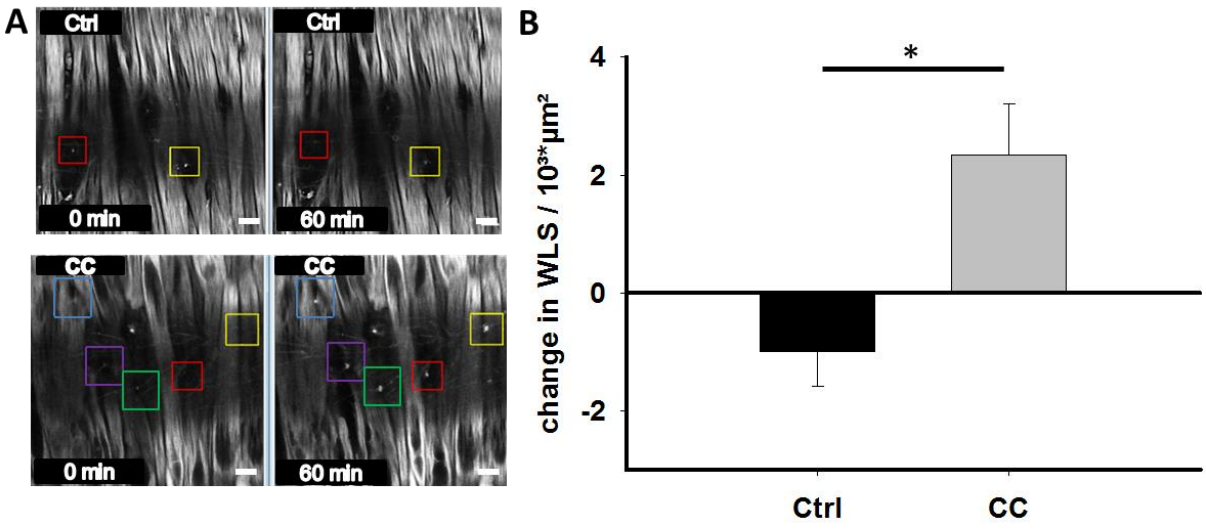

Figure 16. AMPK inhibition boosted MEJ development compared to time control.

Two examples of mesenteric arteries of LifeAct-GFP mice were incubated with CC (10µM) or DMSO as vehicle control for 60 minutes. **(A)**: The box depicts areas where actin bridge areas disappear or newly developing of the actin bridge. **(B)**: Change of the number actin bridges detectable per unit area after a 60 minutes' observation period (Normality Test (Shapiro-Wilk), $p<0.05$, $n = 3$). Scale bar is 10µm.

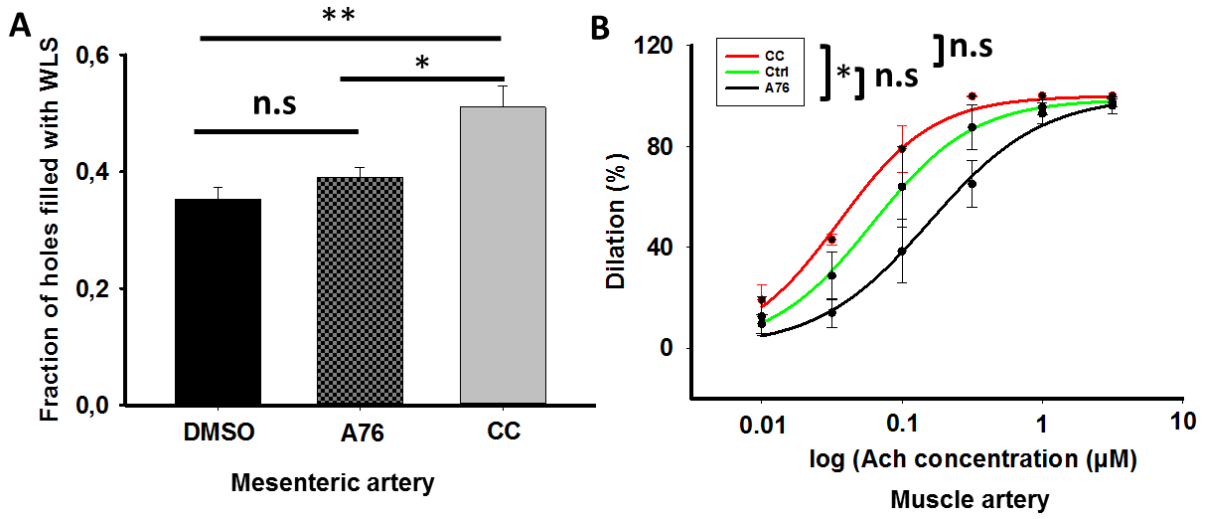

Figure 17. Inhibition of AMPK increased the fraction of holes filled by WLS and enhanced Ach-mediated dilation of the artery.

Mesenteric and muscle arteries from C57BL6/N mice were incubated with A76 10µm, CC 10 µm or DMSO as control for 3 hours. **(A):** CC significantly increased the fraction of holes filled with WLS compared to time control and A76 (One Way ANOVA, *$p < 0.05$ CC vs. A76, **$p < 0.05$ CC vs. time ctrl, $n=10$ or 4). **(B):** Saphenous arteries showed a significant left shift of the

ACh DRC in CC treated arteries compared to A76 treated arteries (Two Way ANOVA, n.s p > 0.05, n = 3).

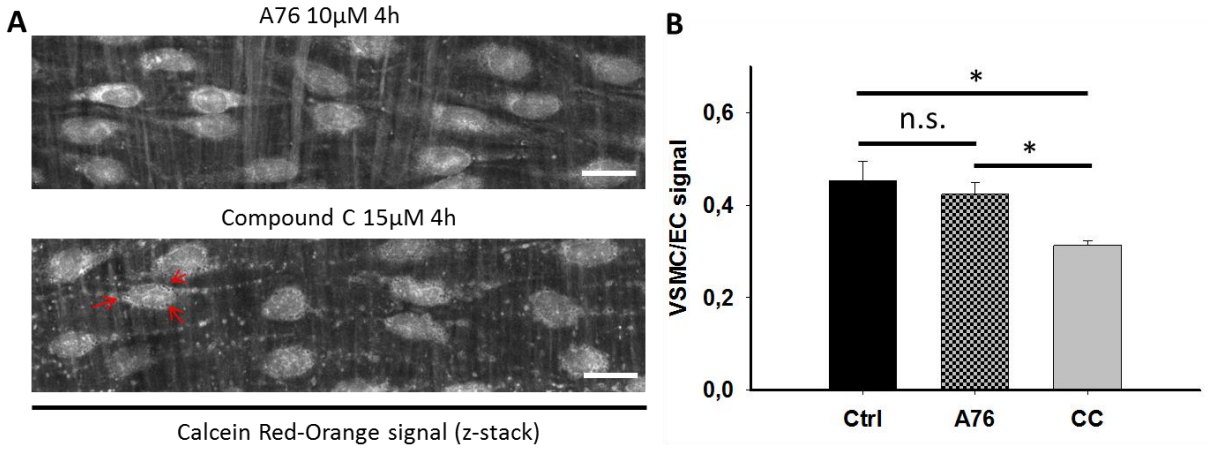

Figure 18. Inhibition of AMPK decreased calcein transfer from EC to VSMC, and enhanced formation of vesicles along nuclei.

Mesenteric arteries from C57BL6/N mice were incubated with A76 10µM, CC 15 µM or DMSO as control for 4 hours, and then stained with calcein Red-Orange. Compared to the control, CC treatment decreased heterocellular dye transfer. **(A)** Representative images with and without CC incubation **(B)**: CC incubation significantly reduced the dye transfer from EC to VSMC compared to other two groups (One Way ANOVA, *p<0.05 CC vs. Ctrl or A76, n=4). Scale bar is 20µm.

3.5. AMPK α1-KO, but not α2-KO, enhanced ACh-induced artery dilation

In view of the enhancing effects of CC on the ACh mediated dilation we studied the vasomotor responses to ACh in AMPK knockout mice. ACh is known to induce dilation in microvessels mainly via endothelium dependent hyperpolarization (EDH). Moreover, it has been shown that MEJs play a role in it. To test EDH dependent dilation, we pre-treated these arteries with L-NAME and INDO to inhibit NO and prostaglandin mediated effects. Dilation to ACh was significantly enhanced in AMPK α1-KO vessels compared to their respective WT controls and went along with respective calcium decreases **(Figure 19)**. An enhanced dilation and calcium decrease to ACh was observed only in vessels from AMPK α1-KO mice but not in AMPK α2-KO vessels (**Figure 20**).

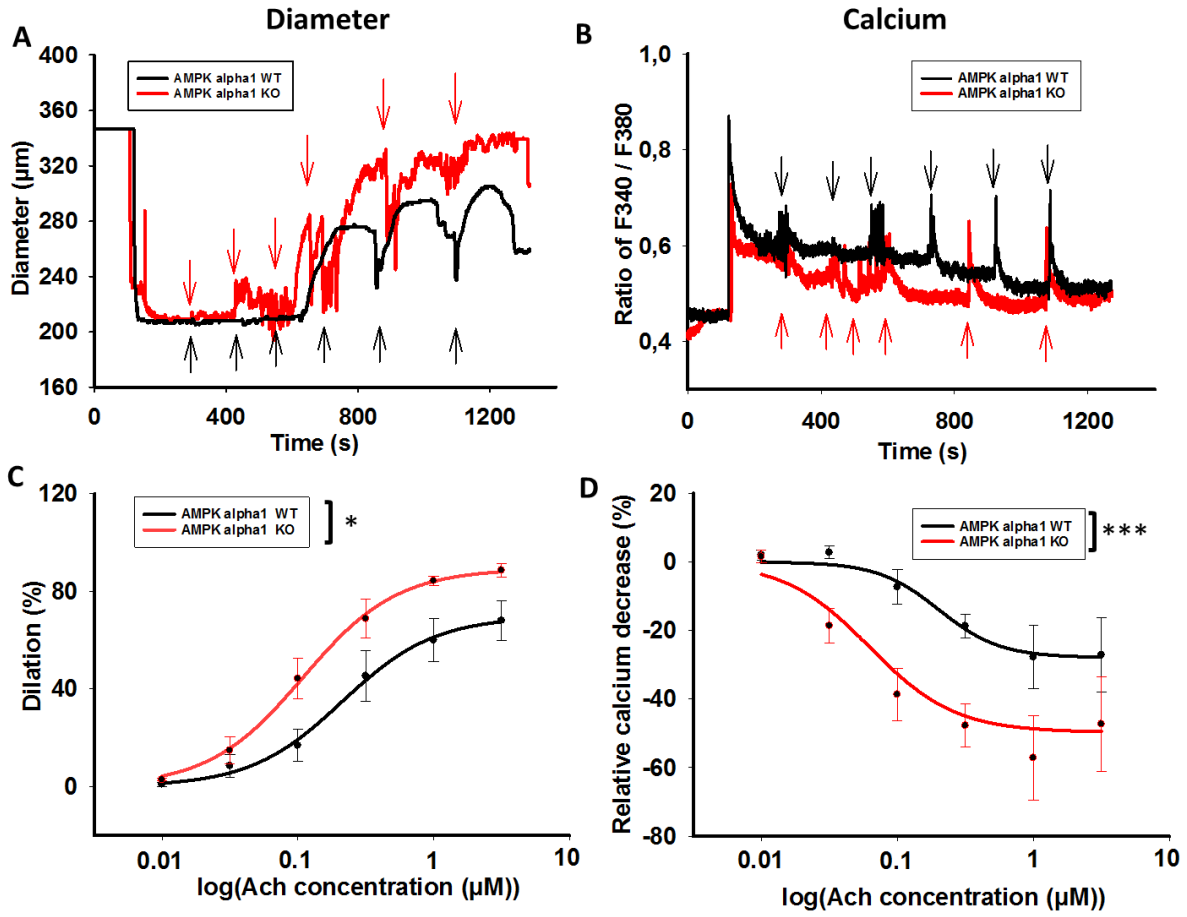

Figure 19. Left shift of the Ach dose response curve in AMPKα1-KO mice compared to their respective WT controls.

Dilator effects of ACh in L-NAME and INDO treated muscle arteries from AMPK α1 WT and KO mice. **(A, B)**: Representative diameter and Calcium recordings of a single vessel each from both groups. **(C and D):** Dose effect curves of ACh showing a significant left shift of the dilation curve and an enhanced calcium decrease in AMPK α1 KO arteries (Two way ANOVA, *p<0.05, ***p<0.001; AMPK α1 KO n = 6/3, AMPK α1 KO n = 7/4).

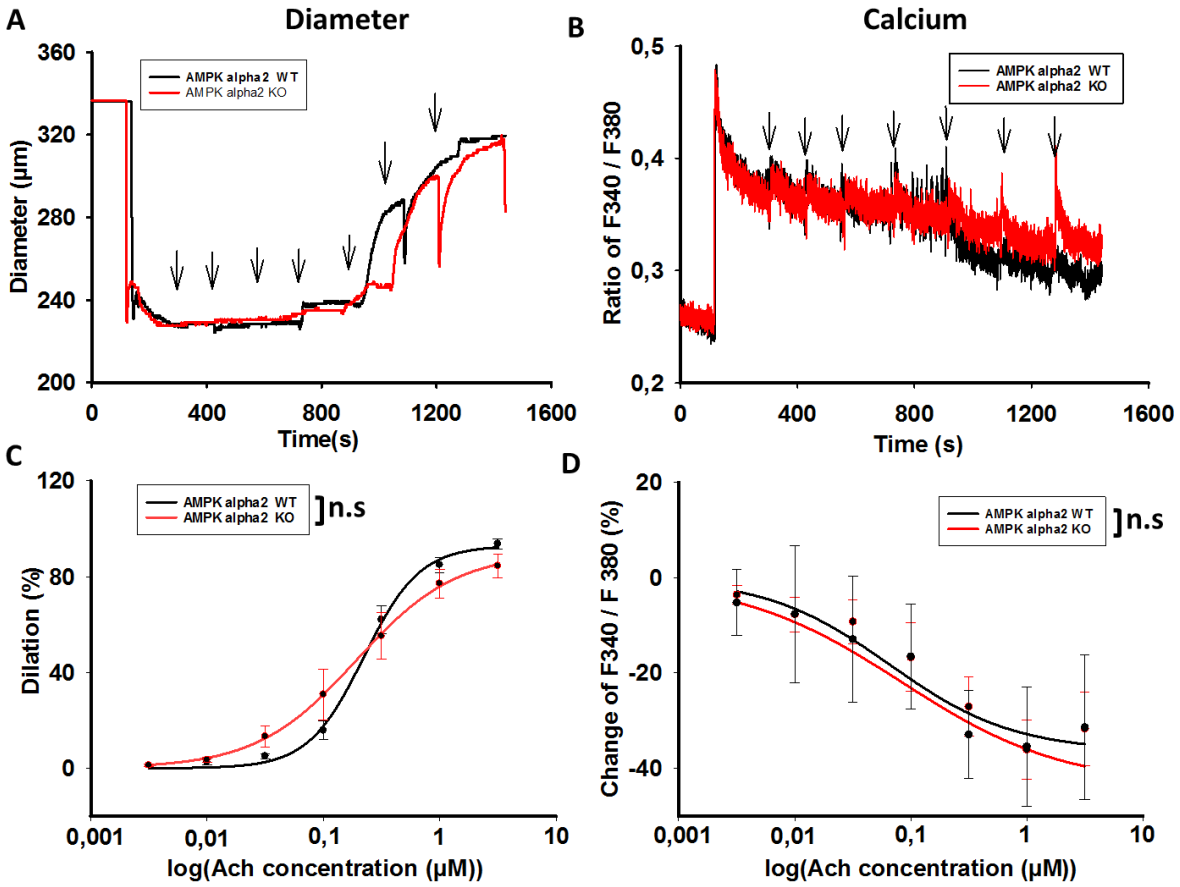

Figure 20. Ach dose response curve was not changed in AMPKα2-KO mice, compared to their respective controls (WT).

Dilator effects of ACh in L-NAME and INDO treated muscle arteries from AMPK α2 WT and KO mice. **(A, B)**: Representative diameter and calcium recordings of a single vessel each from both groups. **(C, D):** Dose effect relations show no differences with regard to diameter and calcium (Two way ANOVA, n.s p>0.05. AMPK α2 KO n = 9/5, AMPK α2 WT n = 4/3).

3.6. More MEJs and IEL holes in AMPK α1-KO, but not in AMPK α2-KO mice.

We also checked whether the knockout of AMPK α1 affects the number of IEL holes. Indeed, we found that the IEL hole number increased by 27.2 % (n=12 or 10) resulting in an respective increase of the hole (fenestrated) area (increase by 28.5.6 % as compared to WT (**Figure 21**). Although the number of holes was higher the fraction of holes "containing" MEJ also increased in AMPK α1-KO when compared with vessels of WT littermates in first branch mesenteric vessels (41.4 % ± 4.43 % AMPK α1-WT vs. 55.7 % ± 1.6 % AMPK α1-KO (t-test, ***p<0.001, n=8 or 4), as well as in muscle saphenous arteries (15.2 % ± 1.8 % AMPK α1-WT vs. 38.3 % ± 3 % AMPK α1-KO, (t-test, *p<0.05, n = 9 or 7)) **(Figure 22).** In AMPK α1-KO CC did not

any more increase the fraction of holes containing MEJ (55.7 % ± 1.6 % non-treated with CC vs 52.7 % ± 2.1% treated with CC ($p>0.05$, n=4)), whereas it still did so in WT littermates from 41.4 % ± 4.4 % to 52.8 % ± 1.6 % ($p<0.01$, n=8) (**Figure 23**), whereas the fraction of holes filled with WLS did not differ between AMPK α2 WT and KO mouse arteries (**Figure 24**).

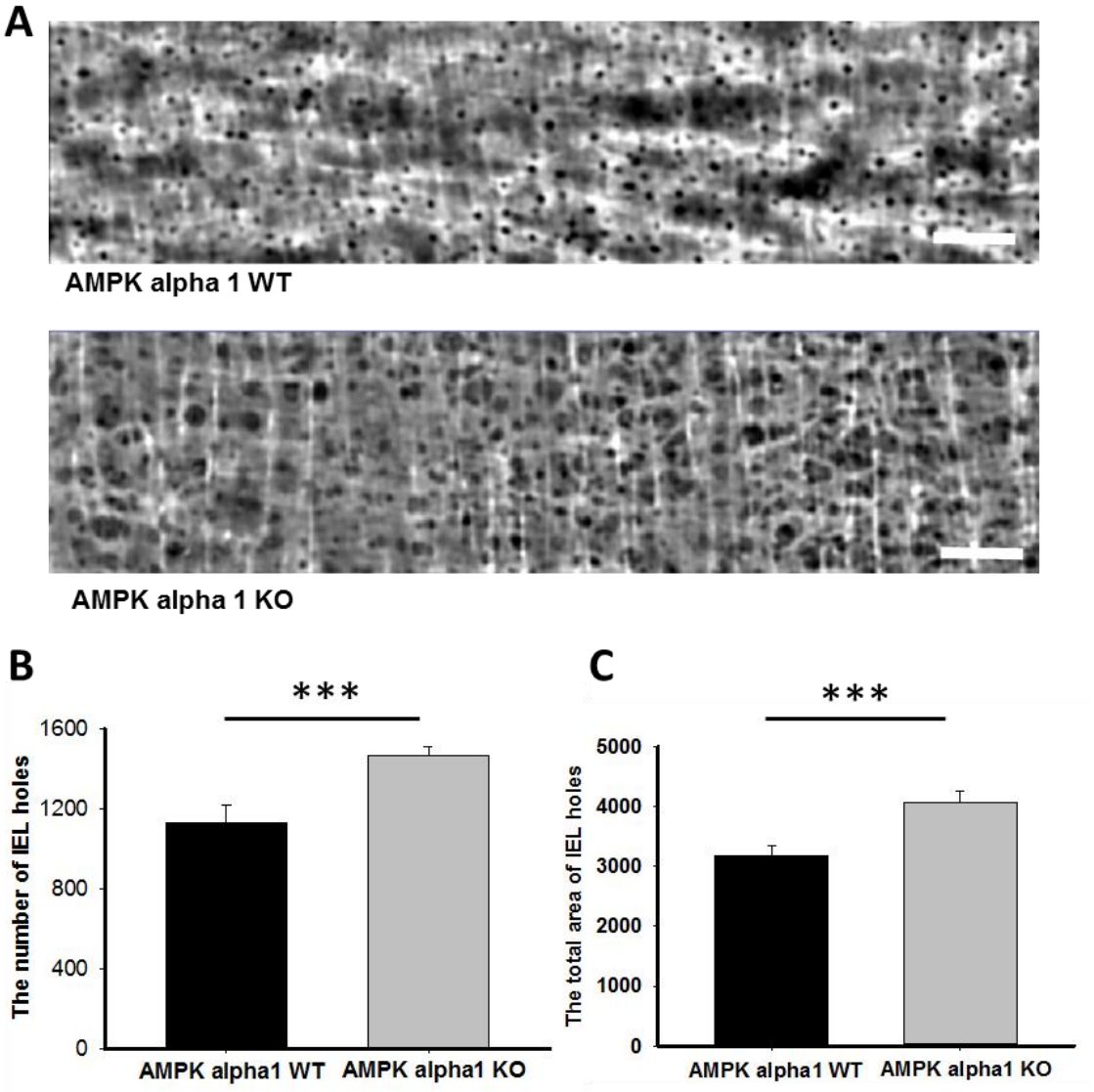

Figure 21. The total hole area per unit IEL was higher in vessels of AMPKα1-KO mice.

Mesenteric arteries from AMPK α1 WT and KO mice were analyzed with regard to IEL holes. **(A)**: Representative images of IEL and its holes from AMPK α1 WT and KO mice. **(B):** The number of holes in IEL was significantly higher in AMPKα1 KO arteries as compared to WT (t-test, ***$p<0.001$, n = 12 or 10). **(C):** Likewise**,** the total hole area in IEL was significantly larger in AMPKα1 KO (t-test, *** $p<0.001$, n = 12 or 10). Scale bar is 20 µm.

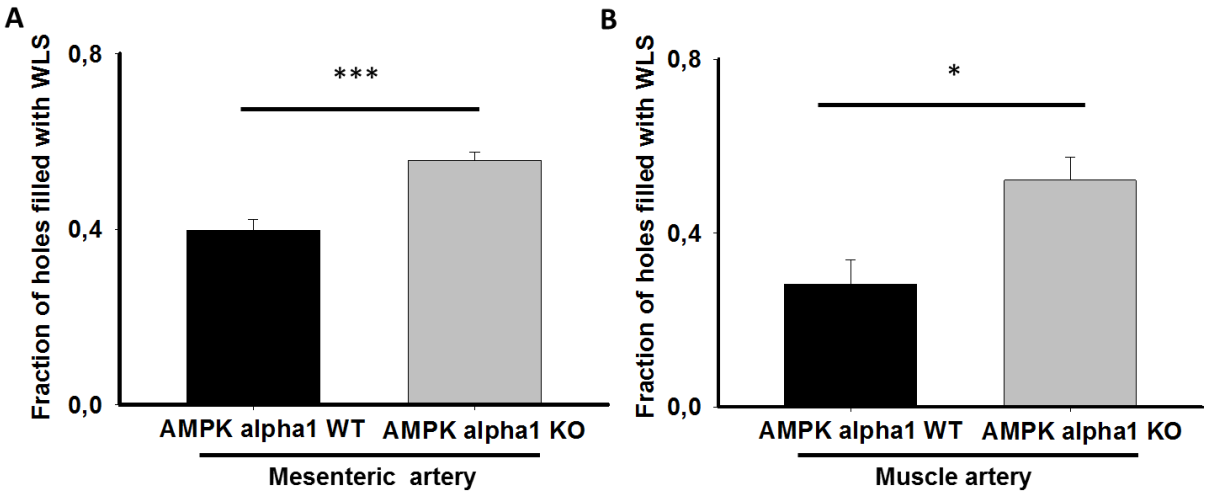

Figure 22. The fraction of hole filled with WLS was higher both in mesenteric and muscle arteries from AMPK α1-KO mice.

(A): In mesenteric arteries a significantly higher fraction of holes filled with WLS was observed in AMPK α1 KO than WT littermates (t-test, ***p<0.001, n=8 or 4). **(B):** Similar results were obtained in skeletal muscle arteries (t-test, *p<0.05, n = 9 or 7).

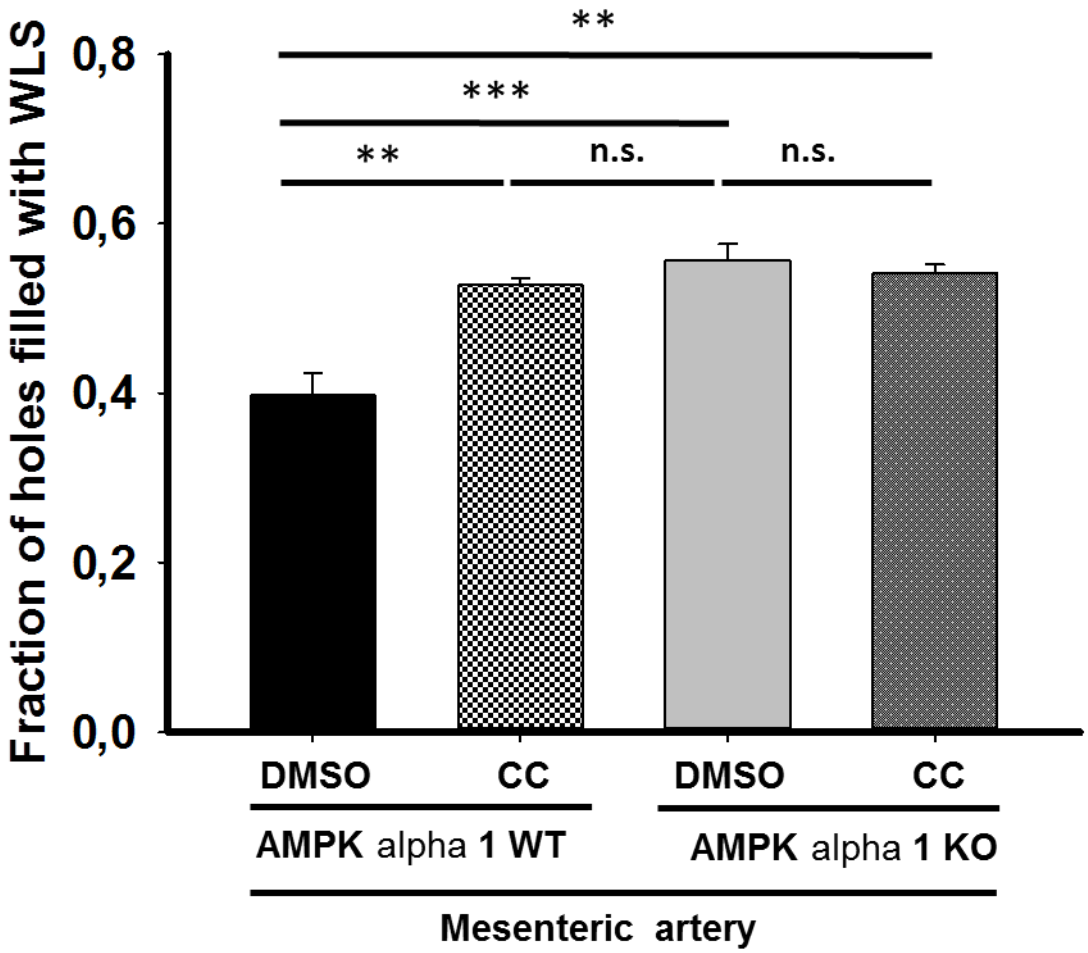

Figure 23. Compound C increased the fraction of hole filled with WLS in mesenteric arteries from WT mice, but not in AMPK α 1 KO mice.

The fraction of holes filled with WLS was significantly increased from 41.4 % ± 4.4 % to 52.8 % ± 1.6 % when the arteries were treated with CC in WT but not in AMPK α1 KO arteries (55.7 % ± 1.6 % non-treated with CC % VS 52.7 % ± 2.1% treated with CC, n.s. $p > 0.05$, n=4) (One Way ANOVA, **$p<0.01$, *** $p<0.001$, n = 8 or 4).

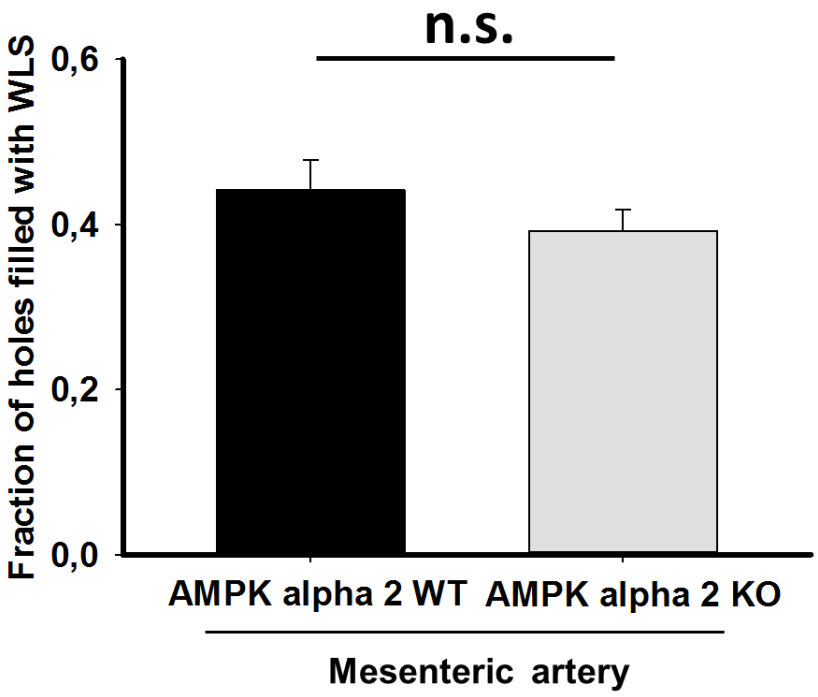

Figure 24. No difference with regard to the fraction of holes filled with WLS in mesenteric arteries between AMPKα2-KO and WT mice.

Mesenteric arteries from AMPK α2 WT and KO mice showed no difference regarding the fraction of holes filled with WLS. There was no difference between WT and AMPK α2 KO arteries (t-test, n.s $p>0.05$, n=7 or 9 from three mice).

3.7. PAI-1 expression was higher in AMPK α1-KO than WT artery, but not in AMPK α2-KO.

To search the mechanism by which AMPK could regulate MEJ dynamics, we studied the expression of PAI-1 which has been shown a stimulator of MEJ (Heberlein et al. 2010). For PAI-1 western blot, the whole mesenteric artery was isolated and equally divided into two parts. The vessels were then isolated and pooled for harvesting the proteins. The total AMPK (α1 and α2) in AMPK α1 KO was significantly reduced by 41.2% as compared to AMPK α1 WT mouse MA **(Figures 25 B and C)**. PAI-1 in AMPK α1 KO mice MA was significantly increased compared to WT littermates (t-test, $p<0.05$, n=6) **(Figures 25 B and D)**. In contrast, both total AMPK and PAI-1 expression in AMPK α2 KO mice MA were not different from their WT mice MA **(Figure 26)**.

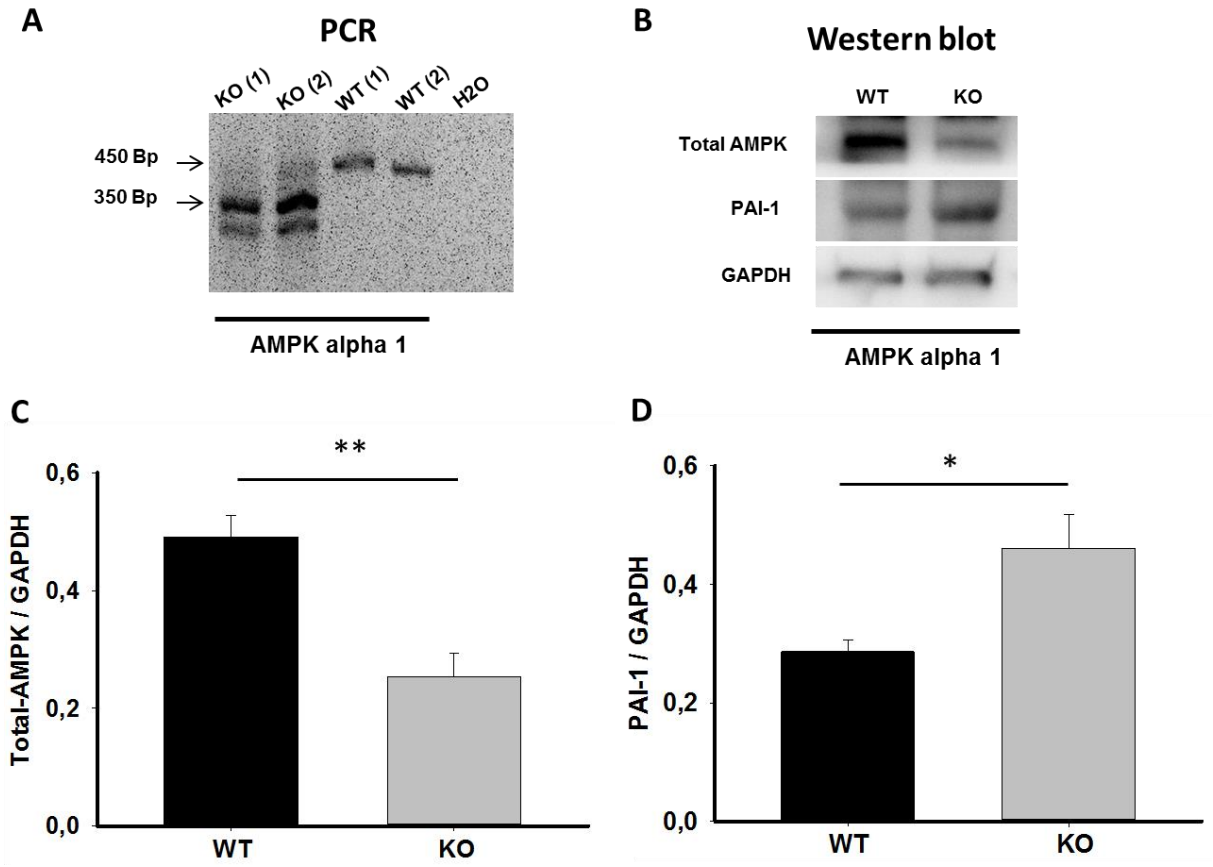

Figure 25. AMPK α1 KO arteries expressed more PAI-1 protein.

(A, B): PCR and Western blot of single arteries demonstrating knockout of AMPK α1 subunit. **(C):** Reduction of the AMPK protein in KO mice (t-test, **p<0.01, n=4). Note that the antibody stains α1 and α2 subunits. **(D):** Western blots revealed a significantly higher expression of PAI-1 in vessels of AMPK α1 KO mice (t-test, *p < 0.05, n=6).

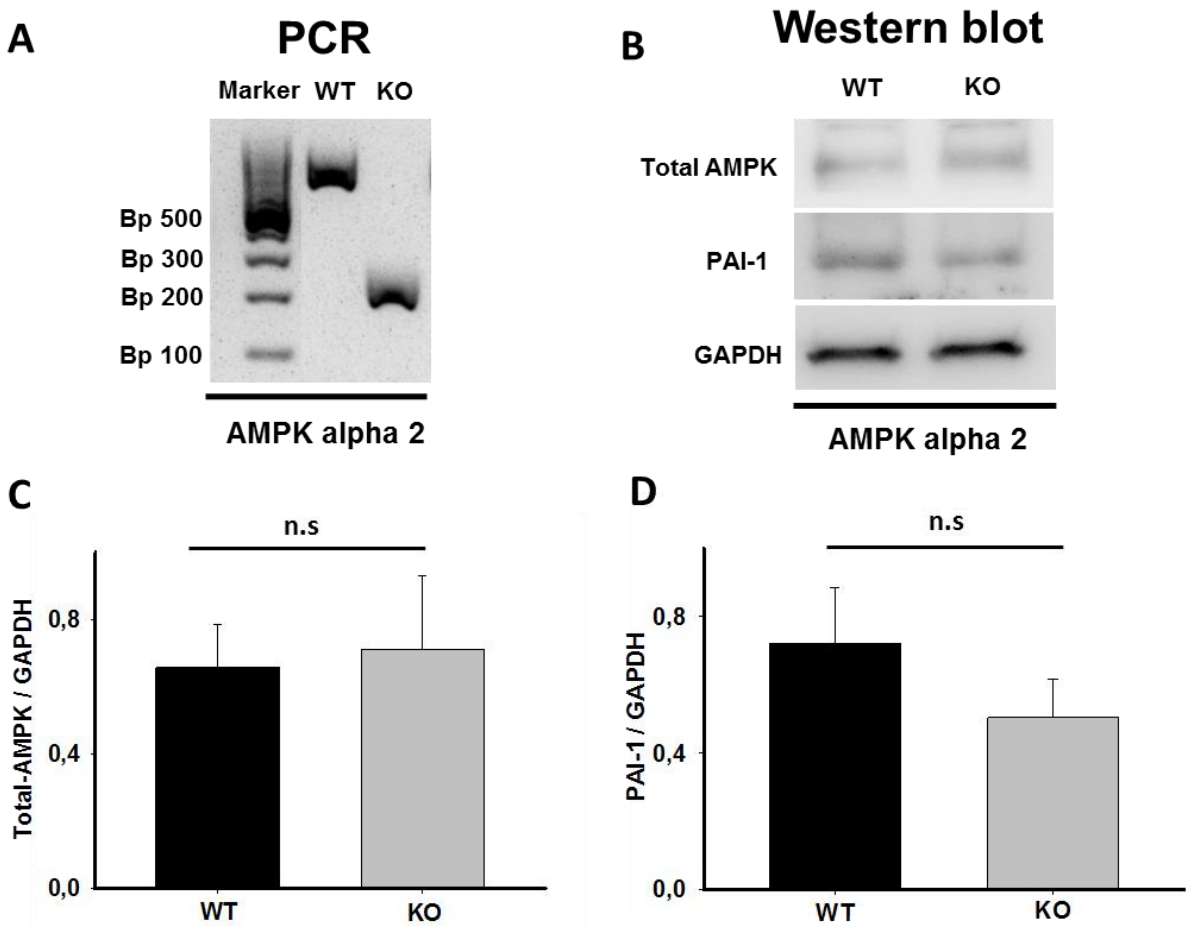

Figure 26. No change of PAI-1 expression in AMPK α2 KO artery compared to WT.

(A, B): PCR and Western blot of single arteries demonstrating knockout of AMPK α2 subunit. **(C):** No significant reduction of the total AMPK protein in KO mice (t-test, n.s $p>0.05$, n=3). Note that the antibody stains α1 and α2 subunits. **(D)**: Western blots revealed no significant difference of expression of PAI-1 in vessels of AMPK α2 KO mice (t-test, n.s $p > 0.05$, n=3).

3.8. Active-PAI-1 increased MEJs in intact artery.

MAs from C57BL6/N mice were isolated, cannulated, pressurized, and incubated with active PAI-1 (1 µg / ml) or DMSO as control at 37 °C for 6 hours. After this, the arteries were co-stained with calcein-AM red-orange from the luminal side and Alexa 633 from the abluminal side for the detection of MEJ and the IEL, respectively. PAI-1 treatment significantly increased the fraction of holes covered by MEJ by 26.3% ± 19.7% compared to the time control (n=4) (**Figure 27**).

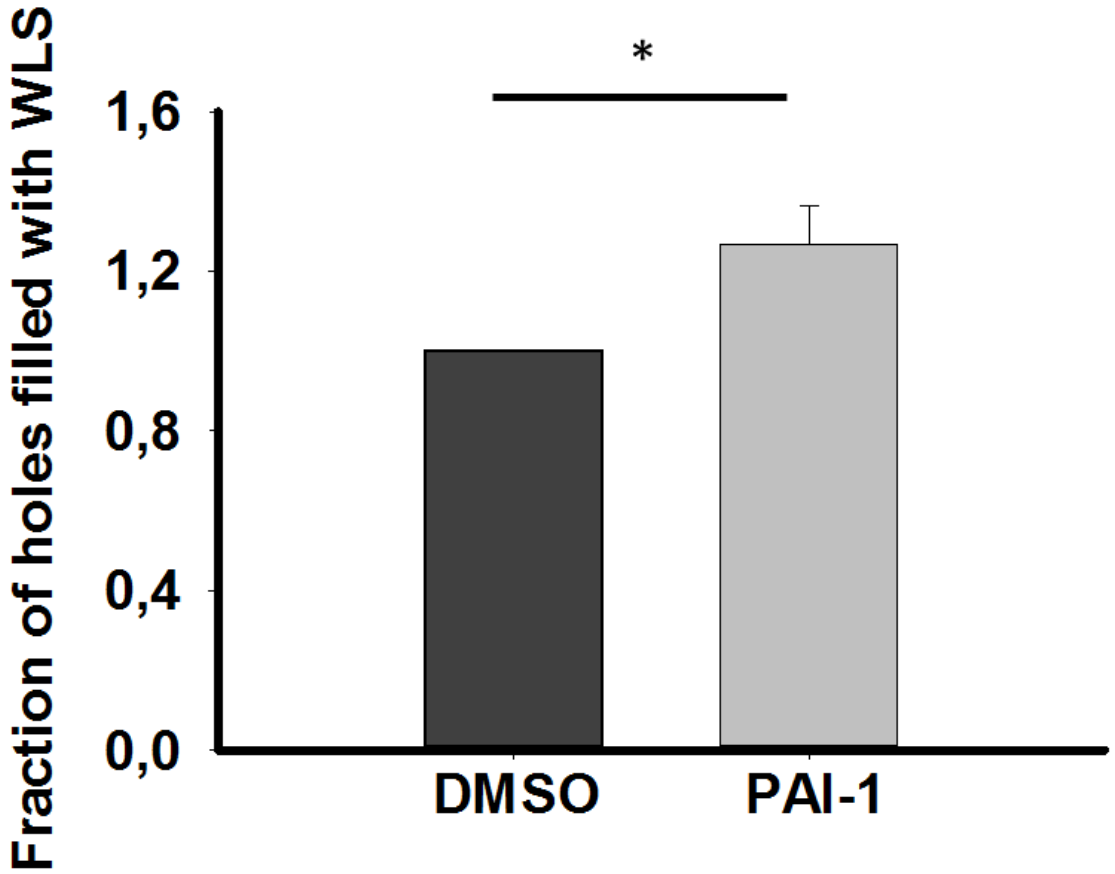

Figure 27. Active PAI-1 increased the fraction of holes filled with WLS.

Incubation with PAI-1 (or DMSO as control) for 6 hours significantly increased the fraction of holes filled with WLS. Values are normalized to the DMSO control (Mann-Whitney Rank Sum Test**,** * $p<0.05$, $n=4$).

3.9. AMPK activation reduced PAI-1 expression in intact artery.

Single intact mesenteric arteries were isolated from C57BL6/N mice and treated with 0.03% DMSO, A76 (10 µM) or A76 (10 µM) plus CC (10 µM) for 1 hour respectively, and then prepared for Western blot. The PAI-1 expression in arteries treated with A76 was significantly lowered by 39.9% of control arteries (n=6) (**Figures 28 A and D**). When A76 was combined with the AMPK inhibitor CC, the decrease of PAI-1 was blunted (One Way ANOVA, $p<0.05$, n=5 or 6) (**Figures 28 A and D**). The activation of AMPK by A76 as well as the inhibition by CC was assessed by the T172 phosphorylation level of the alpha subunit and by the phosphorylation of classic AMPK substrate protein ACC. Both, AMPK T172 and ACC phosphorylation levels were significantly increased in arteries after incubation with the AMPK activator A76 compared to DMSO control arteries **(Figures 28 A, B and C)**. In A76 and CC treated arteries, the increase of p-ACC was virtually blunted compared to A76 treated arteries (One Way ANOVA, $p<0.05$, n=3). Surprisingly the AMPK T172 phosphorylation level was even higher compared to other groups **(Figures 28 A, B and C).**

In contrast, CC did not exert any effect on PAI-1 expression and ACC phosphorylation in unstimulated arteries after incubation for 1 hour. However p-AMPK T172 was again significantly increased after incubation with CC compared to DMSO control (Mann-Whitney Rank Sum Test, $p<0.05$, n=3) **(Figure 29).**

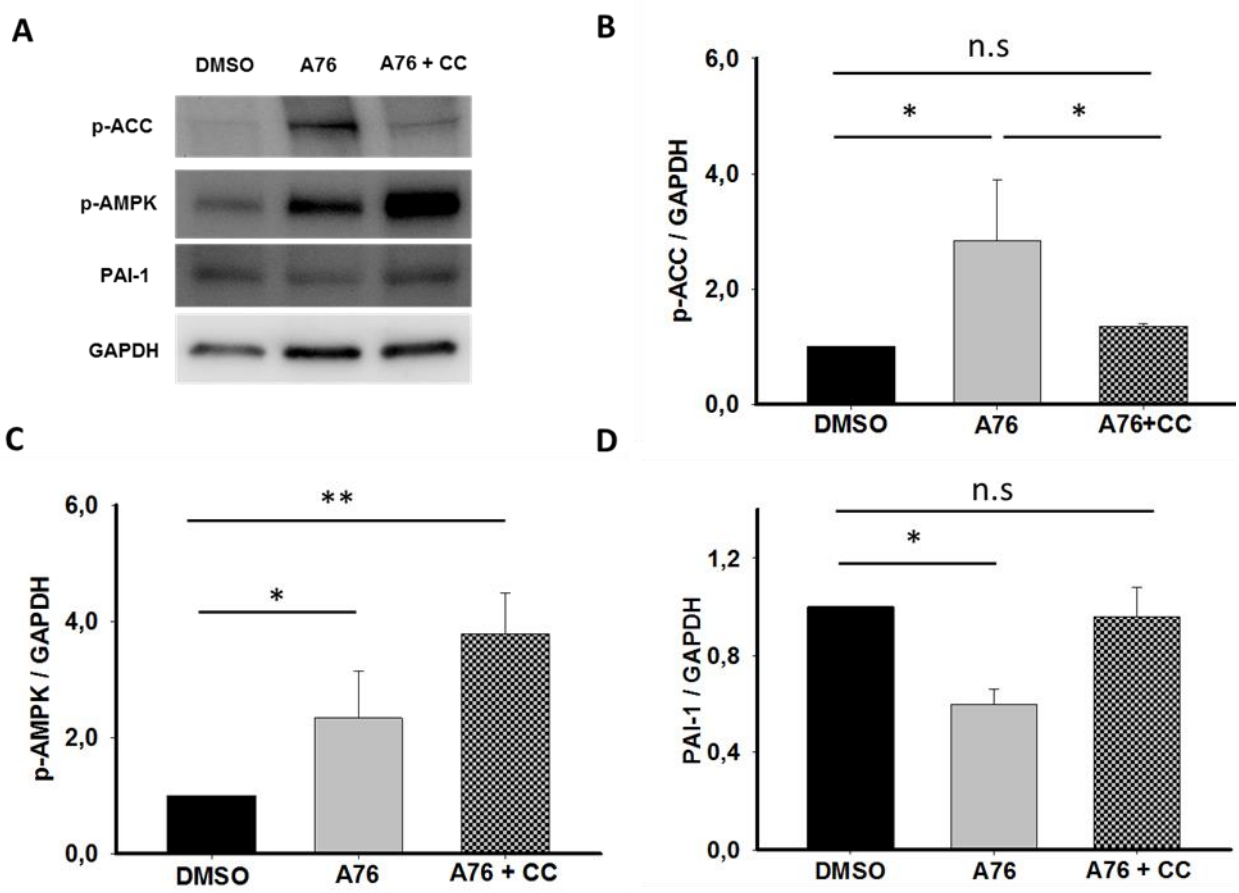

Figure 28. Activated AMPK reduced the PAI-1 expression in intact artery.

(A): Representative western blot demonstrating AMPK activation by A76 and its inhibition by CC. **(B):** A76 significantly increased the phosphorylation of the AMPK target ACC which was inhibited by CC (One Way ANOVA,*p<0.05, n.s p>0.05, n=3). **(C):** Phosphorylation of AMPK T172 in intact arteries. The phosphorylation was significantly increased by A76 but was even higher after combined treatment with CC (One Way ANOVA, *p<0.05, **p<0.01, n=6 or 5). **(D):** PAI-1 expression in intact arteries was significantly lowered after AMPK stimulation with A76 (One Way ANOVA, *p<0.05, n.s p>0.05, n=5 or 6). Values are normalized to DMSO control.

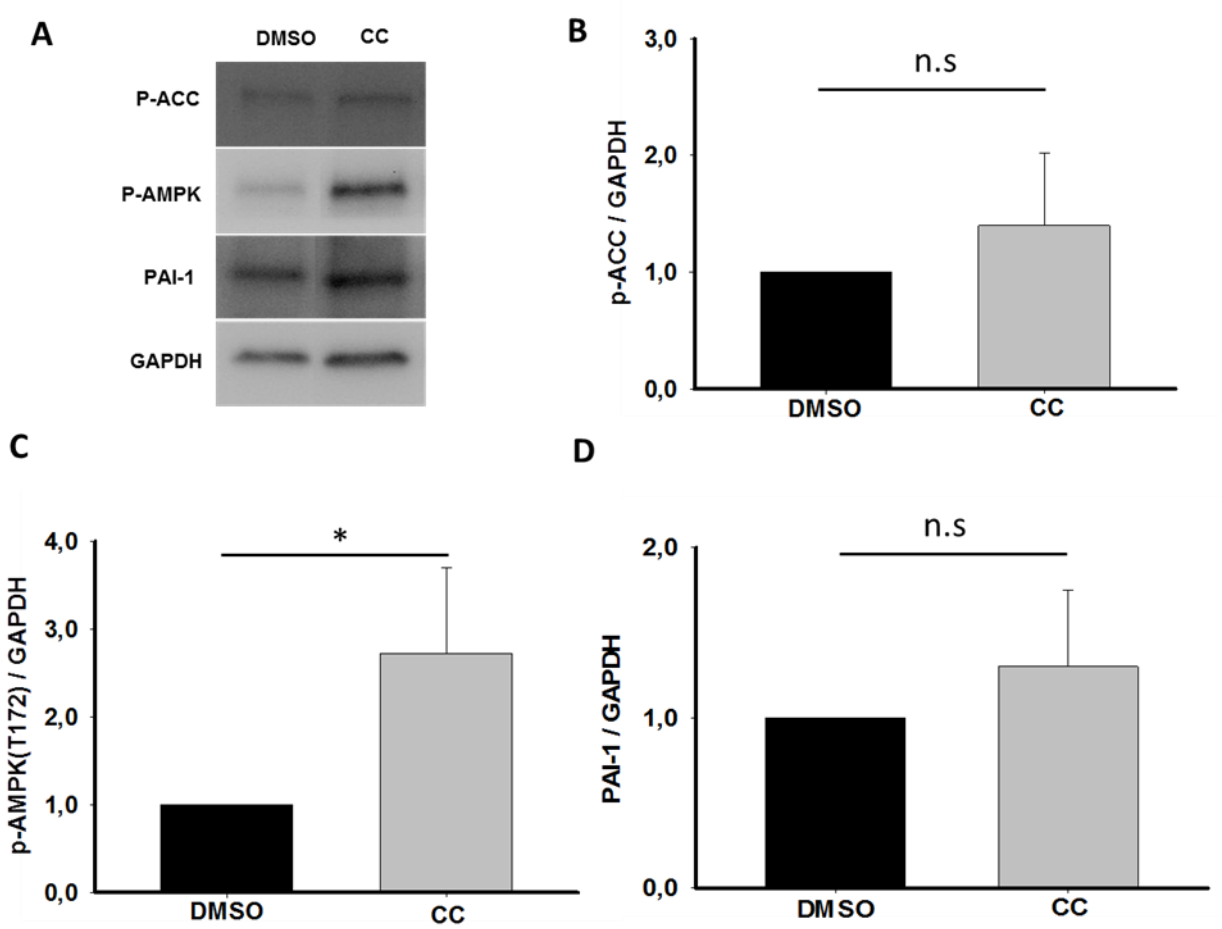

Figure 29. CC alone did not affect PAI-1 expression in unstimulated arteries.

(A): Representative Western blot showing no effect of CC on PAI or ACC phosphorylation **(B)**: No effect of CC on ACC phosphorylation (Mann-Whitney Rank Sum Test, n.s $p>0.05$, n=3). **(**C**)**: p-AMPK T172 was significantly increased in arteries after incubation with CC similar as in A76 treated vessels (Mann-Whitney Rank Sum Test, *$p<0.05$, n=3). **(D):** PAI-1 expression was not changed by CC treatment alone. (Mann-Whitney Rank Sum Test, n.s $p>0.05$, n=3). Values are normalized to DMSO control.

3.10. AMPK activation reduced the PAI-1 expression in PCASMC.

Cultured PCASMC were used to study whether the AMPK effects observed in intact vessels occurred at the level of vascular smooth muscle. The cells (3-6 passage, confluent 70 %-80 %) were treated with 0.03 % DMSO, A76 (100 µM) and A76 (100 µM) plus CC (15 µM) for 2 hours respectively, then detected the PAI-1 expression, p-ACC and p-AMPK by Western blot. PAI-1 expression was significantly lowered compared to control after AMPK activation with A76. Again, pretreatment with CC, virtually blunted the decrease of PAI-1 (One Way ANOVA, Mann-Whitney Rank Sum Test, n=4, $p<0.05$) **(Figures 30A and D)**. Like in intact vessels, AMPK T172 and ACC phosphorylation were significantly increased after A76 **(Figures 30A, B and C)**. While co-incubation with CC again blunted the increase of p-ACC, the AMPK T172 phosphorylation level was higher compared to other groups as observed in intact arteries **(Figures 30A, B and C).**

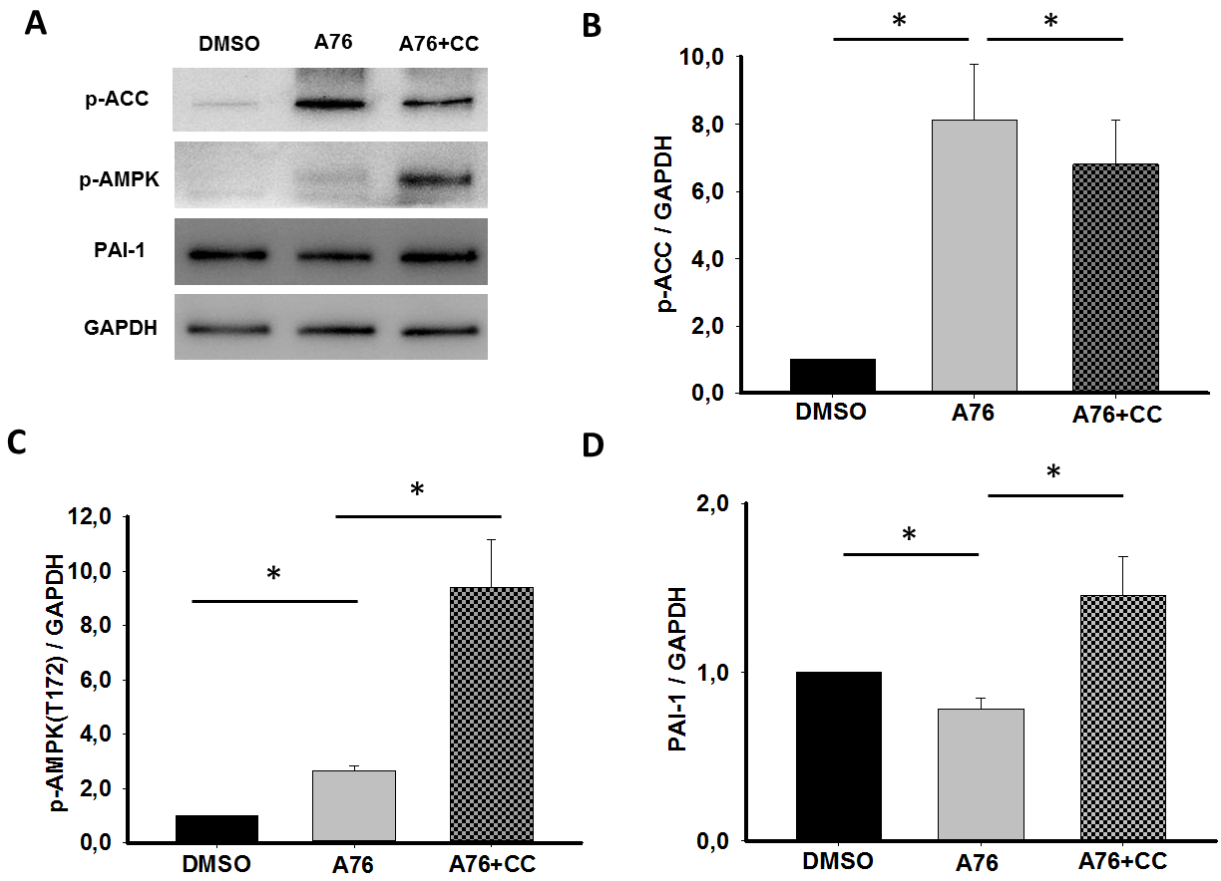

Figure 30. Activated AMPK reduced the PAI-1 expression in PCASMC.

(A): Representative Western blot demonstrating phosphorylation of the AMPK, its substrate ACC, and expression of PAI-1 under A76. **(B)**: ACC phosphorylation after AMPK stimulation and partial inhibition by CC (Mann-Whitney Rank Sum Test, *p<0.05, n=4) **(C)**: AMPK T172 phosphorylation was increased after A76 but further increased after CC, similar as observed in intact arteries (Mann-Whitney Rank Sum Test, *p<0.05, n=4). **(D)**: PAI-1 expression upon activation of AMPK was significantly lowered The AMPK inhibitor CC reversed this effect (One Way ANOVA and Mann-Whitney Rank Sum Test, *p<0.05, n=4). Values are normalized to DMSO control.

3.11. PAI-1 expression was increased after AMPK silencing with SiRNA in porcine and human VSM.

Additionally, in order to detect the influence of AMPK on PAI-1 expression in smooth muscle cells, cultured PCASMCs and HUVSMCs were studied. Cultures were either transfected with Ctrl siRNA or siRNA designed to silence the expression of both AMPK α-subunits (α1 and α2). After three days, AMPK-siRNA significantly inhibited AMPK protein expression in both of the two different type VSMCs. In PCASMCs, the level of AMPK protein was down regulated by 64.5 % compared to control by siRNA treatment (t-test, p<0,001, n = 7) **(Figures 31A and B)**. At the same time, PAI-1 expression in siRNA AMPK cells was significantly enhanced by 2.9 ± 1.5 fold compared to siRNA ctrl cells (t-test, ***p<0.001, n=10) **(Figures 31A and C)**. Similar results were obtained in HVUSMCs: the level of AMPK protein after siRNA treatment decreased by 69.7 % compared to control (t-test, p<0,01, n = 4) **(Figures 32 A and B)**. Whereas the PAI-1 expression was significantly increased by 2.6 ± 0.6 fold (t-test, ***p<0.001, n=4) **(Figures 32A and C).**

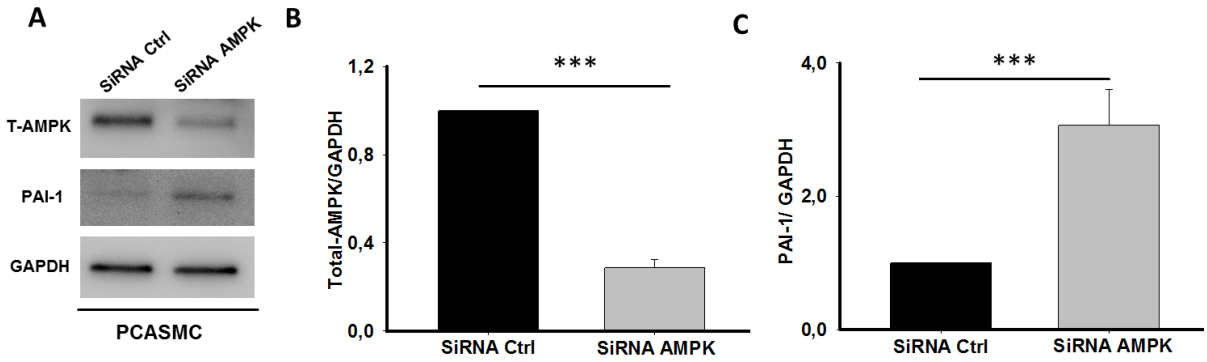

Figure 31. AMPK silencing increased the PAI-1 protein expression in PCASMC.

(A). Representative Western blot showing successful reduction of total AMPK (T-AMPK) expression and a concomitant increase in PAI-1 expression. **(B)**: Total AMPK expression in siRNA AMPK cells was significantly lower than in siRNA ctrl cells (t-test ***p<0,001, n=7). (C): PAI-1 expression in siRNA AMPK cells was significantly higher than in siRNA ctrl cells (t-test, ***p<0.001, n=10). Values are normalized to DMSO control.

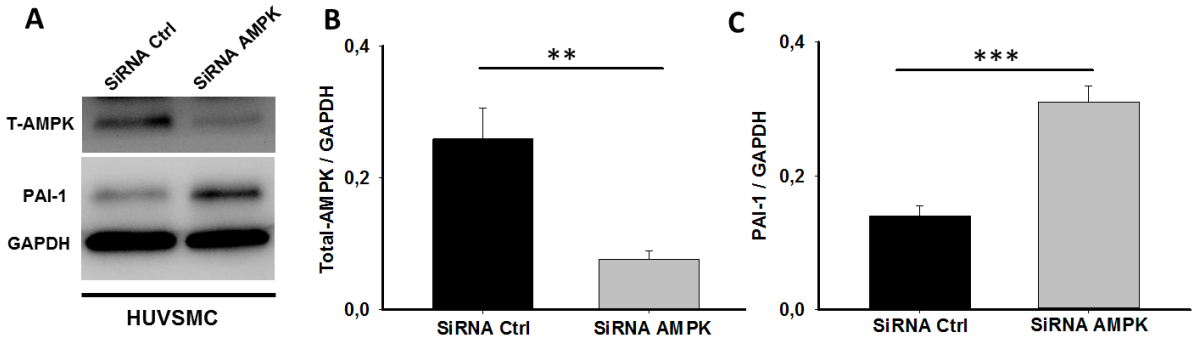

Figure 32. AMPK silencing increased the PAI-1 protein expression in HUVSMC.

(A). Representative Western blot demonstrating successful reduction of total AMPK expression (T-AMPK). **(B)**: Total AMPK expression in siRNA AMPK cells was significantly lower than in siRNA ctrl cells (t-test **p<0.01, n=4). (C): PAI-1 expression in siRNA AMPK cells was significantly higher than in siRNA ctrl cells (t-test, ***p<0.001, n=4).

3.12. PAI-1 expression was not significantly changed after AMPK silencing in HUVEC.

In order to detect the influence of AMPK on PAI-1 expression in endothelial cells, HUVEC were studied. The cells were transfected with AMPK siRNA (including α1 and α2 subunits) or Ctrl siRNA for two days, then harvested and lysed. siRNA AMPK treatment inhibited AMPK protein expression by 42 % of control (t-test, p<0,001, n=7) **(Figures 33 A and B).** However, PAI-1 expression in siRNA AMPK cells was not significantly altered (t-test, p>0.05, n=7) (**Figure 33 A and C**).

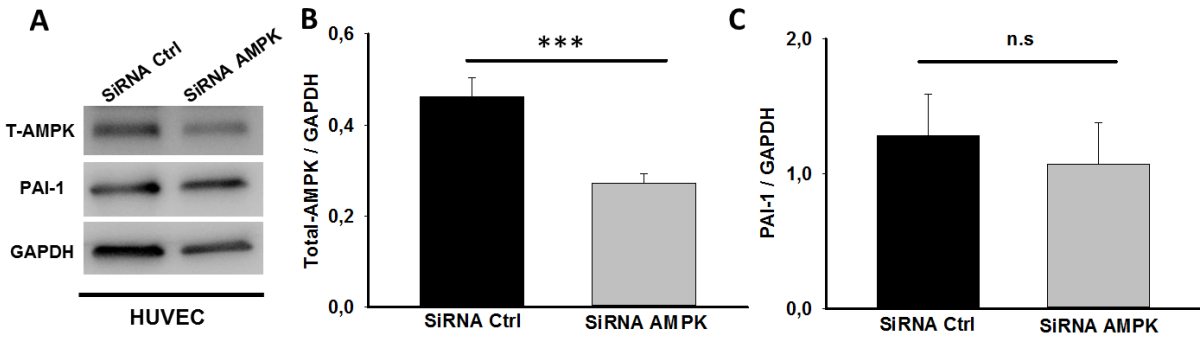

Figure 33. AMPK silencing did not change the PAI-1 protein expression in HUVEC.

(A): Representative Western blot demonstrating partial reduction of total AMPK (T-AMPK) protein after siRNA treatment. **(B):** Total AMPK expression in siRNA AMPK cells was significantly lower than in siRNA ctrl cells (t-test, ***p<0,001, n=7). **(C)**: In contrast to smooth muscle cells, PAI-1 expression in siRNA AMPK EC was not significantly changed compared to siRNA ctrl cells (t-test, n.s p>0.05, n=7).

3.13. SHP expression was inhibited in vessels of both AMPK α1 and AMPK α2-KO mice.

SHP has been reported to play a pivotal role on the transcriptional repression of many genes (Seol et al. 1996) including PAI-1. Total AMPK in AMPK α1 KO mouse MA was significantly reduced by 41.2% as compared to AMPK α1 WT mice MA (samples were the same which were used for detection of PAI-1) **(Figures 25B and C)**, SHP in AMPK α1 KO mouse MA was significantly decreased as compared to AMPK α1 WT mouse MA (p<0.001) **(Figure 34)**. However, virtually the same changes were observed in AMPK α2 KO mouse MA, SHP was significantly decreased in vessels of AMPK α2 KO mouse MA as well (t-test, **p<0,01, n=3) (**Figure 35**).

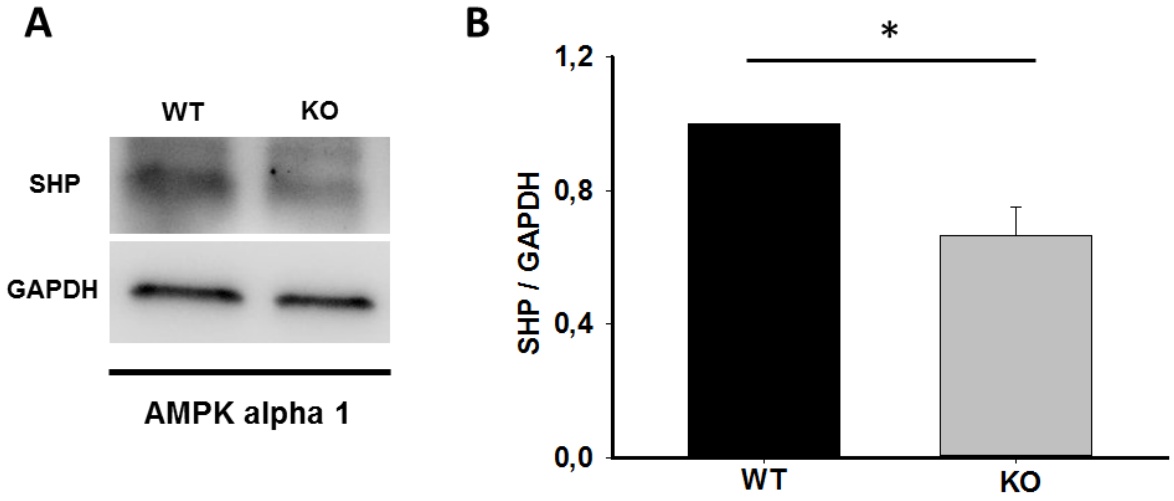

Figure 34. Lower SHP expression in AMPK α1 KO mice.

(A): Representative Western blot. **(B):** SHP expression was significantly lower in AMPK α1 KO than in WT mouse arteries (t-test, *p < 0,05, n = 7/5). Values are normalized to AMPK α1 WT mouse artery.

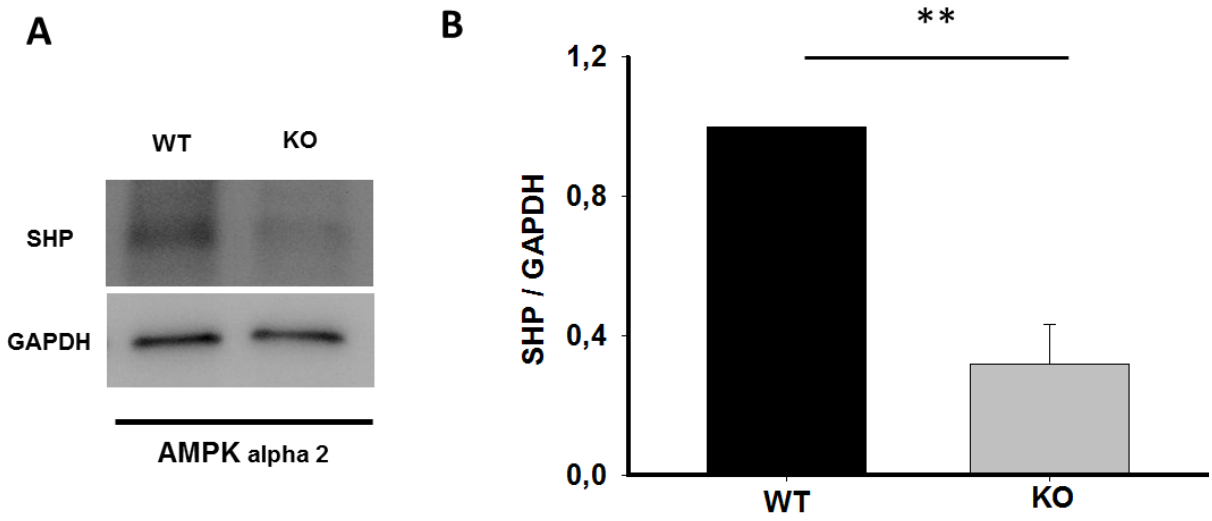

Figure 35. Lower SHP expression in AMPK α2 KO mice.

(A): Representative Western blot. **(B):** SHP expression in AMPK α2 mouse arteries was significantly lower in AMPK α2 KO than in WT mouse arteries. (t-test, **p<0,01, n=3). Values are normalized to AMPK α2 WT mouse artery.

4. Discussion

4.1. A short recapitulation of the most important findings.

In this thesis, results are presented which support a novel role of AMPK, in particular its alpha1 subunit, in controlling the formation of cell protrusions / MEJs. AMPK exerts its effects by modulating PAI-1, most likely via the SHP pathway. These findings were made in intact microvessels in which MEJs are known to play an important role in the control of vascular tone via EDH. Indeed, the magnitude of EDH dependent dilation by acetylcholine correlates well with changes in the expression of MEJ in these vessels. For the first time we can observe the dynamics of the formation of MEJ. Complementary studies in cultured smooth muscle cells suggest that the effect of AMPK occurs predominantly at the level of vascular smooth muscle.

4.2. Research models for MEJ.

Our studies were performed in intact small blood vessels which allow studying cell-cell contacts of MEJ in a physiological environment especially with respect to their dynamics which have not been in focus so far. Many, more artificial, models to study EC-VSMC communications via MEJ have been reported. EC-VSMC co-culture models allow investigation of intercellular communication, as well as the influence of co-culture on VSMC's protein expression and morphology (Wallace et al. 2007) Since cells can be better manipulated and connexin expression can be better controlled, this model allows to study regulation and permeability of MEJ, though these cells may lack some components present in intact vessels such as IEL proteins. Our laboratory has successfully used this model to study the regulatory effect of NO on calcium propagation via MEJ (Pogoda et al. 2014). A model which allows to study myoendothelial interactions and to harvest tissue components enriched in MEJ is a model where cultured EC and VSMC are cultured on opposite sides of transwell filters which to some extent mimics the vessel biological structure (D'Amore 1992; Fillinger et al. 1993). One of the major features of this model is that there is a membrane between EC and VSMC which separates the cells as the IEL does and spatially structures EC and VSMC interaction in a similar way as the IEL does. Due to these characteristics, this model is widely applied to investigate the MEJ functions in

vascular wall biology (Isakson & Duling 2005; Heberlein et al. 2010; Gairhe et al. 2011; Zhang et al. 2016; Jing Xu et al. 2017). There are also some other models, such as EC-VSMC co-culture separated with collagen gels (van Buul-Wortelboer et al. 1986), and spheroid-bound EC-VSMC co-culture (Korff et al. 2001). Recently, the three-dimensional sandwich co-culture model has also been created. In this model, EC and VSMC are separated by the membrane which is produced by VSMC autonomously, and they can contact each other closely by puncturing the membrane (Ganesan & Finsterwalder 2016). A common shortcoming of these models is that they rely on the properties of cultured cells. However culture conditions may decisively alter the characteristics of cells and their mutual interaction (Abdeen et al. 2016). Moreover, these models are not suitable to assess simultaneously for potential effects of MEJ manipulation on vascular tone which is only possible in intact vessels. This is an advantage of our model. Moreover, this model allows to study the dynamic behavior of cell-cell contacts and MEJ without potential alterations by culture conditions. The intact, cannulated vessel under physiological pressure, also known as the pressure myograph system, has been widely applied in vessel function research (Holger. Schneider et al. 2015; Schubert et al. 2017). Using this model, we can now confirm that an actin bridge, which has been described as a typical marker of MEJ in cell culture systems (Isakson, A. Best, et al. 2008; Heberlein et al. 2013), can also be observed in MEJ *in situ*. This actin bridge could be detected when using LifeAct mice. LifeAct is a peptide analogous to the first 17 aa of the actin binding protein 140, and can be used as a F-actin marker in mammalian cells. LifeAct can bind to F-Actin and can be detected by fluorescence microscopy when it is tagged with GFP (Riedl 2010). The transgenic LifeAct mouse is widely used to study the F-actin dynamics in intact cells (Richter et al. 2010). Our findings in small arteries of LifeAct mice could be confirmed using the F-actin staining compound phalloidin (Riedl 2010), which however could only be obtained under static conditions, since the cells need to be permeabilized for phalloidin to reach the cellular actin (Faulstich et al. 1980). Much to our surprise we found that incubation of endothelial and smooth muscle cells *in situ* with the calcium indicator calcein reproduced exactly the same imaging of the structures that were obtained with LifeAct and phalloidin. It is not clear at present, that calcein binds to actin and it should be emphasized that calcein staining did not reproduce the pattern of LifeAct actin staining throughout the whole cell but rather in MEJ. It is therefore more likely that the dynamics of F-Actin

formation in MEJ may require local elevation of calcium (eliciting local calcein fluorescence) that comes from the adjacent endoplasmic reticulum which is a cellular calcium store. However, more studies are necessary to prove this explanation. Nevertheless, calcein staining allowed us to study the formation of MEJ and to dispense LifeAct which gave us better possibilities to stain other structures simultaneously.

4.3. Cell protrusions and / or MEJ?

Using microscopic techniques we identified primarily wheel like structures (WLS)with spokes and a hub consisting of F-actin. These structures had diameters between 5 µm and 9 µm which may comprise the range of diameters of fully developed and growing and of vanishing cell protrusions as well. We know from electron microscopic studies that gap junctions are usually clusters of intercellular channels which cover a whole area of connexons in the cell membrane (Sosinsky & Nicholson 2005), obviously still much smaller than the observed WLS. As a consequence we did not directly observe gap junctions. We propose, however, that all these WLS contained gap junctions for the following reasons. Actin-rich structures along cell membranes have been found to be the scaffold for functional microdomains such as MEJ, podosomes and focal adhesions (Isakson, A. K. Best, et al. 2008; Murphy & Courtneidge 2011; Yamin & Morgan 2012). We could distinguish these cell protrusions from podosomes produced by in EC and VSMC since they had no direct contact to each other and showed a different staining pattern e.g with cortactin and MMP-14. The podosomes were even more dynamic actin structures with a clear circular assembly. They also showed a different localization than the actin rich WLS and could not be assigned to holes in the IEL. In contrast the cone-like structures characterized as WLS were always located in IEL holes and stained positive for Cx37, Cx43, and PAI-1 proteins which are enriched in MEJ (Isakson, A. K. Best, et al. 2008; Heberlein et al. 2012). MEJs were located in holes of the IEL the only sites which allow direct gap junctional contact of VSM and EC in these small vessels (Straub et al. 2014).

Moreover, the amount of WLS as quantified by fluorescent microscopy in our vessels were expressed to the same amount as observed with independent methods such electron microscopy in vessels of similar size (Sandow et al. 2009). Thus, we

conclude that the WLS allowed us to study indirectly the myoendothelial gap junctions present in these vessels.

4.4. Dynamics of MEJs vs. connexins / Gap junctions.

Gap junction function can be regulated acutely via phosphorylation of the key residues on connexin subunits (Segal & Bagher 2010). Our group has found that NO can modulate calcium signal propagation through MEGJ by protecting Cx37 from dephosphorylation at Y332 via inhibition of the phosphatase SHP-2 (Pogoda et al. 2014; Pogoda et al. 2017). The gap junction protein complexes in the cell membrane undergo hourly high turnover with half life times around two hours (Segal & Bagher 2010). For example, connexin 26, connexin 30 and connexin 43 can be down-regulated within 6 hours of wounding at the wound edge (Davis et al. 2013). But only few studies focus on the kinetics of MEJ formation and regression (Heberlein et al. 2010). Until now, there is no information about the detection of MEJ dynamics in intact arteries. To the best of our knowledge, in this project, we can present for the first time results on the dynamics of MEJs, observed here as WLS structures. We were, however, not able to study whether all MEJ also contained MEGJ. Dynamic changes could be observed in the presence of the gap junction inhibitor compound C, whereas the vessels of AMPK a1 KO mouse reflected a new steady state. The effect of CC was specific, since in AMPKa1 KO mice, it did not increase MEJ any further. Interestingly acute AMPK stimulation did not acutely reduce the number of MEJ, which could suggest a full inhibitory effect already of basal AMPK activity in the cells.

4.5. MEJ as interactomes

MEJ represent important EC-VSMC signal communication domains in the resistance artery wall (Straub et al. 2014) which are enriched in channels, enzymes and regulatory molecules. For example, it has been demonstrated that the endoplasmic reticulum (ER), caveolae and ribosome organelles are enriched in MEJ in vitro and in vivo (Straub et al. 2011; Isakson et al. 2007; Heberlein et al. 2013). ER enrichment at MEJ may be required to serve as local calcium pool which is important for the local activation of cell signaling cascades. There is also evidence the ER is enabling local protein translation in the area (Straub et al. 2014). In the current study, using ER-Tracker™ ER-Bodipy staining in the living, intact artery we could show the presence

of ER in the MEJ. ER-Tracker™ ER-Bodipy dye is a live-cell stain and highly selective for ER (Zünkler et al. 2004). It has also been confirmed that scaffolding proteins such as actin and microtubules, are extensively localized in MEJ (Isakson, A. Best, et al. 2008). This is considered important for protein trafficking towards these areas. The enrichment of F-actin in MEJ could be detected in living LifeAct as well as after fixation and phalloidin staining.

MEJ play also a critical role in the tone regulation of resistance arteries (Straub et al. 2014). Nitric oxide (NO) is an important dilator, and endothelial NO synthase also localizes in MEJ (Straub et al. 2011; Straub et al. 2012). In resistance arteries, endothelial dependent hyperpolarization (EDH) is considered functional more important than NO signaling. Most of EDH related channels and proteins, (such as transient receptor potential 4 (TRPV4), IP3-R, Na^+/K^+ -ATPase, K_{IR} channel, SKca channels and BKca-channel) (Ledoux et al. 2008; Tian & Xie 2008; Sonkusare et al. 2012; Absi et al. 2007), as well as epoxyeicosatrienoic acid and caveolin-1 are enriched in MEJ (Isshiki & Anderson 2003). Connexins were also been shown to be enriched in MEJ (Langlois et al. 2008) and they may not only function to firm gap junctions but also serve as scaffolds for protein complexes (Pogoda et al. 2017).

4.6. AMPK, a universal cell regulator.

AMPK is a heterotrimeric enzyme including a catalytic α subunit and two regulatory subunits β and γ, with a different combination and unequal distribution in diverse tissues (Hardie 2007). It has been characterized as a critical sensor of cellular energy status in all eukaryotic cells and can be activated by the increase in AMP:ATP and ADP:ATP ratios (Lin & Hardie 2017). In general, AMPK inhibits anabolic metabolism to restore energy, and promotes catabolic metabolism to generate ATP (Garcia & Shaw 2017). These catabolic processes include glucose uptake, glycolysis, fatty acid oxidation and mitochondrial biogenesis (Hardie 2008). All of these processes require the supply of cells with substrates and oxygen which is delivered by blood flow. Enhancement of catabolic metabolism therefore implies that the microcirculation allows a higher blood flow which can be achieved when resistance arteries dilate. Indeed, we have found before that AMPK activation can dilate resistance artery via calcium-dependent and -independent pathways (Holger. Schneider et al. 2015; Schubert et al. 2017).

4.7. AMPK expression in blood vessels.

AMPK is expressed both in endothelium and smooth muscle (Stahmann et al. 2010; Pyla et al. 2015), and exerts an important function for the regulation of vascular tone (I. P. Salt & Hardie 2017). In our former studies we have described that all of the isoforms of AMPK α (α1 and α2) and β (β1 and β2) subunits are expressed in hamster microvascular system (Holger. Schneider et al. 2015). Like others, we find that AMPK α1 is the major isoform and accounts for the majority of total AMPK in vascular system (Francoise Goirand et al. 2007; Stahmann et al. 2010). Our results obtained in this study from intact small mouse arteries also show the knockout of AMPK α1 but not of AMPK α2 went along with a drastic reduction of the total AMPK α expression in western blots, further supporting the view that AMPK α1 was the predominantly expressed catalytic isoform. The subcellular distribution of AMPK in various cell types has been shown to be very different, which seems to be dependent on the subunit composition with a more dispersed subcellular distribution of AMPK α2 and γ2, and predominantly cytoskeletal location of α1 and γ1 subunits (Pinter et al. 2013; Pinter et al. 2012). In heart, the AMPK γ2 subunit has been found to co-localize with the T-tubule system and SERCA2 (Pinter et al. 2013). Furthermore, we have found previously that AMPK is essential for SERCA function via regulating the phosphorylation status of PLN on Thr17 in VSMC of small arteries (Holger. Schneider et al. 2015). Moreover, in a study conducted in pancreatic cells, AMPK was capable to change ER (inhibition caused ER expansion and ER stress) and mitochondrial morphology via phosphorylation and thus regulating Dynamin-related protein 1 (DRP-1) (Wikstrom et al. 2013). AMPK activation is also involved in regulating the F-actin dynamics (Schubert et al. 2017) in smooth muscle cells. F-actin cytoskeletal components are enriched in MEJs as shown here by us and before by others (Heberlein et al. 2009).

4.8. Verification of the AMPK activation state

It is important for the interpretation of our findings to confirm that AMPK stimulators indeed activated AMPK. On the other hand it is important to verify that siRNA treatment as well as treatment with the unspecific pharmacologic inhibitor of AMPK, compound CC really affected expression or in the latter case – the activity of the enzyme. According to the literature as an indicator for activation of AMPK, two

protein phosphorylation are accepted. One is the phosphorylation of Thr-172 of the AMPK alpha units (S. a Hawley et al. 1996). The other one is the phosphorylation state of its direct cellular substrate acetyl-CoA carboxylase (ACC) (Salt & Hardie 2010; C. Zhang et al. 2017). Higher level of ACC phosphorylation are indicating stronger AMPK activation. Here we could indeed show that treatment with A76, an activator of AMPK, significantly enhanced AMPK phosphorylation at Thr-172 and ACC phosphorylation in intact vessels, which is in accordance with former studies in animal and culture cells (Göransson et al. 2007). Conversely, treatment with CC or treatment with siRNA reduced ACC phosphorylation as expected, thus confirming efficacy of the treatment.

However, CC unexpectedly also increased AMPK α phosphorylation at Thr-172. This is at variance with several studies (Chakrabarti et al. 2015; Zhou et al. 2017), but at least one study in yeast cells showed that binding of a adenylate ligand at the interface between AMPK kinase domain and the heterotrimeric core can significantly reduce AMPK's catalytic activity without affecting phosphorylation level of Thr 172 (Chandrashekarappa et al. 2013). Since it is not known how CC exactly acts as the inhibitor of AMPK, it is possible that Thr172 phosphorylation is not a reliable indicator of AMPK activity in the presence of CC.

4.9. AMPK α1 modulation of MEJ dynamics

In our experiments we observed that arteries of AMPK α1 KO mice expressed significantly more WLS. This was not the case in AMPK α2 KO which suggests that the effect was dependent on AMPK α1. Though proper littermates were used as control, these experiments alone cannot exclude that the effect was only an indirect one based on unspecific side effects of chronic AMPK rundown. However we could show that treatment with CC and acute siRNA treatment had the same effects within a few hours, i.e an acute increase of the number of WLS in intact vessels which to our knowledge is the first time that short term, dynamic alterations of WLS formation could be observed. We therefore conclude that AMPK via the α1 subunit reduces the formation of WLS and hence of MEJ. Such an effect of AMPK has not yet been described before.

Using co-culture models Heberlein et al. have described that less MEJs went along with less formation of actin bridges (Heberlein et al. 2010). Therefore it is possible

that part of the AMPK effects are due to inhibitory AMPK effects on F-actin formation. We have shown before, that AMPK can degrade F-actin via activation of the actin severing protein cofilin (Schubert et al. 2017).

4.10. AMPK regulates MEJ dynamics via PAI-1.

Our findings suggest that AMPK is exerting its inhibitory effects on MEJ at least in part via downregulation regulating PAI-1 expression. Indeed PAI-1 consistently showed changes which were inverse to changes of AMPK activity or expression under such different conditions as genetic AMPK knockout, siRNA treatment and pharmacological inhibition in vascular smooth muscle.

This is in accordance with a report demonstrating that PAI-1 gene can be down-regulated via AMPK pathway (Chanda et al. 2009). A signaling cascade comprising adiponectin-AMPK-PAI-1 was also shown to play a significant role in the gender specific difference regarding susceptibility to develop nonalcoholic fatty liver disease (NAFLD) (Spruss et al. 2012).

Local translocation and knock-out models of PAI-1 have suggested that this compound, also elevated under obese conditions, is essential for MEJ formation with more MEJ formed with higher PAI-1 amounts (Heberlein et al. 2010; Heberlein et al. 2013). Other authors have also described a similar effect of PAI-1 on MEJ in murine corporal tissue vessel system (Kavoussi et al. 2015).

Interestingly, Heberlein et al also have shown that the amount of PAI-1 expressed depends on microtubule binding ability and local translation of PAI-1 mRNA at the rough ER near MEJ (Heberlein et al. 2012). AMPK can also modulate microtubule stability via phosphorylation of CLIP-170 (Nakano et al. 2010) and ER function by SERCA (Holger. Schneider et al. 2015).

PAI-1 does not only influence coagulation and fibrinolysis, but has been shown to have other functions (Rijken & Lijnen 2009). In the context of MEJ, it may play a compensatory role to maintain MEJ dependent endothelial dependent hyperpolarization and dilation in obesity, as elevated amounts of MEJs were found in the coronary arteries of C57Bl/6 mice fed with a high-fat diet. This went along with an elevation of PAI-1 levels (Heberlein et al. 2010). In the same study, they also found a faster endothelial Ca^{2+}-increase to phenylephrine in a vascular cell co-culture model

when recombinant PAI-1 was present. Since only smooth muscle cells respond to phenylephrine , the increase in endothelial calcium was considered to be due to MEJ calcium transfer (Heberlein et al. 2010).

It is not yet clear however, how AMPK regulates PAI-1 expression. PAI-1 synthesis is regulated by many factors and on many levels (Agirbasli 2005). Its expression can be stimulated by inflammatory state (Emeis & Kooistra 1986; Sawdey et al. 1989) and hypoxia in human EC etc. (Gerber et al. 1993)**.** High fat diet and TNF-α stimulation facilitate the increase of PAI-1 by stabilization of PAI-1 mRNA at MEJs location via mRNA binding protein-serine binding protein-1 (Heberlein et al. 2012). Recently, it was shown in HepG2 cells that AMPK can negatively regulate PAI-1 via increase of the silencer small heterodimer partner (SHP) (Chanda et al. 2009). Our current study shows that SHP was indeed down-regulated in AMPK α1 KO mice which would result in an increased PAI-1 expression as observed. However, such a downregulation was also observed in vessels of AMPK α2 KO mice which did not show alterations in MEJ. Thus, more research appears to be necessary to elucidate the concrete mechanism of AMPK modulating PAI-1 expression.

4.11. Endothelial vs. smooth muscle regulation

Of note, western blots of small isolated vessels do not help to differentiate between whether changes of protein expression occur in the endothelium or in smooth muscle. There are techniques to remove the endothelium such as perfusion with air (Holger. Schneider et al. 2015) but complete removal cannot be confirmed when the vessel is supposed to be used for western blot. Thus, we performed further studies using cultured cells. These could not be isolated in sufficient amounts and purity from the small vessels so that endothelial cells from other origin and species had to be used, HUVEC and porcine or human coronary artery smooth muscle cells. Interestingly, all findings from isolated vessels could be confirmed in cultured smooth muscle cells using siRNA and Compound C. In contrast, in HUVEC, PAI-1 was not significantly changed with silencing of AMPK. The results may be species or tissue specific. Alternatively, the endothelial AMPK was not suppressed sufficiently so that the residual AMPK could still exert an effect on PAI-1 expression. This requires further research especially since the work of Heberlein et al appears to indicate that PAI-1 changes at the endothelial side are important for the effects on MEJ which they

observed (Heberlein et al. 2010). Of note, data from arteries of inducible endothelial AMPK α1 KO mice showed a loss of EDH function (Enkhjargal et al. 2014) whereas we found an increase in a global knockout model, i.e. after (additional) KO of smooth muscle AMPK.

4.12. ACh-induced dilatation in AMPK α1 KO mice: related to the higher amount of MEJ?

In many studies including some from our own lab (Steffen-Sebastian Bolz et al. 1999; Hoepfl et al. 2002) it has been shown that acetylcholine (ACh) elicits an endothelium dependent dilatation. The endothelium dependency of ACh mediated dilation has been shown by us before in the mesenteric arteries, the same vessels type which was studied here (Pogoda et al. 2017). When ACh binds with its receptor on EC, mainly M1 and M3, VSMC dilators (NO, PGI and EDHFs) are produced, and these dilators induce VSMC relaxation (Rubanyi 1991). NO and PGI are synthesized by nitric oxide synthase (NOS) and cyclooxygenase respectively from their respective precursors L-arginine and arachidonic acid (Shu et al. 2015; Hara 2017) and diffuse from EC to VSMC to elicit dilation. Their formation can be inhibited by the NOS inhibitor L-NAME and the cyclooxygenase inhibitor INDO respectively. Endothelium dependent hyperpolarization (EDH) also leads to vasodilation of smooth muscle. There is some evidence that several EDHFs can be produced by the endothelium to elicit vasodilation (Garland & Dora 2017). Potassium ions which are released from the endothelium after activation of SKca and IKca channels (Rasmussen et al. 2016) are thought to represent one EDHF since they can hyperpolarize underlying smooth muscle cells by activation K_{ir} channels AND Na^+/K^+ ATPase (Jackson 2017). Endothelial potassium channels are enriched in myoendothelial junctions (Ledoux et al. 2008; Tian & Xie 2008; Sonkusare et al. 2012; Absi et al. 2007). This is the potential basis for the findings first reported by Tudor Griffith, that “EDH” effects require the presence and intact function of MEJ (Griffith et al. 2004). The calcium in VSMC will increase and induce VSMC contraction when ACh directly binds to the M1 or M3 on VSMC (Rourke & Vanhoutte 1992) but this effect is weak and does not affect the net dilation observed with intact endothelium.

In accordance with this, we found that in small arteries exhibiting higher amounts of WLS/MEJ there was an enhanced ACh induced endothelium dependent dilation. This

dilation was elicited in the continuous presence of L-NAME and Indo which excludes NO and PGI_2 as mediators so that it was an EDH-induced dilation confirming that MEJ plays an important role for this type of dilation. It should be mentioned here, however, that our findings obtained with CC do not fully support this conclusion. While we could show that CC increases the amount of MEJ, we also observed a reduction of the calcium signal passing into smooth muscle cells from endothelium, suggesting a reduction of MEJ permeability. This may be due to an unspecific effect of CC on gap junction permeability which reduces the transfer in spite of a higher number of MEJ. Though we consider it unlikely, we can also not exclude at this point that AMPK KO could also have some changes of MEJ permeability which would make it difficult to assume a linear correlation between the number of MEJ and the resulting dilation.

4.13. Potential physiological relevance of the mechanism.

The vast majority of studies have shown that AMPK activation is beneficial for artery relaxation and blood flow (E. a Bradley et al. 2010; Enkhjargal et al. 2014; Wang et al. 2012; Ford & Rush 2011), For example, AMPK inhibition and deletion has been reported to be neuroprotective and reduce infarct size (Li et al. 2007).

In accordance with this we have also shown that AMPK is a potent vasodilator which exerts its dilator effects at the level of vascular smooth muscle by reducing the cytosolic calcium level and the calcium sensitivity of the contractile apparatus (Holger. Schneider et al. 2015; Schubert et al. 2017).

Under these conditions it is difficult to understand why AMPK should reduce expression of MEJ. A recent study from our lab, analyzing the effect of NO on Cx37 dependent control of MEJ permeability appears to shed some light on this question (Pogoda et al. 2014; Pogoda et al. 2017). In this work it could be shown that an inhibition of MEJ permeability preserved endothelial calcium losses towards the underlying smooth muscle and increased endothelial sensitivity to vasoactive agonists. Therefore, too many MEJ could reduce endothelial vasomotor function implying that the number of MEJ needs to be tightly regulated. It is also conceivable that we observe a compensatory mechanism: when AMPK dilation is reduced, e.g. in obesity being characterized by reduced levels of the endogenous AMPK stimulator adiponectin, an increased EDH could partly compensate for it.

In summary, our study provides first data on MEJ dynamics. In the model of isolated intact vessels, MEJ regulation can be studied while the cells remain in their natural environment. The data also provide evidence for a hitherto unknown role of AMPK in the regulation of MEJ expression. Further studies have to show whether this disturbances of this function and related changes of PAI-1 expression, e.g. in inflammation, have pathophysiologic relevance and whether specific treatment of AMPK activity will offer new therapeutic options.

References

Abdeen, A.A., Lee, J. & Kilian, K.A., 2016. Capturing extracellular matrix properties in vitro: Microengineering materials to decipher cell and tissue level processes. *Experimental biology and medicine (Maywood, N.J.)*, 241(9), pp.930–8. Available at: http://www.ncbi.nlm.nih.gov/pubmed/27075930\nhttp://www.pubmedcentral.nih.gov/articlerender.fcgi?artid=PMC4950351.

Abounit, S. & Zurzolo, C., 2012. Wiring through tunneling nanotubes – from electrical signals to organelle transfer.

Absi, M. et al., 2007. Effects of methyl beta-cyclodextrin on EDHF responses in pig and rat arteries; association between SK(Ca) channels and caveolin-rich domains. *British journal of pharmacology*, 151(3), pp.332–40. Available at: http://www.pubmedcentral.nih.gov/articlerender.fcgi?artid=2013982&tool=pmcentrez&rendertype=abstract.

Agirbasli, M., 2005. Pivotal role of plasminogen-activator inhibitor 1 in vascular disease. *Ltd Int J Clin Pract*, (January), pp.102–106.

Alba, G. et al., 2004. Stimulators of AMP-activated protein kinase inhibit the respiratory burst in human neutrophils. , 573, pp.219–225.

An, H. et al., 2016. Journal of Diabetes and Its Complications Metformin attenuates fluctuating glucose-induced endothelial dysfunction through enhancing GTPCH1-mediated eNOS recoupling and inhibiting NADPH oxidase. *Journal of Diabetes and Its Complications*, 30(6), pp.1017–1024. Available at: http://dx.doi.org/10.1016/j.jdiacomp.2016.04.018.

Angin, Y. et al., 2016. Regulation of Carbohydrate Metabolism , Lipid Metabolism , and Protein Metabolism by AMPK. , pp.23–43.

Bain, J. et al., 2007. The selectivity of protein kinase inhibitors : a further update. , 315, pp.297–315.

Bang, S. et al., 2017. Novel regulation of melanogenesis by adiponectin via the AMPK/CRTC pathway. *Pigment cell Melanoma Res*, 8.

Bathany, C. et al., 2011. High throughput assay of diffusion through Cx43 gap junction channels with a microfluidic chip. *Analytical Chemistry*, 83(3), pp.933–939.

Bergheim, I.N.A. et al., 2009. Metformin prevents alcohol induced liver injury in the mouse critical role of plasminogen activator inhibitor-1. , 130(7), pp.2099–2112.

Biwer, L.A. et al., 2016. Two functionally distinct pools of eNOS in endothelium are facilitated by myoendothelial junction lipid composition. *Biochimica et Biophysica Acta - Molecular and Cell Biology of Lipids*, 1861(7), pp.671–679. Available at: http://dx.doi.org/10.1016/j.bbalip.2016.04.014.

Bloemendal, S. & Kück, U., 2013. Cell-to-cell communication in plants, animals, and fungi: A comparative review. *Naturwissenschaften*, 100(1), pp.3–19.

Bolz, S.-S., de Wit, C. & Pohl, U., 1999. Endothelium-derived hyperpolarizing factor but not NO reduces smooth muscle Ca2+ during acetylcholine-induced dilation of microvessels. *British Journal of Pharmacology*, pp.124–134.

Bolz, S.-S., Wit, C. De & Pohl, U., 1999. Endothelium-derived hyperpolarizing factor but not NO reduces smooth muscle Ca2+ during acetylcholine-induced dilation of microvessels. *British journal of pharmacology*, 128(1), pp.124–34.

Bradley, E. a et al., 2010. Activation of AMP-activated protein kinase by 5-aminoimidazole-4-carboxamide-1-beta-D-ribofuranoside in the muscle microcirculation increases nitric oxide synthesis and microvascular perfusion. *Arteriosclerosis, thrombosis, and vascular biology*, 30(6), pp.1137–42.

Bradley, E.A. et al., 2010. Activation of AMP-activated protein kinase by 5-aminoimidazole-4-carboxamide-1-beta-D-ribofuranoside in the muscle microcirculation increases nitric oxide synthesis and microvascular perfusion. *Arteriosclerosis, thrombosis, and vascular biology*, 30(6), pp.1137–42.

Brogren, H. et al., 2004. Platelets synthesize large amounts of active plasminogen activator inhibitor 1. *Blood*, 104(13), pp.3943–3948.

Buhl, E.S. et al., 2002. Long-Term AICAR Administration Reduces Metabolic Disturbances and Lowers Blood Pressure in Rats Displaying Features of the Insulin Resistance Syndrome. *Diabetes*, 51(7), pp.2199–2206.

van Buul-Wortelboer, M.. et al., 1986. Reconstitution of the Vascular Wall In Vitro Cultures of endothelial cells seeded on solid impermeable substrates have proven useful for the study of several processes implicated in the physiology of the vessel wall including biosynthesis of prostaglandin. *Experimental Cell Research*, 162, pp.151–158.

Cacicedo, J.M. et al., 2004. AMPK inhibits fatty acid-induced increases in NF-. *Biochemical and Biophysical Research Communications*, 324, pp.1204–1209.

Carling, D. et al., 2012. AMP-activated protein kinase : new regulation , new roles ? , 27, pp.11–27.

Carling, D. et al., 1989. Purification and characterization of the AMP-activated protein kinase. *Eur J Biochemistry*, 136(186), pp.129–136.

Carlson, C. & Kim, K., 1973. Regulation of hepatic acetyl coenzyme a carboxylase by phosphorylation and dephosphorylation. *The journal of biological chemistry*, 248(1), pp.378–380.

Chakrabarti, K.R. et al., 2015. Pharmacologic regulation of AMPK in breast cancer affects cytoskeletal properties involved with microtentacle formation and re-attachment. , 6(34).

Chanda, D. et al., 2009. Fenofibrate differentially regulates PAI-1 gene expression via AMPK-dependent induction of orphan nuclear receptor SHP. *Hepatology*, 50(3), pp.880–892.

Chandrashekarappa, D.G., Mccartney, R.R. & Schmidt, M.C., 2013. Ligand Binding to the AMP-activated Protein Kinase Active Site Mediates Protection of the

Activation Loop from. *The jounal of biological chemistry*, 288(1), pp.89–98.

Chen, Y. et al., 2017. Adiponectin Inhibits TNF-α-Activated PAI-1 Expression Via the cAMP-PKA-AMPK-NF-κB Axis in Human Umbilical Vein Endothelial Cells. *Cellular Physiology and Biochemistry*, pp.2342–2352. Available at: https://www.karger.com/?doi=10.1159/000480006.

Chen, Y. et al., 1998. Sp1 Sites Mediate Activation of the Plasminogen Activator Inhibitor-1 Muscle Cells Sp1 Sites Mediate Activation of the Plasminogen Activator Inhibitor-1 Promoter by Glucose in Vascular Smooth Muscle Cells. *The journal of biological chemistry*, 273(3), pp.8225–8231.

Chen, Z. et al., 1999. AMP-activated protein kinase phosphorylation of endothelial NO synthase. , 443, pp.285–289.

Corton, J.M. et al., 1995. A specific method for activating AMP-activated protein kinase in intact cells ? , 565, pp.558–565.

Coven, D.L. et al., 2003. Physiological role of AMP-activated protein kinase in the heart : graded activation during exercise. , 8017, pp.0–7.

D'Amore, P., 1992. Endothelial cell-mural cell interactions. *J Cell Biochem (Supplement)*, 16(Supplement), pp.A1–5.

Daskalopoulos, E.P. et al., 2016. AMP-activated Protein Kinase. *EXS*, 107, pp.179–201. Available at: http://link.springer.com/10.1007/978-3-319-43589-3.

Davis, N.G., Phillips, A. & Becker, D.L., 2013. Connexin dynamics in the privileged wound healing of the buccal mucosa. *Wound Repair and Regeneration*, 21(4), pp.571–578.

Deyoung, M.B., Tom, C. & Dichek, D.A., 2001. Formation in Balloon-Injured Rat Carotid Arteries. , 1.

Dimova, E.Y. & Kietzmann, T., 2008. Metabolic , hormonal and environmental regulation of plasminogen activator inhibitor-1 (PAI-1) expression : Lessons from the liver. , 1, pp.992–1006.

Dora, K.A., 2001. Cell-cell communication in the vessel wall. *Vascular Medicine*, 6(1), pp.43–50. Available at: http://vmj.sagepub.com/cgi/doi/10.1177/1358836X0100600108.

Dora, K.A. et al., 2009. Europe PMC Funders Group Modulation of endothelial cell K Ca 3 . 1-channels during EDHF signaling in mesenteric resistance arteries. , 102(10), pp.1247–1255.

Emeis, J. & Kooistra, T., 1986. Interleukin 1 and lipopolysaccharide induce an inhibitor of tissue-type plasminogen activator in vivo and in cultured endothelial cells. *J Exp Med*, 163(May), pp.1260–1266.

Enkhjargal, B. et al., 2014. Endothelial AMP-Activated Protein Kinase Regulates Blood Pressure and Coronary Flow Responses Through Hyperpolarization Mechanism in Mice. *Arteriosclerosis, thrombosis, and vascular biology*, pp.1505–1513.

Erickson, L.A., Ginsberg, M.H. & Loskutoff, D.J., 1984. Detection and partial characterization of an inhibitor of plasminogen activator in human platelets. *The Journal of clinical investigation*, 74(4), pp.1465–72. Available at: http://www.pubmedcentral.nih.gov/articlerender.fcgi?artid=425316&tool=pmcentrez&rendertype=abstract.

Evans, A.M. et al., 2016. The emerging role of AMPK in the regulation of breathing and oxygen supply. , 0, pp.2561–2572.

Faulstich, H. et al., 1980. Virotoxins: Actin-Binding Cyclic Peptides of Amanita Virosa Mushrooms. *Biochemistry*, 19(14), pp.3334–3343.

Festa, A. et al., 2002. Plasminogen Activator Inhibitor-1 Predict the The Insulin Resistance Atherosclerosis Study. , 51(May 2001).

Figueroa, X.F. & Duling, B.R., 2009. Gap junctions in the control of vascular function. *Antioxidants & redox signaling*, 11(2), pp.251–266.

Fillinger, M.F. et al., 1993. The effect of endothelial cell coculture on smooth muscle cell proliferation. *Journal of vascular surgery*, 17(6), pp.1058–1068.

Ford, R.J. et al., 2012. AMP-activated protein kinase activator AICAR acutely lowers blood pressure and relaxes isolated resistance arteries of hypertensive rats. *Journal of hypertension*, 30(4), pp.725–33.

Ford, R.J. & Rush, J.W.E., 2011. Endothelium-dependent vasorelaxation to the AMPK activator AICAR is enhanced in aorta from hypertensive rats and is NO and EDCF dependent. *American journal of physiology. Heart and circulatory physiology*, 300(55), pp.H64–H75.

Fujimura, N. et al., 2012. 90 / AMP-Activated Protein Kinase / Endothelial Nitric Oxide in Humans. , (32), pp.153–160.

Fukuda, M., 2011. TBC proteins : GAPs for mammalian small GTPase Rab ? , 31, pp.159–168.

Gairhe, S. et al., 2011. Myoendothelial gap junctional signaling induces differentiation of pulmonary arterial smooth muscle cells. *American journal of physiology. Lung cellular and molecular physiology*, 301(4), pp.L527–35. Available at: http://ajplung.physiology.org/content/301/4/L527.abstract%5Cnpapers3://publication/doi/10.1152/ajplung.00091.2011.

Ganesan, M.K. & Finsterwalder, R., 2016. 3D co-culture model to analyze the crosstalk between endothelial and smooth muscle cells. , pp.1–42.

Garcia, D. & Shaw, R.J., 2017. AMPK: Mechanisms of Cellular Energy Sensing and Restoration of Metabolic Balance. *Molecular Cell*, 66(6), pp.789–800. Available at: http://dx.doi.org/10.1016/j.molcel.2017.05.032.

Garland, C.J. & Dora, K.A., 2017. EDH: endothelium-dependent hyperpolarization and microvascular signalling. *Acta Physiologica*, 219(1), pp.152–161.

Gerber, J.P. et al., 1993. Ambient oxygen tension modulates endothelial fibrinolysis. *Journal of vascular surgery*, pp.939–946.

Goirand, F. et al., 2007. Activation of AMP kinase alpha1 subunit induces aortic vasorelaxation in mice. *The Journal of physiology*, 581(Pt 3), pp.1163–71.

Goirand, F. et al., 2007. Activation of AMP kinase α 1 subunit induces aortic vasorelaxation in mice Franc. *J Physiol*, 3, pp.1163–1171.

Gomez-Galeno, J.. et al., 2010. A Potent and Selective AMPK Activator That Inhibits de Novo Lipogenesis. *ACS Med Chem Lett*, 1(9), pp.478–482.

Göransson, O. et al., 2007. Mechanism of action of A-769662, a valuable tool for activation of AMP-activated protein kinase. *The Journal of biological chemistry*, 282(45), pp.32549–60. Available at: http://www.jbc.org/content/282/45/32549.long.

Gowans, G.J. et al., 2013. AMP Is a True Physiological Regulator of AMP-Activated Protein Kinase by Both Allosteric Activation and Enhancing Net Phosphorylation. *Cell Metabolism*, 18(4), pp.556–566. Available at: http://dx.doi.org/10.1016/j.cmet.2013.08.019.

Griffith, T.M., Chaytor, A.T. & Edwards, D.H., 2004. The obligatory link : role of gap junctional communication in endothelium-dependent smooth muscle hyperpolarization. *Pharmacological Research*, 49, pp.551–564.

Gruzman, A., Babai, G. & Sasson, S., 2009. Adenosine Monophosphate-Activated Protein Kinase (AMPK) as a New Target for Antidiabetic Drugs: A Review on Metabolic, Pharmacological and Chemical Considerations. *The review of diabetic studies : RDS*, 6(1), pp.13–36.

Ha, D., Yang, N. & Nadithe, V., 2016. Exosomes as therapeutic drug carriers and delivery vehicles across biological membranes : current perspectives and future challenges. *Acta Pharmaceutica Sinica B*, 6(4), pp.287–296. Available at: http://dx.doi.org/10.1016/j.apsb.2016.02.001.

Haddock, R.E. et al., 2006. Endothelial coordination of cerebral vasomotion via myoendothelial gap junctions containing connexins 37 and 40. , pp.2047–2056.

Hara, S., 2017. Prostaglandin terminal synthases as novel therapeutic targets. *Proc. Jpn. Acad*, 93(9), pp.703–723.

Hardie, D.G., 2007. AMP-Activated Protein Kinase as a Drug Target. *Annual Review of Pharmacology and Toxicology*, 47(1), pp.185–210. Available at: http://www.annualreviews.org/doi/10.1146/annurev.pharmtox.47.120505.105304.

Hardie, D.G., 2013. AMPK: a target for drugs and natural products with effects on both diabetes and cancer. *Diabetes*, 62(7), pp.2164–72.

Hardie, D.G., 2015. AMPK: Positive and negative regulation, and its role in whole-body energy homeostasis. *Current Opinion in Cell Biology*, 33, pp.1–7. Available at: http://dx.doi.org/10.1016/j.ceb.2014.09.004.

Hardie, D.G., 2008. Role of AMP-activated protein kinase in the metabolic syndrome and in heart disease. *FEBS Letters*, 582(1), pp.81–89.

Hardie, D.G. & Ashford, M.L.J., 2014. REVIEWS AMPK : Regulating Energy Balance at the Cellular and Whole Body Levels. , pp.99–107.

Hardie, D.G., Ross, F.A. & Hawley, S.A., 2012. AMP-activated protein kinase: A target for drugs both ancient and modern. *Chemistry and Biology*, 19(10), pp.1222–1236. Available at: http://dx.doi.org/10.1016/j.chembiol.2012.08.019.

Hardie, D.G., Ross, F.A. & Hawley, S.A., 2012. F O C U S O N m e ta o l l R b E is AMPK : a nutrient and energy sensor that maintains energy homeostasis. , 13(April), p.2012.

Hawley, S. a et al., 1996. Characterization of the AMP-activated Protein Kinase Kinase from Rat Liver and Identification of Threonine 172as the Major Site at Which It Phosphorylates AMP-activated Protein Kinase. *Journal of Biological Chemistry*, 271(44), pp.27879–27887.

Hawley, S.A. et al., 2005. Calmodulin-dependent protein kinase kinase- β is an alternative upstream kinase for AMP-activated protein kinase. , 2(July), pp.9–19.

Hawley, S.A. et al., 1996. Characterization of the AMP-activated Protein Kinase Kinase from Rat Liver and Identification of Threonine 172 as the Major Site at Which It Phosphorylates AMP-activated Protein Kinase *. , 271(44), pp.27879–27887.

Hawley, S.A. et al., 2010. Use of cells Expressing gammar Subunit Subunit Subunit Variants to Identify Diverse Mechanisms of AMPK Activation. *Cell Metabolism*, 11(6), pp.554–565. Available at: http://dx.doi.org/10.1016/j.cmet.2010.04.001.

He, C. et al., 2015. AMPK Suppresses Vascular In fl ammation In Vivo by Inhibiting Signal Transducer and Activator of Transcription-1. , 64(January), pp.4285–4297.

Heberlein, K., Straub, A. & Isakson, B.E., 2009. The myoendothelial junction : breaking through the matrix ? *Microcirculation*, 16(4), pp.307–322.

Heberlein, K.R. et al., 2012. A novel mRNA binding protein complex promotes localized plasminogen activator inhibitor-1 accumulation at the myoendothelial junction. *Arteriosclerosis, Thrombosis, and Vascular Biology*, 32(5), pp.1271–1279.

Heberlein, K.R. et al., 2013. A novel mRNA binding protein complex promotes localized plasminogen activator inhibitor-1 accumulation at the myoendothelial junction. , 70(4), pp.646–656.

Heberlein, K.R. et al., 2010. Plasminogen activator inhibitor-1 regulates myoendothelial junction formation. *Circulation Research*, 106(6), pp.1092–1102.

Hoepfl, B. et al., 2002. EDHF, but not NO or prostaglandins, is critical to evoke a conducted dilation upon ACh in hamster arterioles. *American Journal of Physiology - Heart and Circulatory Physiology*, 283(3), pp.H996–H1004. Available at: http://ajpheart.physiology.org/lookup/doi/10.1152/ajpheart.01082.2001.

Hurley, R.L. et al., 2005. The Ca 2 □ / Calmodulin-dependent Protein Kinase Kinases

Are AMP-activated Protein Kinase Kinases * □. , 280(32), pp.29060–29066.

Isakson, B.E., Best, A. & Duling, B.R., 2008. Incidence of protein on actin bridges between endothelium and smooth muscle in mouse arterioles demonstrates heterogeneous connexin expression and phosphorylation. *Am J Physiol Heart Circ Physiol*, 294(6), pp.H2898–H2904.

Isakson, B.E., Best, A.K. & Duling, B.R., 2008. Incidence of protein on actin bridges between endothelium and smooth muscle in arterioles demonstrates heterogeneous connexin expression and phosphorylation. *American journal of physiology. Heart and circulatory physiology*, 294(6), pp.H2898–904.

Isakson, B.E. & Duling, B.R., 2005. Heterocellular contact at the myoendothelial junction influences gap junction organization. *Circulation Research*, 97(1), pp.44–51.

Isakson, B.E., Ramos, S.I. & Duling, B.R., 2007. Ca2+ and inositol 1,4,5-trisphosphate-mediated signaling across the myoendothelial junction. *Circulation Research*, 100(2), pp.246–254.

Isshiki, M. & Anderson, R.G.W., 2003. Function of Caveolae in Ca 2 + Entry and Ca 2 + -Dependent Signal Transduction. , pp.717–723.

Jackson, W.F., 2017. *Potassium Channels in Regulation of Vascular Smooth Muscle Contraction and Growth* 1st ed., Elsevier Inc. Available at: http://linkinghub.elsevier.com/retrieve/pii/S1054358916300606.

Jacob, M., Chappell, D. & Becker, B.F., 2016. Regulation of blood flow and volume exchange across the microcirculation. *Critical Care*, 20(1), p.319. Available at: http://ccforum.biomedcentral.com/articles/10.1186/s13054-016-1485-0.

Kameritsch, P. et al., 2015. Cx43 increases serum induced filopodia formation via activation of p21-activated protein kinase 1. *Biochimica et Biophysica Acta - Molecular Cell Research*, 1853(11), pp.2907–2917. Available at: http://dx.doi.org/10.1016/j.bbamcr.2015.08.004.

KAPABIOSYSTEMS, 2016. *Technical Data Sheet KAPA Mouse Genotyping Kit*,

Kavoussi, P.. et al., 2015. Recombinant PAI-1 therapy restores myoendothelial junctions and erectile function in PAI-1 deficient mice. *Andrologia*, 47(10), pp.1147–1152.

Kim, Y.D. et al., 2012. Metformin ameliorates IL-6-induced hepatic insulin resistance via induction of orphan nuclear receptor small heterodimer partner (SHP) in mouse models. *Diabetologia*, 55(5), pp.1482–1494.

Koh, H., 2016. Regulation of exercise-stimulated glucose uptake in skeletal muscle. , pp.61–65.

Komiya, M. et al., 2014. Bi-directional regulation between adiponectin and plasminogen activator-inhibitor-1 in 3T3-L1 cells. *In Vivo*, 28(1), pp.13–19.

Korff, T. et al., 2001. Blood vessel maturation in a 3-dimensional spheroidal coculture model : direct contact with smooth muscle cells regulates endothelial cell

quiescence and abrogates VEGF responsiveness. *The FASEB Journal*, 15(10), pp.447–457.

Kowal, J. et al., 2016. Proteomic comparison defines novel markers to characterize heterogeneous populations of extracellular vesicle subtypes. *Proceedings of the National Academy of Sciences*, 113(8), pp.E968–E977. Available at: http://www.pnas.org/lookup/doi/10.1073/pnas.1521230113.

Kreutz, C.-P., 2013. *Die Rolle der AMP-Kinase bei der Regulation des Vasotonus*.

Kubli, D. & Gustafsson, A., 2014. Cardiomyocyte health: adapting to metabolic changes through autophagy. *Trends in Endocrinol Metab*, 25(3), pp.156–164.

Kudo, N. et al., 1995. High rates of fatty acid oxidation during reperfusion of ischemic hearts are associated with a decrease in malonyl-CoA levels due to an increase in 5-AMP-activated protein kinase inhibition of acetyl-CoA carboxylase.pdf. *The journal of biological chemistry*, 270(21), pp.17513–17520.

Langlois, S. et al., 2008. Caveolin-1 and -2 Interact with Connexin43 and Regulate Gap Junctional Intercellular Communication in Keratinocytes. *Molecular biology of the cell*, 19(1), pp.912–926.

Ledoux, J. et al., 2008. Functional architecture of inositol 1,4,5-trisphosphate signaling in restricted spaces of myoendothelial projections. *Proceedings of the National Academy of Sciences*, 105(28), pp.9627–9632. Available at: http://www.pnas.org/cgi/doi/10.1073/pnas.0801963105.

Li, J. et al., 2013. effects to activate AMP-activated protein kinase in the heart. , 110(40).

Li, J. et al., 2007. Neuroprotective effects of adenosine monophosphate-activated protein kinase inhibition and gene deletion in stroke. *Stroke*, 38(11), pp.2992–2999.

Lin, S.-C. & Hardie, D.G., 2017. AMPK: Sensing Glucose as well as Cellular Energy Status. *Cell Metabolism*, (2017). Available at: http://linkinghub.elsevier.com/retrieve/pii/S1550413117306228.

Lindahl, T., Sigurdardottir, O. & Wiman, B., 1989. Stability of plasminogen activator inhibitor 1 (PAI-1). *Thromb Haemost*, 62(2), pp.748–751.

Maeda, S. & Tsukihara, T., 2011. Structure of the gap junction channel and its implications for its biological functions. , pp.1115–1129.

Michel, R., Hu, F. & Meyrick, B., 1995. Myoendothelial junctional complexes in postobstructive pulmonary vasculopathy a quantitative electron microscopic study. *Exp Lung Res*, 21(3), pp.437–452.

Miller, L., 2010. Analyzing gels and western blots with ImageJ. *lukemiller.org*.

Moore, D.H. & Ruska, H., 1957. The fine structure of capillaries and small arteries. *The Journal of biophysical and biochemical cytology*, 3(3), pp.457–462.

Murphy, D.A. & Courtneidge, S.A., 2011. The “ins” and “outs” of podosomes and

invadopodia: characteristics, formation and function. *NATURE REVIEWS | MOLECULAR CELL BIOLOGY*, 12(7), pp.413–426.

Nakano, A. et al., 2010. AMPK controls the speed of microtubule polymerization and directional cell migration through CLIP-170 phosphorylation. *Nature cell biology*, 12(6), pp.583–590.

Nawaz, M., Fatima, F. & Elia, L., 2017. Extracellular Vesicles , Tunneling Nanotubes , and Cellular Interplay : Synergies and Missing Links. , 4(July), pp.1–12.

Onselaer, M. et al., 2014. The Ca 2 + / calmodulin-dependent kinase kinase b - AMP-activated protein kinase- a 1 pathway regulates phosphorylation of cytoskeletal targets in thrombin-stimulated human platelets. *J Thromb Haemost*, 12, pp.973–986.

Pang, T. et al., 2008. Small Molecule Antagonizes Autoinhibition and Activates AMP-activated Protein Kinase in Cells *. , 283(23), pp.16051–16060.

Pannekoek, H. et al., 1986. Endothelial plasminogen activator inhibitor(PAI): a new member of the serpin gene family. *The EMBO Journal*, 5(10), pp.2539–2544.

Patten, I.S. & Arany, Z., 2012. PGC-1 coactivators in the cardiovascular system. *Trends in Endocrinology & Metabolism*, 23(2), pp.90–97. Available at: http://dx.doi.org/10.1016/j.tem.2011.09.007.

Pinter, K. et al., 2013. Localisation of AMPK γ subunits in cardiac and skeletal muscles. *Journal of muscle research and cell motility*, 34(5-6), pp.369–78.

Pinter, K. et al., 2012. Subunit composition of AMPK trimers present in the cytokinetic apparatus: Implications for drug target identification. *Cell Cycle*, 11(5), pp.917–921.

Pogoda, K. et al., 2017. NO Augments Endothelial Reactivity by Reducing Myoendothelial Calcium Signal Spreading A Novel Role for Cx37 (Connexin 37) and SHP-2. *Arterioscler Thromb Vasc Biol*, (12), p.2017.

Pogoda, K. et al., 2014. NO, via its target Cx37, modulates calcium signal propagation selectively at myoendothelial gap junctions. *Cell communication and signaling : CCS*, 12(1), p.33. Available at: http://www.pubmedcentral.nih.gov/articlerender.fcgi?artid=4036488&tool=pmcentrez&rendertype=abstract.

Prisco, D. et al., 2001. Postprocedural PAI-1 Activity is a Risk Marker of Subsequent Clinical Restenosis in Patients Both with and without Stent Implantation After Elective Balloon PTCA. *Thrombosis Research*, 104, pp.181–186.

Pyla, R. et al., 2015. Altered energy state reversibly controls smooth muscle contractile function in human saphenous vein during acute hypoxia-reoxygenation Role of glycogen AMP-activated protein kinase and insulin-independent glucose uptake. *Biochemical Pharmacology*, 97(1), pp.77–88.

Randriamboavonjy, V. et al., 2010. PLATELETS AND THROMBOPOIESIS AMPK ␣ 2 subunit is involved in platelet signaling , clot retraction , and thrombus stability. *Blood*, 116(12), pp.2134–2141.

Rasmussen, K.M.B. et al., 2016. Contribution of K+channels to endothelium-derived hypolarization-induced renal vasodilation in rats in vivo and in vitro. *Pflugers Archiv European Journal of Physiology*, 468(7), pp.1139–1149. Available at: http://dx.doi.org/10.1007/s00424-016-1805-x.

Revel, J.P. & Karnovsky, M.J., 1967. Hexagonal array of subunits in intercellular junctions of the mouse heart and liver. *Journal of Cell Biology*, 33(3).

Rhodin, J., 1967. The ultrastructure of mammalian arterioles and precapillary sphincters. *J Ultrastruct Res*, 18(1), pp.181–223.

Richter, S.H. et al., 2010. Lifeact mice for studying F-actin dynamics. *Nature Methods*, 7(3), pp.168–169. Available at: http://dx.doi.org/10.1038/nmeth0310-168.

Riedl, J., 2010. Development and Characterization of Lifeact - a versatile marker for the visualization of F-actin -. *PhD Thesis*.

Rijken, D. & Lijnen, R., 2009. New insights into the molecular mechanisms of the fibrinolytic system. *Journal of thrombosis and Haemostasis*, 7(1), pp.4–13.

Röder, P. V et al., 2016. Pancreatic regulation of glucose homeostasis. *Experimental & Molecular Medicine*, 48(3), p.e219. Available at: http://www.nature.com/doifinder/10.1038/emm.2016.6.

Ross, F.A., Jensen, T.E. & Hardie, D.G., 2016. Differential regulation by AMP and ADP of AMPK complexes containing different γ subunit isoforms. , pp.189–199.

Ross, F.A., MacKintosh, C. & Hardie, D.G., 2016. AMP-activated protein kinase: a cellular energy sensor that comes in 12 flavours. *FEBS Journal*, 283, pp.2987–3001.

Rourke, S.T.O. & Vanhoutte, P.M., 1992. Adrenergic and Cholinergic Regulation of Bronchial Vascular Tone. *An Rev Respir Dis*, 146(5 Pt 2), pp.S11–S14.

Rubanyi, G.M., 1991. Endothelium-Derived Relaxing and Contracting Factors. *Journal of Cellular Biochemistry*, 36(1 991), pp.27–36.

Rubin, L.J. et al., 2005. Metabolic activation of AMP kinase in vascular smooth muscle. *Journal of applied physiology (Bethesda, Md. : 1985)*, 98(1), pp.296–306.

Russo, G.L., Russo, M. & Ungaro, P., 2013. AMP-activated protein kinase: A target for old drugs against diabetes and cancer. *Biochemical Pharmacology*, 86(3), pp.339–350. Available at: http://dx.doi.org/10.1016/j.bcp.2013.05.023.

Rustom, A. et al., 2014. Nanotubular Highways for Intercellular Organelle Transport. , 1007(2004).

Rutherford, C. et al., 2016. Phosphorylation of Janus kinase 1 (JAK1) by AMP-activated protein kinase (AMPK) links energy sensing to anti-inflammatory signaling. , 109(November), pp.1–11.

Sakamoto, K. et al., 2004. Activity of LKB1 and AMPK-related kinases in skeletal

muscle : effects of contraction , phenformin , and AICAR. , pp.310–317.

Salt, I. & Hardie, D.G., 2017. AMP-Activated Protein Kinase An Ubiquitous Signaling Pathway With Key Roles in the Cardiovascular System. *Circulation Research*, (120), pp.1825–1842.

Salt, I.P. & Hardie, D.G., 2010. AMP-Activated Protein Kinase. *Handbook of Cell Signaling*, pp.551–557. Available at: http://linkinghub.elsevier.com/retrieve/pii/B9780123741455000735.

Salt, I.P. & Hardie, D.G., 2017. in the Cardiovascular System Occurrence of Subunit Isoforms. , pp.1825–1842.

Sandow, S.L. et al., 2002. Involvement of myoendothelial gap junctions in the actions of endothelium-derived hyperpolarizing factor. *Circulation Research*, 90(10), pp.1108–1113.

Sandow, S.L. et al., 2012. Myoendothelial Contacts, Gap Junctions, and Microdomains: Anatomical Links to Function? *Microcirculation*, 19(5), pp.403–415.

Sandow, S.L. et al., 2006. Spatial separation of endothelial small- and intermediate-conductance calcium-activated potassium channels (K Ca) and connexins : possible relationship to vasodilator function ? , (August), pp.689–698.

Sandow, S.L., Gzik, D.J. & Lee, R.M.K.W., 2009. Arterial internal elastic lamina holes: Relationship to function? *Journal of Anatomy*, 214(2), pp.258–266.

Sandow, S.L. & Hill, C.E., 2000a. Incidence of Myoendothelial Gap Junctions in the Proximal and Distal Mesenteric Arteries of the Rat Is Suggestive of a Role in Endothelium-Derived Hyperpolarizing Factor – Mediated Responses.

Sandow, S.L. & Hill, C.E., 2000b. Incidence of myoendothelial gap junctions in the proximal and distal mesenteric arteries of the rat is suggestive of a role in endothelium-derived hyperpolarizing factor-mediated responses. *Circulation research*, 86(3), pp.341–346.

Sarelius, I. & Pohl, U., 2010. Control of muscle blood flow during exercise: Local factors and integrative mechanisms. *Acta Physiologica*, 199(4), pp.349–365.

Sawdey, M., Podor, T.J. & Loskutoffs, J., 1989. Regulation of Type 1 Plasminogen Activator Inhibitor Gene Expression in Cultured Bovine Aortic Endothelial Cells. *The journal of biological chemistry*, 264(25), pp.10396–10401.

Schmidt, V.J. et al., 2008. Gap junctions synchronize vascular tone within the microcirculation. *Pharmacol Rep*, 60(1), pp.68–74.

Schneider, C.A., Rasband, W.S. & Eliceiri, K.W., 2012. NIH Image to ImageJ: 25 years of image analysis. *Nature Methods*, 9(7), pp.671–675. Available at: http://www.nature.com/doifinder/10.1038/nmeth.2089.

Schneider, H. et al., 2015. AMPK Dilates Resistance Arteries via Activation of SERCA and BK Ca Channels in Smooth Muscle. *Hypertension*, 66(1), pp.108–116.

Schneider, H. et al., 2015. AMPK dilates resistance arteries via activation of SERCA and BKCa channels in smooth muscle. *Hypertension*, 66(1), pp.108–116.

Schubert, K. et al., 2017. The AMP-Related Kinase (AMPK) Induces Ca 2 + - Independent Dilation of Resistance Arteries by Interfering with Actin Filament Formation. *Circulation research*, 121(2), pp.149–161.

Segal, S.S. & Bagher, P., 2010. Regulation of myoendothelial junction formation: Bridging the gap. *Circulation Research*, 106(6), pp.1014–1016.

Seol, W., Choi, H. & Moore, D.D., 1996. An Orphan nuclear Hormone Receptor That Lacks a DNA Binding Domain and Heterodimerizes with Other Receptors. , 2(12).

Shaw, R.J. et al., 2004. The tumor suppressor LKB1 kinase directly activates AMP-activated kinase and regulates apoptosis in response to energy stress. , 101(10), pp.3329–3335.

Shu, X. et al., 2015. Endothelial nitric oxide synthase in the microcirculation. *Cellular and Molecular Life Sciences*, 72(23), pp.4561–4575.

Siragusa, M., Fleming, I. & Fleming, I., 2016. The eNOS signalosome and its link to endothelial dysfunction. *Pflügers Archiv - European Journal of Physiology*. Available at: http://dx.doi.org/10.1007/s00424-016-1839-0.

Smith, B. et al., 2016. Treatment of nonalocholic fatty liver disease role of AMPK. *Am J physiol Endocrinol Metab*, 311(4), pp.E730–E740.

Sonkusare, S.K. et al., 2012. Elementary Ca2+ Signals Through Endothelial TRPV4 Channels Regulate Vascular Function. *Science*, 336(6081), pp.597–601.

Sosinsky, G.E. & Nicholson, B.J., 2005. Structural organization of gap junction channels. *Biochimica et Biophysica Acta (BBA) - Biomembranes*, 1711(2), pp.99–125. Available at: http://linkinghub.elsevier.com/retrieve/pii/S0005273605000878.

Spruss, A. et al., 2012. Female Mice Are More Susceptible to Nonalcoholic Fatty Liver Disease: Sex-Specific Regulation of the Heptatic AMP-Activated Protein Kinase-Plasminogen Activator Inhibitor-1 Cascade, but Not the Hepatic Endotoxin Response. *Molecular Medicine*, 18(9), p.1. Available at: http://www.molmed.org/pdfstore/12_223_Spruss.pdf.

Stahmann, N. et al., 2010. Activation of AMP-activated Protein Kinase by Vascular Endothelial Growth Factor Mediates Endothelial Angiogenesis Independently of Nitric-oxide Synthase * □. , 285(14), pp.10638–10652.

Steinberg, G.R. & Kemp, B.E., 2009a. AMPK in Health and Disease BACKGROUND. , pp.1025–1078.

Steinberg, G.R. & Kemp, B.E., 2009b. AMPK in Health and Disease. *Physiological reviews*, 89(3), pp.1025–1078.

Straub, A.C. et al., 2011. Compartmentalized connexin 43 s-nitrosylation/denitrosylation regulates heterocellular communication in the vessel

wall. *Arteriosclerosis, thrombosis, and vascular biology*, 31(2), pp.399–407.

Straub, A.C. et al., 2012. Endothelial cell expression of hemoglobin α regulates nitric oxide signaling. *Nature*, 491(7424), pp.473–477.

Straub, A.C., Zeigler, A.C. & Isakson, B.E., 2014. The Myoendothelial Junction : Connections That Deliver the Message. , pp.242–249.

Tennant, M. & Mcgeachie, J. k, 1990. REVIEW ARTICLE BLOOD VESSEL STRUCTURE AND FUNCTION : A BRIEF UPDATE ON RECENT ADVANCES. *Aust N Z J Surg*, (October), pp.747–753.

Tian, J. & Xie, Z., 2008. The Na/K-ATPase and Calcium Signaling Microdomains. *Physiology (Bethesda)*, 23, pp.205–211.

Tran, C.H.T. et al., 2012. Endothelial Ca2+ wavelets and the induction of myoendothelial feedback. *AJP: Cell Physiology*, 302(8), pp.C1226–C1242.

Wallace, C.S., Champion, J.C. & Truskey, G.A., 2007. Adhesion and Function of Human Endothelial Cells Co-cultured on Smooth Muscle Cells. *Annals of Biomedical engineering*, 35(3), pp.375–386.

Wang, S. et al., 2012. Activation of AMP-activated protein kinase α2 by nicotine instigates formation of abdominal aortic aneurysms in mice in vivo. *Nature medicine*, 18(6), pp.902–10.

Watt, M.J. et al., 2008. CNTF reverses obesity-induced insulin resistance by activating skeletal muscle AMPK. , 12(5), pp.541–548.

Welsh, D.G. & Taylor, M.S., 2012. Cell-Cell Communication in the Resistance Vasculature: The Past, Present, and Future. *Microcirculation*, 19(5), pp.377–378.

Wikstrom, J.D. et al., 2013. AMPK regulates ER morphology and function in stressed pancreatic β-cells via phosphorylation of DRP1. *Molecular endocrinology (Baltimore, Md.)*, 27(10), pp.1706–23.

Woods, A. et al., 2005. Ca 2 + / calmodulin-dependent protein kinase kinase- β acts upstream of AMP-activated protein kinase in mammalian cells. , 2(July), pp.21–33.

Woods, A. et al., 2003. LKB1 Is the Upstream Kinase in the AMP-Activated Protein Kinase Cascade. *Current Biology*, 13, pp.2004–2008.

Xiao, B. et al., 2013. Structural basis of AMPK regulation by small molecule activators. *Nature communications*, 4(3017), pp.1–17. Available at: http://www.pubmedcentral.nih.gov/articlerender.fcgi?artid=3905731&tool=pmcentrez&rendertype=abstract.

Xu, J. et al., 2017. Myoendothelial gap junctions mediate regulation of angiopoietin-2-induced vascular hyporeactivity after hypoxia through connexin 43-gated cAMP transfer. *Am J Physiol cell Physiol*, 68757421.

Xu, J., Chen, G. & Yang, Y., 2017. Exosomes : A Rising Star in Falling Hearts. , 8(July).

Yamin, R. & Morgan, K.G., 2012. Deciphering actin cytoskeletal function in the contractile vascular smooth muscle cell. *The Journal of physiology*, 590(Pt 17), pp.4145–54.

Yeager, M. & Harris, A.L., 2007. Gap junction channel structure in the early 21th centurey: facts and fantasies. , 19(5), pp.1–14.

Zhang, C. et al., 2017. Fructose-1,6-biphosphate and aldolase mediate glucose sensing by AMPK. *Nature Publishing Group*. Available at: http://dx.doi.org/10.1038/nature23275.

Zhang, L. & Ducsay, C.A., 2014. Advances in Fetal and Neonatal Physiology. *Adv EXP Med Biol*, 814, pp.117–132.

Zhang, M. et al., 2017. Protective benefits of AMP-activated protein kinase in hepatic ischemia-reperfusion injury. , 9(3), pp.823–829.

Zhang, Z. et al., 2016. Role of myoendothelial gap junctions in the regulation of human coronary artery smooth muscle cell differentiation by laminar shear stress. *Cellular Physiology and Biochemistry*, 39(2), pp.423–437.

Zhou, H. et al., 2017. Rosmarinic Acid Alleviates the Endothelial Dysfunction Induced by Hydrogen Peroxide in Rat Aortic Rings via Activation of AMPK. *Oxidative Medicine and Cellular Longevity*, 2017, pp.1–9. Available at: https://www.hindawi.com/journals/omcl/2017/7091904/.

Zhu, Y., Farrehi, P.M. & Fay, W.P., 2001. Plasminogen Activator Inhibitor Type 1 Enhances Neointima Formation After Oxidative Vascular Injury in. *Circulation*, 103(25), pp.3105–3110.

Zünkler, B.J., Wos-Maganga, M. & Panten, U., 2004. Fluorescence microscopy studies with a fluorescent glibenclamide derivative, a high-affinity blocker of pancreatic β-cell ATP-sensitive K+ currents. *Biochemical Pharmacology*, 67(8), pp.1437–1444.

Acknowledgements

Traveling thousands of miles is better than reading thousands of books, and with longing for the unknown, I began my doctoral study in Ludwig Maximilian University of Munich Germany from the summer of 2014. How time flies, more than three years has gone forever, but everything happened during this time is visible before my eyes, as if it was yesterday. During this period, I got much help from my supervisors, teachers and classmates, and support from my family. I would like to express my heartfelt thanks to all of them at the moment when I completing my thesis.

First of all, as the saying goes, a teacher for a day is a father for a life. I would like to thank both Prof Ulrich Pohl and Thomas Koeppel from the bottom of my heart. For Prof Thomas Koeppel, he gave me the opportunity to study in Munich. As luck would have it, with the recommendation from Prof Thomas Koeppel, I finally carried out my doctoral research project on understanding of the roles of AMPK in vascular system under supervision of Prof Ulrich Pohl. Prof Ulrich Pohl is a model for me to follow for his knowledgeable, honest, rigorous and realistic scientific attitude, scientific thinking, and his life style, courteous, accessible, amiable and easy of approach. Prof Ulrich Pohl not only helped me in the course of research and the completion of thesis, but also in life. I will remember him all my life. And I would like to express my sincere respect to both supervisors!

Secondly, I'd like to thank postdoctoral Holger Schneider from the bottom of my heart. There is a folk adage in China: a man depends upon his parents at home and upon his friends abroad. In life, Holger Schneider has given a great help to me. He is also my co-supervisor. He carefully guided me into the research with the German specific and meticulous way, and I learned various experimental techniques, skills and research thinking from him. And I also need to thank him for his revision of my thesis. Kai-Michael Schubert is another guy to whom I need to express my sincere thanks. He paid a lot of time on this project. Meanwhile, I need to thank Sibgha Tahir. For the last three years, I have been taking great help from her to improve my English pronunciation and to help me in the experiment. At the same time, I also need to thank Stephanie Blodow, Margarethe Wiedenmann, Reinhard Fässler, Eloi Montanez, Felizitas Kiemer, Kristin Pogoda, Petra Kameritsch, Anke Lübeck, Claudia Fahney, Meipin Wu and Hellen for their guidance and help for my study.

I would like to thank the Second Affiliated Hospital of Nanchang University and the chairman of my vascular department in China for great support for my studies abroad, and I also thank the EU ITN SmArter project for the grant.

Sincere thanks to the brothers and sisters from China who are also studying in Germany, such as Tian Weili, Zhang Zhe, He Kuang and so on.

At the moment of finishing my thesis, my heart is full of gratitude, and I would like to thank my parents for their selfless support. And I need to express my sincere gratitude from the bottom of my heart to my wife. In order to live together, she gave up her own job and came to Germany to support and take care of family and the education of my son. I will never forget the sacrifices and selfless devotion of my wife to our family. I hope we will have nice, healthy life in the future.

Conference and Publications Papers during doctor study:

Conference:

1. The 3th Annual European meeting on AMPK- September 10th to 13th, 2017, Ile De Porquerolles, France.
   Oral presentation: AMPK causes vasodilation by reducing calcium sensitivity and altering actin filament dynamics in microvascular smooth muscle.

2. The 2nd Joint Meeting of the European Society for Microcirculation (ESM) and European Vascular Biology Organisation (EVBO) –May 29th to June 1st , 2017, Geneva, Switzerland.
   Poster presentation: AMPK causes vasodilation by reducing calcium sensitivity and altering actin filament dynamics in microvascular smooth muscle.

3. 29th European Society of Vascular surgery Annual Meeting – September 23th to 25th, 2015, Porto, Portugal.
   Poster presentation: The Treatment of Infected Femoral Artery Pseudo aneurysms Secondary to Drug Abuse: 11 Years of Experience at a Single Institution.

4. Joint Meeting of the 28th European Society for Microcirculation (ESM) and the 8th European Vascular Biology Organization (EVBO) June 03rd to 06th, 2015, Pisa, Italy.
   Poster presentation: AMPK Dilates Resistance Arteries via Activation of SERCA and BKCa Channels in Smooth Muscle.

Publication:

1. Pogoda K, Mannell H, Blodow S, Schneider H, Schubert KM, **Qiu J**, Schmidt A, Imhof A, Beck H, Tanase LI, Pfeifer A, Pohl U, Kameritsch P. NO Augments Endothelial Reactivity by Reducing Myoendothelial Calcium Signal Spreading: A Novel Role for Cx37 (Connexin 37) and SHP-2. ArteriosclerThrombVasc Biol. 2017 Oct 12.

2. Schubert KM*, **Qiu J***, Blodow S, Wiedenmann M, Lubomirov LT, Pfitzer G, Pohl U, Schneider H. The AMP-Related Kinase (AMPK) Induces Ca2+-Independent Dilation of Resistance Arteries by Interfering With Actin Filament Formation. Circ Res. 2017 Jul 7;121(2):149-161. doi: 10.1161/CIRCRESAHA.116.309962. Epub 2017 Jun 6.

3. Kirsch J, Schneider H, Pagel JI, Rehberg M, Singer M, Hellfritsch J, Chillo O, Schubert KM, **Qiu J**, Pogoda K, Kameritsch P, Uhl B, Pircher J, Deindl E, Müller S, Kirchner T, Pohl U, Conrad M, Beck H. Endothelial Dysfunction, and A Prothrombotic, Proinflammatory Phenotype Is Caused by Loss of Mitochondrial Thioredoxin Reductase in Endothelium. ArteriosclerThrombVasc Biol. 2016 Sep;36(9):1891-9. doi: 10.1161/ATVBAHA.116.307843. Epub 2016 Jul 7.

4. Schneider H*, Schubert KM*, Blodow S, Kreutz CP, Erdogmus S, Wiedenmann M, **Qiu J,** Fey T, Ruth P, Lubomirov LT, Pfitzer G, Mederos Y Schnitzler M, Hardie DG, Gudermann T, Pohl U. AMPK Dilates Resistance Arteries via Activation of SERCA and BKCa Channels in Smooth Muscle. Hypertension. 2015 Jul;66(1):108-16. doi: 10.1161/HYPERTENSIONAHA.115.05514. Epub 2015 Jun 1.

LMU LUDWIG-MAXIMILIANS-UNIVERSITÄT MÜNCHEN

Dean's Office
Medical Faculty

Afidavit

Qiu, Jiehua

Surname, first name

Street

Zip code, town

Country

I hereby declare, that the submitted thesis entitled

5'-adenosine monophosphate-activated protein kinase (AMPK) modulates myoendothelial junctions

is my own work. I have only used the sources indicated and have not made unauthorised use of services of a third party. Where the work of others has been quoted or reproduced, the source is always given.

I further declare that the submitted thesis or parts thereof have not been presented as part of an examination degree to any other university.

Munich Germany, 06.03.2018 — Place, date

Jiehua Qiu — Signature doctoral candidate